POST-IR IRSL DATING OF THE NENANA DUNE FIELD IN THE TANANA LOWLANDS, CENTRAL ALASKA

by

Claire Anna Messner

Submitted to the graduate degree program in Geography and the Graduate Faculty of the University of Kansas in partial fulfillment of the requirements for the degree of Master of Science.

_____

Chairperson William C. Johnson, Ph.D.

_____

Stephen L. Egbert, Ph.D.

_____

Leigh A. Stearns, Ph.D.

_____

Alan F. Halfen, Ph.D.

Date Defended: July 17th, 2015

The Thesis Committee for Claire Anna Messner

certifies that this is the approved version of the following thesis:

POST-IR IRSL DATING OF THE NENANA DUNE FIELD IN THE TANANA LOWLANDS, CENTRAL ALASKA

_____

Chairperson William C. Johnson, Ph.D.

Date approved: July 17th, 2015

Abstract

Sand dunes record paleoclimatic change within their stratigraphy as they respond to climatic shifts through sequences of activation and stabilization. Developing chronologies documenting periods of dune activity and stabilization can thus provide information about past climatic conditions. Consequently, the need for accurate chronological determinations of aeolian features has stimulated the advancement of dating techniques. In Alaskan sand dune settings, radiocarbon dating of organic material and optical dating of quartz grains have proven to be problematic due to insufficient organic material and a weak optical signal, respectively. In such cases, feldspar grains can be dated using Infrared Stimulated Luminescence (IRSL) dating, but are often avoided due to inherent anomalous fading that results in age underestimation. The lack of a viable dating technique has resulted in a paucity of chronostratigraphic Alaskan dune studies, particularly within central Alaska. This research tests the use of a post-infrared (pIR) IRSL protocol, specifically designed to limit the effects of anomalous fading, on the Nenana dune field within the Tanana River Lowlands of central Alaska. Results indicate that dune activity occurred as far back as ~16 ka for the Nenana dunes, as deglaciation of the surrounding area provided an influx of sediment into glacial streams throughout the Tanana River Lowlands. IRSL ages indicate a switch from sand to silt accumulation between 11 ka and 10 ka and stabilization of the dune field that is likely tied to the spread of boreal forest throughout the region around this time. These IRSL ages align with regional proxy data indicating similar timing of activation and stabilization of aeolian features during the transition between the Late Pleistocene and early Holocene. This research represents one of the first IRSL sand dune studies

of central Alaska and supports further use of a pIR IRSL protocol to expand aeolian research within Alaska.

Acknowledgements

This research would not have been possible without funding support from a variety of sources, including the Geological Society of America, University of Kansas General Research Fund, U.S. Army Cultural Resources Program at Fort Wainwright, Alaska, and University of Kansas Department of Geography. I am also grateful for field support provided by Wright Air Service and Quicksilver Air of Fairbanks, Alaska.

I would like to especially acknowledge my advisor, Bill Johnson, who has not only generously supported me throughout the entirety of this research, but also stuck out long days in the field battling relentless mosquitos. Overall, it was a wonderful experience conducting fieldwork in Alaska, and one that was only made possible by your efforts and support. I am also grateful to my committee members, Leigh Stearns, Alan Halfen, and Steve Egbert. Thank you for your guidance, encouragement, and feedback that have greatly improved this thesis.

A significant portion of time spent on this research revolved around luminescence dating, to which I was introduced during the Optical Dating Short Course offered at the University State University Luminescence Laboratory. I owe my interest in and knowledge of luminescence dating to Tammy Rittenour and am incredibly grateful for the laboratory support and mentorship that she and Michelle Nelson have provided throughout the past two years. Thank you for the time and effort you have both put forth on behalf of my research and for walking me through the complexities of the technique. I am also grateful for laboratory support from Carlie Ideker, who offered her time on more than one occasion to help me around the lab and so generously clean sieves. My time spent working at the lab in Logan, Utah, has been a highlight of my graduate

work, and I am grateful for the experience and for the many friendships that have resulted from collaboration with Utah State University.

This thesis has also benefitted greatly from my peers at the University of Kansas, especially those of my writing group. Jen, Anna, Awesta, and Jean, thank you for your time, dedication, and willingness to read through endless drafts. Your comments, critiques, and mentoring made all the difference.

The steadfast support of my family, especially my parents Bill and Wanita, has been indispensable throughout my schooling. Thank you for your words of encouragement and guidance along the way. I am lucky to have such incredible role models. Lastly, I am indebted to my husband, Lewis, whose help and generosity have been invaluable. Thank you for encouraging me to pursue graduate school, even when it was far from home, and for your unwavering support throughout the years.

Table of Contents

Abstract ..... **iii**

Acknowledgements ..... **v**

Table of Contents ..... **vii**

List of Tables ..... **ix**

List of Figures ..... **ix**

List of Appendices ..... **x**

Chapter 1 Introduction **1**

Chapter 2 Background **8**

2.1 Aeolian Deposits of Northwest North America 8

2.1.1 Summary of Regional Aeolian Activity 15

2.2 Luminescence Dating 21

2.2.1 Basics of Optical Luminescence 21

2.2.2 Optical Luminescence Age Determination 24

2.3 Applications and Developments of Luminescence Dating 25

2.3.1 Applications of Luminescence Dating 25

2.3.2 Limitations of Luminescence Dating 27

2.3.3 Development of IRSL Techniques 29

2.3.4 Aeolian Luminescence Studies of Alaska 31

Chapter 3 Regional Setting and Study Area **36**

Chapter 4 Methods **44**

4.1 Field Methods 44

4.2 Laboratory Pretreatment of Luminescence Samples 49

4.3 Post-IR IRSL Age Determination 49

Chapter 5 Results 50

5.1 Post-IR IRSL Results 50

5.2 Site Stratigraphy 53

5.2.1 Cosna site (64.533, -149.060) 53

5.2.2 Jacobson site (64.531, -149.059) 56

5.2.3 Red Tower site (64.526, -149.067) 58

5.2.4 Three Towers site (64.524, -149.068) 59

5.2.5 Beekeeper site (64.505, -149.071) 60

5.2.6 Boulden site (64.506, -149.074) 61

5.2.7 Chevron site (64.494, -149.078) 61

Chapter 6 Discussion 63

6.1 Comparison of Nenana Ages with Regional Proxies 64

6.1.1 Wood River Age Comparison 68

6.2 Future Studies 68

Chapter 7 Conclusions 72

References 76

Appendix A. Supplemental Data 88

Appendix B. Sample Site Images 104

List of Tables

Table 2.1. Treatment process of the applied post-IR IRSL SAR protocol..... 31

Table 2.2. Wood River dune IRSL age estimates 34

Table 3.1. Temperature and precipitation data for Nenana from 1981–2010 38

Table 5.1: Equivalent dose, dose rate, and post-IR IRSL age estimates for the Nenana dunes... 51

List of Figures

Figure 2.1. Expanse of aeolian deposits of Alaska 9

Figure 2.2. Expansive Gold Hills loess bluffs 11

Figure 2.3. Deglaciation of interior Alaska between 17 ka and 10 ka 18

Figure 2.4. Generalized depiction of luminescence principles 22

Figure 3.1. Physiographic regions of central Alaska (Wahrhaftig, 1965) 37

Figure 3.2. Seasonal wind rose showing prevailing wind direction during June 1961–1990..... 39

Figure 3.3. Seasonal wind rose showing prevailing wind direction during Dec. 1961–1990 39

Figure 3.4. Proximal extent of the expansive Kantishna sand sea 41

Figure 3.5. Remnants of aeolian deposits 42

Figure 3.6. Multiple vegetated, stabilized dunes of the Nenana dune field 43

Figure 3.7. Aerial and ground views of several of the Wood River dunes 43

Figure 4.1. Aerial survey of Nenana area 45

Figure 4.2. Sample sites (yellow triangles) labeled by site location code 46

Figure 4.3. Various sampling techniques used in the field 48

Figure 5.1. Post-IR IRSL age estimates from the Nenana dunes and generalized stratigraphy .. 52

Figure 5.2. Present and original slip face of the Cosna dune 55

Figure 5.3. East-facing road-cut exposure at the Cosna site 55

Figure 5.4. Patches of darker colored sediment indicate several krotovina..... 58

Figure 5.5. Human disturbance (ATV tracks) at the Three Towers site..... 60

List of Appendices

Appendix A. Supplemental Data

Appendix B. Sample Site Images

Chapter 1 Introduction

The field of Quaternary geomorphology has directed a large portion of its research towards developing chronologies of sedimentary deposits as effects of global climate change become more widely recognized by the scientific community and the general public. Examining periods of formation or alteration of sedimentary features, such as sand dunes, reveals information about past environmental conditions. For example, a shift toward a drier climate, as seen at the end of the Pleistocene, can reduce vegetative cover and, with sufficient wind velocities, induce the mobility of sediment and thus dune formation or reformation. Such interest regarding past environments generates the need for the advancement of dating techniques to aid Quaternary researchers.

Sand dunes maintain records of paleoclimatic change within their stratigraphy as they respond to climatic changes through activation and stabilization (Lancaster, 1995; Wolfe et al., 2011). Their formation requires the mobilization of sand, which can be influenced by factors including transport capacity of the wind, sediment supply, and sediment availability (Kocurek and Lancaster, 1999). An increase in sediment availability, for example, instigates sand mobilization and the formation of dunes. Meanwhile, a decrease in sediment availability results in a decrease in dune field area and an increase in dune stability (Lancaster, 2009). These three primary factors are driven by alterations in climate, vegetative coverage, and sediment source (Lancaster, 1995). By identifying when past changes in dune activity occurred, one can infer that a change to any of these factors may have resulted in the change seen in dune activity. Developing accurate chronologies documenting periods of formation and stabilization leads to an

understanding of the regional evolution of an aeolian landscape by using aeolian features as indicators of past changes in climate.

Numerous chronometric dating techniques have been developed to date sediment, radiocarbon being among the most widely used; however, problems arise with radiocarbon dating when insufficient organic material exists within the sediment, which is typically the case with aeolian sand deposits. Accordingly, the application of a non-carbon-based dating method is often needed. In the mid-1980s, significant advances in the field of particle dating resulted in the technique of luminescence dating, which enabled aeolian deposits to be dated directly. Luminescence dating greatly enhanced the capabilities for building more precise chronologies of aeolian landforms and extended the dating range capabilities from around 50,000 years via radiocarbon dating to greater than 1,000,000 years, in some cases, with luminescence dating (e.g., Pickering et al., 2013; Arnold et al., 2014). Since its debut, luminescence dating continues to expand the capabilities of sediment dating and has been extensively used for determining the chronologies of aeolian landforms.

Luminescence dating estimates the time since a sediment grain was last exposed to light and provides the time of burial of the sediment, or dune formation, in the case of aeolian sand (Aitken, 1998; Huntley and Lamothe, 2001). The method measures the natural buildup of radiation over time that is contained within sediment crystal lattices and is based on the concept that the luminescence signal is reset, or "bleached," when the sediment grains are exposed to sunlight or heat (Aitken, 1998). Luminescence dating is an ideal dating method for aeolian sediment because it is a form of absolute dating, rather than relative dating, in that it directly dates periods of aeolian activity. Another advantage of using luminescence dating with aeolian deposits is that it requires ample sediment exposure to sunlight, which aeolian grains typically

experience during wind transport. Additionally, luminescence analysis generally uses quartz or feldspar grains, which are abundant in most aeolian deposits. Luminescence dating has been used to study aeolian systems across Europe, North America, and Asia but much remains to be studied in some of the most critical areas of concern with current climate change.

High-latitudes areas, such as Alaska, are particularly sensitive to changes in climate. While geomorphic system processes that link high-latitude ecosystem responses to climatic changes are not fully understood, moisture is suggested to play an important role within these regions (Hinzman and Kane, 1992). Within interior Alaska, permafrost is prevalent (Péwé, 1965), and changes in temperature can cause flux in depth to permafrost, which directly affects sediment availability. Despite the importance of understanding past responses of landscape features within critical areas like Alaska, sediment dating, particularly of sand dunes, within the high-latitude region remains understudied throughout most of Alaska. Part of this has to do with difficulty of access: in addition to being remote, many interior dune fields are located within marshy lowlands and are not easily accessible by foot or all-terrain vehicles. But even in those areas with access, a lack of viable dating techniques has contributed to the paucity of chronostratigraphic Alaskan dune studies.

In Alaskan aeolian settings, the most frequently used methods of radiocarbon dating and Optical Stimulated Luminescence (OSL) are rarely possible due to insufficient organic material and a weak luminescence signal, respectively. Quartz grains are typically used in luminescence studies; however, in some glaciogenic and neotectonic regions the quartz minerals show a weak luminescence signal that is hard to measure (Pietsch et al., 2008; Rhodes, 2011). Luminescence studies have documented low quartz OSL sensitivity in areas including the Himalaya region (Rhodes and Pownall, 1994), the New Zealand Alps (Preusser et al., 2006), and Peru (Steffen et

al., 2009). While this phenomenon remains understudied, the cause of the weak signal is currently attributed to a short lifetime of the sedimentary particles (i.e., inadequate 'sediment cycling'), which relates to a lack of "traps" in the mineral crystal structure. Similarly, OSL dating of quartz minerals found within aeolian deposits of Alaska and western Canada has yielded dim luminescence signals (Munyikwa et al., 2011; Johnson et al., 2012; Reuther, 2013). In such cases, feldspar grains can be dated using Infrared Stimulated Luminescence (IRSL) dating, but have been avoided in the past due to the inherent signal fading, or 'leaking' of stored radiation that often occurs. This anomalous fading (Wintle, 1973) often affects IRSL samples, and, if unaccounted for, can result in ages that are too young for the sediment being dated.

Because of these complications, luminescence dating of interior Alaskan dunes has remained extremely limited. Several attempts have been made to calculate and account for the effects of anomalous fading (e.g., Huntley and Lamothe, 2001; Auclair et al., 2003; Thomsen et al., 2008), including a recent protocol from Buylaert et al. (2009) that uses post-IR (pIR) IRSL analysis in an effort to limit the effects of anomalous fading. Roberts (2012) tested the potential of using this p-IR protocol to date loess deposits near Fairbanks, AK, and yielded IRSL ages in agreement with independent age control. Because of this success dating central Alaskan loess deposits, the pIR protocol was tested on a limited number of samples from sand dune deposits of the Wood River dune field within central Alaska (Johnson et al., 2012). Both studies serve as impetus for this research to continue testing the potential of a p-IR protocol to expand aeolian research within central Alaska.

This research investigates the chronology of dune deposits within the Nenana dune field of central Alaska using a pIR IRSL protocol (following Buylaert et al., 2009). Specifically, the sampling strategy aims to capture maximum- and minimum-limiting ages of aeolian activity

within the dune field. The Nenana dunes are proximal to the Wood River dune field, where the p-IR protocol has previously been deemed successful during an initial exploratory study (Johnson et al., 2012). This research serves to address the following objectives: (1) to determine maximum- and minimum-limiting ages of aeolian activity and stabilization of the Nenana dune field; (2) to further test the use of a post-IR IRSL protocol for capturing aeolian activity within the Nenana dune field; and (3) to discuss the resulting luminescence ages within a paleoenvironmental context using regional proxy data.

Resulting Nenana ages will be reviewed in relation to the aeolian activity of the proximal Wood River dune field during the initial exploratory study (Johnson et al., 2012), as well as aeolian activity recorded elsewhere in central Alaska and northwestern Canada in order to place the Nenana aeolian activity within a regional context. This research also includes a broad discussion of the timing of Nenana dune activation and stabilization within a paleoenvironmental context, referencing regional proxies primarily related to aeolian activity, but also including records pertaining to pollen levels, lake levels, vegetation changes, as well as paleoclimatic conditions.

Better understanding of timing of aeolian activity in TRL and paleoenvironmental conditions surrounding changes to the landscape can provide helpful information about understanding linkages between geomorphic systems, such as glacial, fluvial, and aeolian systems, that dominate within central Alaska. For example, aeolian chronologies provide periods of sediment transport and subsequent deposition that are linked to changes in transport capacity (i.e., wind) and sediment supply and availability (Kocurek and Lancaster, 1999). This relationship occurred during glacial retreat with an influx of sediment into glaciofluvial and subsequently aeolian systems as a response to the change in glacial system. In a broader sense,

current GCMs have predicted future warming of these areas (Dyke et al., 2003) that will likely cause changes to the landscape. Given the sensitivity of these high-latitude regions to climatic changes, chronological studies of Alaska are important for understanding possible implications of future changes.

Luminescence dating has already advanced aeolian studies globally through its robust capabilities, and the continued development of luminescence techniques would allow for further dating of aeolian deposits within central Alaska. Development of luminescence techniques is particularly important where the use of other dating techniques, including OSL and radiocarbon dating, are not viable. Where quartz suffers from low sensitivity, as has been observed in glaciogenic regions, feldspar dating can provide an alternative (Lukas et al., 2012). Success in the use of dating feldspars using a pIR IRSL protocol would also serve as impetus for use in other high-latitude aeolian settings globally that face similar issues. This research is significant in its novel approach and serves as a starting point for more research of its kind in Alaska and other aeolian sand environments where dating methods previously have been limited.

Finally, central Alaska, and specifically the Nenana and Tanana river valleys, have proven to hold a wealth of information regarding the earliest peopling of Alaska and North America. The earliest evidence of human occupation in North America occurred during the transition from the Late Pleistocene to early Holocene within central Alaska, which coincided with widespread aeolian activity of the region. Determining information regarding aeolian sand dune chronologies for the remaining aeolian deposits can provide useful information regarding the timing and extent of human occupation and association with aeolian environments throughout central Alaska, as well as possible insight for future researchers into use of aeolian

landscapes for prehistoric peoples (e.g., hunting lookouts), proximity to resources, and timing of inhabitance.

The significance of aeolian research within the Arctic region is substantial in relation to understanding paleoenvironmental conditions and the relationships between geomorphic systems. This research aims to expand what limited information is known about the isolated deposits of the Nenana dunes within the TRL. Use of a pIR protocol makes this research one of the first to use IRSL dating on sand dune deposits of central Alaska in light of past difficulties. Success in dating the Nenana dunes could lead to an increased use of luminescence dating in a region where researchers are only beginning to understand the complexities of the timing of past aeolian activity and its relationship with paleoclimatic conditions. Additionally, chronological information regarding the formation and stabilization of the Nenana dunes would prove useful for expanding archaeological studies within an area that has already recognized as rich in potential for learning more about the earliest prehistoric occupations of North America.

Chapter 2 Background

2.1 Aeolian Deposits of Northwest North America

The following introduces the primary aeolian deposits throughout Alaska and western Canada (including the Yukon, Northwest Territories, and Alberta) and provide notable examples of studies focusing on these aeolian deposits. This section of the background will close with a discussion of the timing of regional aeolian activity of central Alaska and northwest Canada during the Late Pleistocene and early Holocene within a paleoenvironmental context.

Aeolian deposits, including sand dunes, sand sheets, and loess, are prevalent throughout Alaska (Péwé, 1975; Hopkins, 1982) (Fig. 2.1). During the last glacial period, 30,000 km^2 of northern Alaska were comprised of aeolian sand sheets and dunes (Hopkins, 1982; Lea and Waythomas, 1990). Aeolian sands and silts span most of the unglaciated portions of Alaska, concentrated in most of the lowland areas and on some uplands proximal to streams draining formerly glaciated uplands (Black, 1951; Hopkins, 1982). Some of the primary aeolian deposits consist of the Great Kobuk Sand Dunes (GKSD) and Little Kobuk Dunes of the Kobuk Valley, the Arctic Coastal Plains in northern Alaska, the vast Kantishna sand sea, and extensive loess deposits prevalent throughout central Alaska.

Northern and central Alaskan aeolian deposits have received the majority of attention (Lea, 1990), likely due to the extent of the GKSD and the presence of extensive loess deposits near Fairbanks that have been researched in great detail (Péwé, 1975; Muhs et al., 2003). Partially stabilized dune fields in central and northern Alaska cover more than 30,000 km^2 (Péwé, 1975; Hopkins, 1982). Within central Alaska, aeolian deposits include the Nogahabara

dunes in the lower Koyukuk Valley, the Kantishna sand sea, and those within the Nenana and Tanana river valleys.

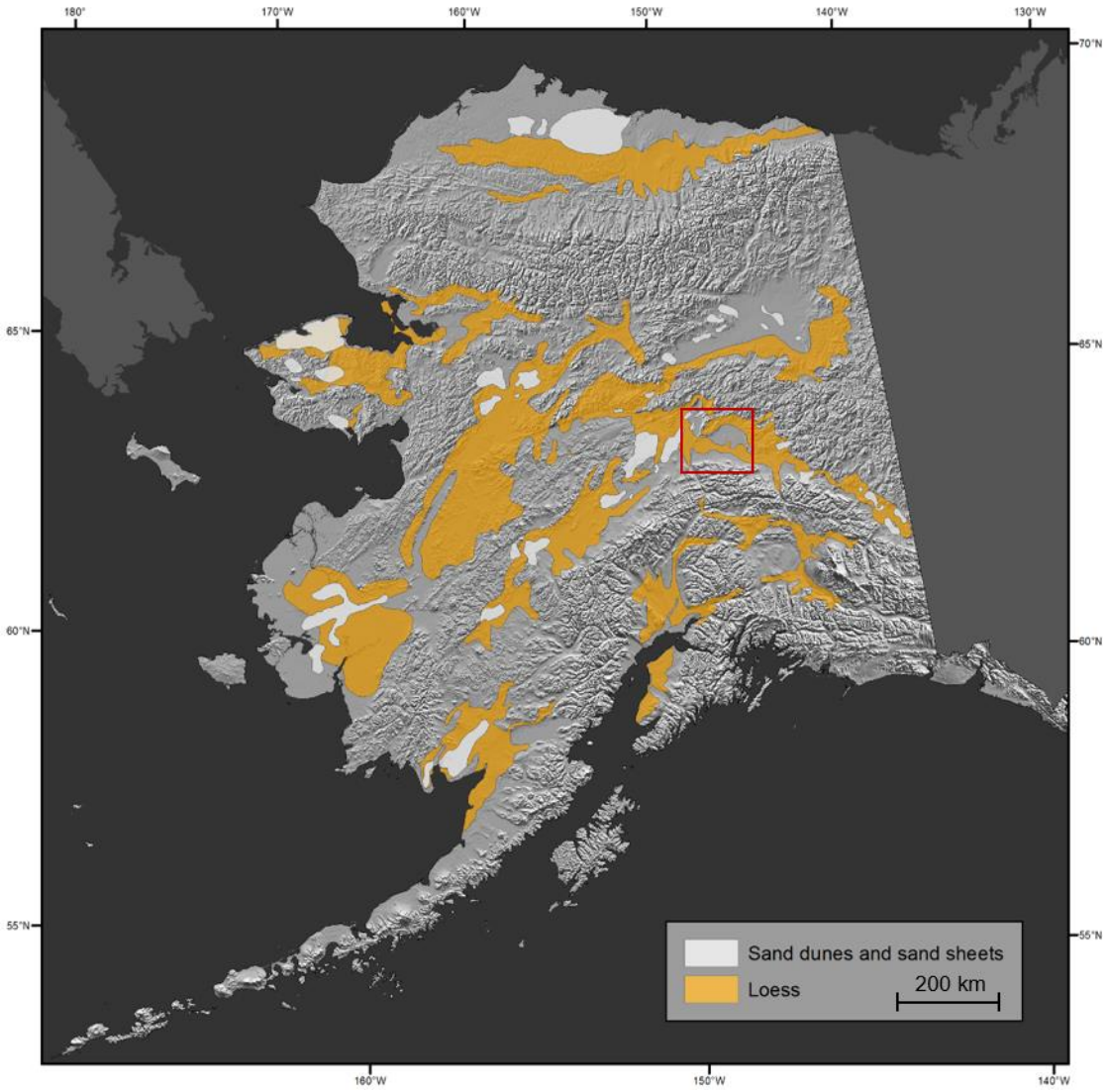

Figure 2.1. Expanse of aeolian deposits of Alaska. Red box indicates study area (data from Wolfe et al., 2009).

The Fairbanks loess belt is comprised of several widespread loess deposits located near Fairbanks, notably the Gold Hills loess (Péwé, 1975) (Fig. 2.2). Since Péwé's initial surficial mapping (1955), Alaskan loess deposits have served in numerous studies, including stratigraphic studies (e.g., Muhs et al., 2003), magnetism (e.g., Vlag et al., 1999; Lagroix and Banjeree, 2002,

2004; Jensen, 2013), and chronological studies using primarily radiocarbon dating and some thermoluminescence (TL) and infrared stimulated luminescence (IRSL) dating of the loess straddling the Old Crow tephra (Westgate et al., 1990; Preece, 1991; Preece et al., 1999) found near Fairbanks (e.g., Berger et al., 1994, 1996). These locations are useful in that they are relatively continuous deposits that contain paleosols and several tephra beds that have been dated back to 142 k cal yrs BP (Berger, 2003).

Figure 2.2. Expansive Gold Hills loess bluffs. These exposures are located approximately 3 km west of Fairbanks along the Parks Highway (Route 3) and extend more than 20 m above the highway (Photographs: W. Johnson and C. Messner).

In northern Alaska, the Alaskan Arctic Coastal Plain consists primarily of stabilized longitudinal, parabolic, and multi-cyclic dunes that cover approximately 12,950 km^2 west of the Colville River (Black, 1951). Loess has been identified along the lower Colville River varying in depths of up to a few meters, but it is believed to be extensive throughout northern Alaska (Black, 1951). Ages of most of the Coastal Plain aeolian features are unknown but are believed to have been formed in a warmer climate (Carter and Robinson, 1978). Smaller aeolian ridges occur south of the coastline, including the Kealok Creek exposure believed to be Holocene in age (Carter and Robinson, 1978). The coastal plain, an area of oriented lakes and dunes, is favorable for aeolian activity due to high winds, low relief, and an abundance of sand and silt, but permafrost and vegetation currently hinder complete aeolian activation (Black, 1951). The Kobuk Valley of northwest Alaska consists of about 650 km^2 of primarily stabilized aeolian sand deposits (Fernald, 1964; Hamilton et al., 1984). The GKSD extend for 62 km^2, and the Little Kobuk dunes cover an area of 8 km^2, and both dune fields are active (Dijkmans and Koster, 1990). Silt and sand deposits of the central Kobuk Valley were derived mainly from sandy till and glacial outwash redeposited by glaciolacustrine, alluvial, and aeolian processes following the Pleistocene glaciations (Dijkmans and Koster, 1990). The GKSD were previously more extensive than they are today (e.g., Fernald, 1964; Hamilton et al., 1984), with episodes of expansion, inactivity, and a subsequent reduction in size throughout the Holocene, a trend controlled largely by changes in effective moisture (Mann et al., 2002).

In southwestern Alaska, Pleistocene aeolian sand sheet deposits and sand-loess intergrades are exposed within the Nushagak, Holitna and Kuskokwim lowlands (Lea, 1990). These areas served as depositional basins during the Pleistocene glaciations and were primarily sourced by sand and silt deflating from the Kuskokwim and Nashagak River floodplains (Lea,

1990). In these lowlands, the presence of sand sheet deposits, rather than dune deposits, was attributed to a limited availability of loose, dry sand necessary for dune development caused by a combination of ice, sparse vegetation, high water tables, and snow cover (Lea, 1990).

In Canada, the northern Great Plains are the largest extent of aeolian deposits, covering over 40,000 km^2 across Alberta, Saskatchewan and Manitoba (Halfen et al., 2015). Aeolian deposits also occur within the Yukon (e.g., Wolfe et al., 2011), Northwest Territories (Bateman and Murton, 2006; Murton et al., 2007) and Alberta (e.g., Muhs and Wolfe, 1999; Wolfe et al., 2004, 2007). While aeolian deposits of the northern Great Plains have been mapped and studied, Wolfe et al. (2011) recognized the lack of information regarding the extent and significance of aeolian deposits within the Yukon Province, and they provided a first attempt at mapping the aeolian deposits of central and southern Yukon, which consist of inland sand dunes, sand sheets, lakeshore and riverside dunes, and cliff-top aeolian deposits, including loess. Using IRSL analysis, Wolfe et al. (2011) concluded that the Whitehorse and Rusty Creek dune fields both indicate maximum-limiting ages of stabilization between 9 ka and 8.5 ka. Stabilization is attributed to the spread of boreal forest between 10 ka and 9 k cal yrs BP (Ager and Brubaker, 1985; Dyke, 2005) and coincides with cooler, moister climatic conditions following the Holocene Thermal Maximum (HTM) (Wolfe et al., 2011).

Sand dunes of Alberta primarily consist of parabolic and some transverse dunes (David, 1977; Wolfe et al., 2004; Munyikwa et al., 2011). The majority of dunes are currently stabilized and are shown to have been active between 15 ka and 14 ka through luminescence dating of quartz and feldspar grains taken from the top portions of dune stratigraphy (Wolfe et al., 2004; Munyikwa et al., 2011). Dune stabilization occurred in a time-transgressive manner from central Alberta into northeastern Saskatchewan following the establishment of boreal forest after ~11.4

ka (Dyke et al., 2004) and decreased wind strength and do not suggest subsequent reactivation (Wolfe et al., 2004). In contrast, some dunes of the southern Canadian prairies, experienced periods of reactivation during the mid-Holocene (e.g., Muhs and Wolfe, 1999; Lian et al., 2002; Wolfe et al., 2004).

Within the Tuktoyaktuk Coastlands of the Northwest Territories, luminescence dating was used to establish aeolian activity spanning 30–8 ka across the same area (Bateman and Murton, 2006; Murton et al., 2007). Subsequently, the landscape transitioned from dune to sand sheet aggradation until stabilization after ~8 ka that resulted from a climatic transition from cold, arid conditions to cooler, moister conditions (Bateman and Murton, 2006). In turn, cooler, moister conditions led to a change from herb tundra to shrub tundra vegetation (Dyke, 2005).

While many of the aeolian deposits of western Canada are separated geographically from central Alaska (e.g., northern Great Plains), similarities exist between the timing of aeolian activity due to comparable geomorphic influences on aeolian systems of Alaska and Canada. For example, the timing of aeolian activity within the boreal forest zone of the northern Great Plains is closely tied to the retreat of the Laurentide Ice Sheet (Wolfe et al., 2004; Munyikwa et al., 2011). Halfen et al. (2015) constructed a conceptual sediment-state history of the boreal dune fields of Canada that highlights periods of high to low potential for dune building within the context of sediment availability, supply, and transport capacity that are widely accepted as the three deciding factors of the aeolian sediment state model (Kocurek and Lancaster, 1999). The conceptual model indicates a phase of influx of sediment supply along the margins of proglacial lakes immediately and contemporaneously following deglaciation (16–13 ka). A lagged influx of sediment supply sustained dune activity following the retreat of the Laurentide Ice Sheet to the east, but was initially influenced by limited sediment availability during a shift to tundra-shrub

vegetation and replacement of glacial winds by the Pacific air mass (~13 to 11 ka). Aeolian activity became limited by sediment availability and transport capacity beginning around 9 ka and extending through the present, which culminated in vegetated, stabilized dune fields throughout the boreal ecozone of western Canada (Halfen et al., 2015).

2.1.1 Summary of Regional Aeolian Activity

While some areas exhibit aeolian activity within central Alaska prior to the LGM, (e.g., Hopkins, 1982; Muhs et al., 2003), the majority of regional aeolian activity within central Alaska and western Canada during the Late Quaternary seems to have occurred between the Last Glacial Maximum (25–20 ka) and the beginning of the Holocene Thermal Maximum (11 ka). Research pertaining to regional aeolian activity (i.e., within central Alaska and northwest Canada) is discussed within the context of current proxies and paleoenvironmental conditions.

2.1.1.1 Last Glacial Maximum (25 to 20 ka)

The LGM (25–20 ka) in central Alaska was characterized by cold, dry, and windy conditions (Hopkins, 1982; Thorson and Bender, 1985). Glacial conditions led to significant changes of the landscape of interior Alaska, as large amounts of silt and sand were produced by massive alluviation occurring as rivers were choked with glacial sediment (Reuther, 2013). The glacial landscape created strong katabatic winds blowing off of the ice that may have helped create higher aridity within the region (Thorson and Bender, 1985; Bateman and Murton, 2006).

Though there was an abundance of sediment produced during the LGM, sediment availability for aeolian activity remained somewhat restricted, likely due to factors including a permafrost-dominated landscape, snow cover, and an increase in groundwater levels (Lea and

Waythomas, 1990). Radiocarbon ages suggest the limited sediment supply primarily resulted in sand sheet deposition during the LGM, rather than sand dune formation (Lea and Waythomas, 1990), although there is some evidence of dune formation occurring between 25 k cal yrs BP and 16 k cal yrs BP in the Shaw Creek Flats area and Upward Sun River Site (USRS) terrace (Reuther, 2013). Similarly, dune building within the central Kobuk Valley of northwest Alaska occurred beginning ~24 k cal yrs BP was attributed to an abundant sediment supply from glacial erosion and river alluviation of the Kobuk River (Hamilton et al., 1984, 1988; Dijkmans and Koster, 1990). The majority of aeolian activity, however, seemed to occur throughout interior Alaska and western Canada during the transition out of the glacial period and into the interglacial phase.

2.1.1.2 Late Glacial Transition (16 to 11 ka)

Transition between the Late Glacial and early Holocene periods was marked by significant environmental change within interior Alaska and the surrounding areas. The Pleistocene deglaciation spanning 16.6 ka and 11.6 ka was accompanied by warmer temperatures and increased moisture (Hopkins, 1982; Edwards et al., 2001). Deglaciation included the retreat of the Laurentide Ice Sheet and Cordilleran Ice Sheets, which released massive amounts of freshwater into the ocean and brought about ~30-m rise in sea level between 18 ka and 15 ka (Manley, 2002). As the ice sheets melted, the regional air masses shifted, bringing increased moisture to interior Alaska as moist, coastal air masses were no longer blocked by the ice. Shifting air masses brought about changes in paleowind directions in the area during the Late Pleistocene and early Holocene (Anderson and Brubaker, 1994; Bartlein, 1997).

Deglaciation also brought the influx of glaciofluvial sediment into the braided stream systems feeding into the surrounding Nenana and Tanana floodplains (Fig. 2.3). Warmer temperatures and deeper thaws increased sediment supply during the Late Pleistocene to Early Holocene transition, and aeolian activity appears to have been widespread during this phase across Alaska and western Canada (e.g., Dilley, 1998; Wolfe et al., 2004, 2011), possibly as a result of this increased sediment supply. Within the Tanana River Lowlands (TRL), Wood River luminescence ages indicate that dune formation occurred as long ago as ~15.5 ka and likely continued until ~9.6 ka (Johnson, et al., 2012).

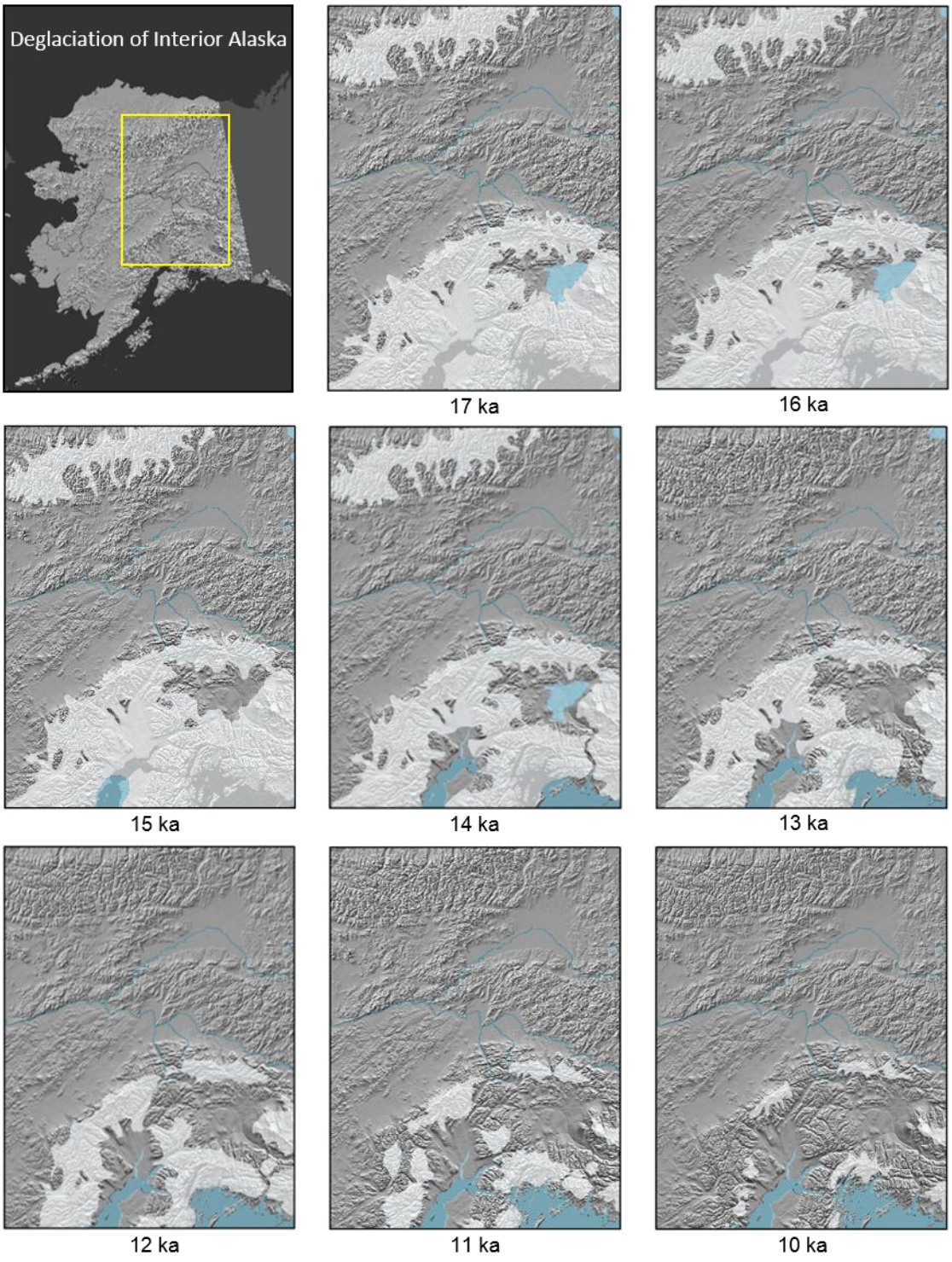

Figure 2.3. Deglaciation of interior Alaska between 17 ka and 10 ka (data from Dyke et al., 2003).

There remains some discrepancy regarding paleowinds during this time of widespread aeolian activity across the TRL. Péwé (1965) hypothesized that winds during the Late Glacial were coming from the southwest. Based on shape, orientation, and distribution of the dunes throughout the Kantishna sand sea that date to ~11 k cal yrs BP (Lea, 1996), Collins (1985) argued that winds from the northeast must have formed the dunes. However, the loess north of Fairbanks, which Muhs and Budahn (2006) identified as primarily sourced from the Tanana River, is believed to have formed during the Late Glacial or early Holocene and would have required winds from the southwest in order to deflate aeolian silt from the Tanana River into the uplands. As the ice sheets retreated, it is possible that katabatic winds originating from the Alaska Range to the south could have been responsible for depositing the Fairbanks loess (Thorson and Bender, 1985; Muhs and Budahn, 2006). While the exact orientation of paleowinds during the Late Glacial remains unknown, evidence exists for both northeasterly winds forming the Kantishna sand sea to the west of the Nenana River, and southerly winds forming the Wood River and Fairbanks loess deposits within a similar timeframe. This enigma could result from localized differences in paleowinds affecting the TRL and the Kantishna valley. For example, differences in wind intensity or a combination of northerly winds with opposing katabatic winds could have affected these areas of central Alaska. This prompts further study of the timing of aeolian activity throughout the TRL, as well as further paleowind and sourcing research in order to better understand the complicated nature of these periglacial landscapes.

Around 14 ka, proxy data indicate wetter and potentially warmer conditions (Finkenbinder et al., 2014). A rise in lake levels suggests that ~14–13 ka experienced increased effective moisture and warmer temperatures (Abbott et al., 2000; Bigelow and Edwards, 2001; Graf and Bigelow, 2011). The vegetation also experienced a shift from herb-tundra vegetation

around this time, which had previously dominated the central Alaskan landscape, to a prevalence of shrub-tundra, dominated by birch (Bigelow and Powers, 2001; Anderson et al., 2004; Graf and Bigelow, 2011). Several radiocarbon records from multiple archaeological sites within the Tanana and Nenana river valleys date artifacts found within loess profiles at 14–11 k cal yrs BP, which supports evidence for aeolian activity occurring during the Late Pleistocene to early Holocene transition period (e.g., Holmes, 1996, 2001; Holmes and Dilley, 1996; Potter et al., 2008, 2011, 2014; Graf and Bigelow, 2011; Esdale et al., 2012;).

The Younger Dryas (YD) Chronozone (12.8–11.7 ka) is characterized as a cooling event that is expressed in some studies throughout Alaska and northern Europe (Bigelow and Edwards, 2001; Bigelow and Powers, 2001; Kokorowski et al., 2008). In general, the effects seemed to be more strongly expressed south of the Alaska Range than in central Alaska, which was suggested to be a result of cool, moist air being blocked from central Alaska by the Alaska Range (Bigelow and Edwards, 2001). Overall, proxy data indicating significantly cooler and drier temperatures during the YD are coarse in resolution, so speculation remains as to whether significant changes were felt in central Alaska (Graf and Bigelow, 2011). Overseas, increased aeolian activity was recorded in northern Europe during the YD (Bigelow and Edwards, 2001).

2.1.1.3 Holocene Thermal Maximum (11 to 8 ka)

YD cooling was followed by the Holocene Thermal Maximum (HTM), reaching central Alaska ~11 ka. An increase in summer insolation (Berger, 1978) produced warming throughout central Alaska, though the strength and exact timing of the HTM varied throughout the western Arctic (Kaufman et al., 2004). Lake levels in the southern Yukon suggest a rapid increase in lake level from 10–9 ka (Kaufman et al., 2004). In central Alaska, lake levels also increased at Birch,

Jan, and Dune lakes (Bigelow, 1997; Abbott et al., 2000; Barber and Finney, 2000). Pollen records from several lakes in central Alaska indicate a brief expansion of *Populus* occurring 11–9 k cal yrs BP (Graf and Bigelow, 2011). Similarly, the expansion and establishment of *Picea* (spruce) throughout Alaska and the Yukon ~10 k cal yrs BP or thereafter, as evidenced from pollen records (e.g., Ager, 1983; Ager and Brubaker, 1985; Bigelow and Powers, 2001; Muhs et al., 2003; Dyke 2005). Dune fields throughout the Yukon, southwest Alberta, and northeast Saskatchewan seemed to stabilize in a time-transgressive manner ~11 ka in the southwest to ~9 ka in the northeast as a result of the expansion of the boreal forest throughout the region (Wolfe et al., 2004, 2011; Bateman and Murton, 2006).

2.2 Luminescence Dating

2.2.1 Basics of Optical Luminescence

Luminescence dating is a technique based on the accumulation of radiation within sediment following deposition (Fig. 2.4). Once sediment is buried, it is "dosed," or exposed to, levels of radiation from the surrounding sediments and a small portion from sunlight dosing (Aitken, 1998). This ionizing radiation consists of alpha and beta particles, as well as gamma rays, which are emitted during the decay of radioactive isotopes and cosmic rays. The gradual dosing occurs as electrons become trapped within structural defects or impurities within the crystal lattice of the mineral. For example, electron traps can form where elemental substitution occurs, such as Ti replacing Si in quartz minerals (Rhodes, 2011). These electron traps continue to fill over time until eventually saturation can be reached, which is the point at which all electron traps have been filled (Rhodes, 2011). The point of saturation is dependent upon the mineral; in general, saturation for quartz sediments occurs more quickly than for feldspar

sediments (Wintle, 1993). This favors the use of feldspar grains to extend the age range of particle dating using luminescence.

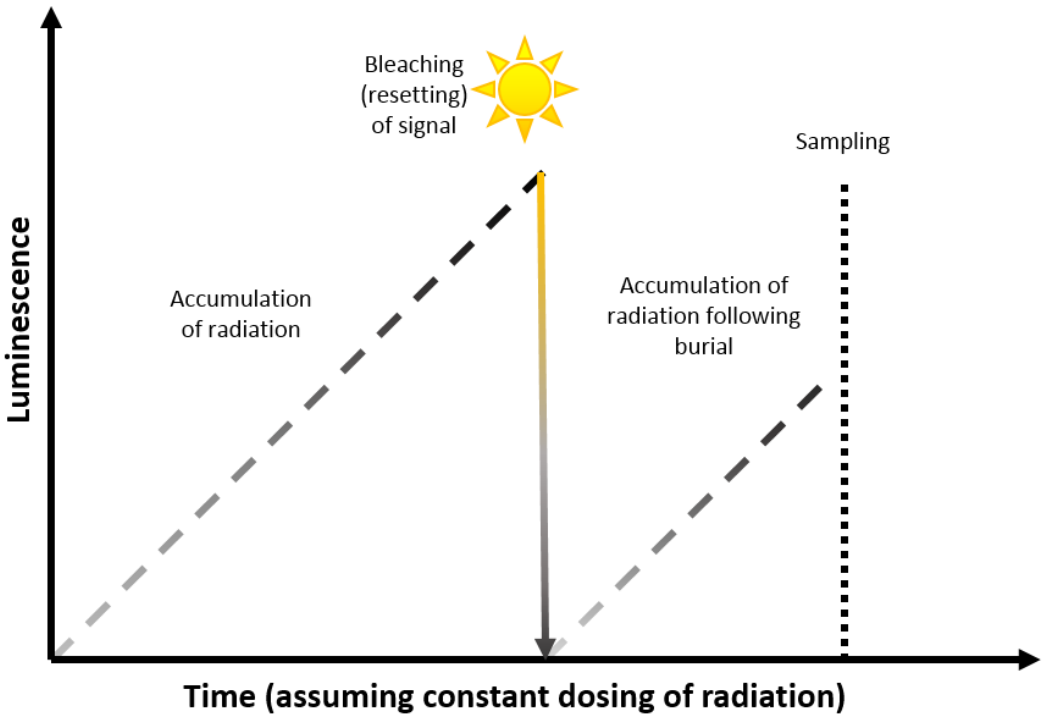

Figure 2.4. Generalized depiction of luminescence principles of the build-up and resetting of a luminescence signal from radiation dosing.

Electron traps can be released through exposure to heat or light ("zeroing," or "bleaching"), which is essentially a resetting of the electron traps and stored radiation (Aitken, 1998). The amount necessary for all traps to be released varies between minerals, but ranges in the magnitude of 10–100 seconds (Rhodes, 2011). For example, bleaching occurs for aeolian sediment as the grains are exposed to sunlight during wind transport. Once the grains have been deposited in a dune, bleaching occurs when the dune becomes active and grains that were previously buried are exposed to sunlight. Because luminescence dating measures the buildup of radiation over time, it is imperative that sediment grains were fully bleached prior to deposition (i.e., received sufficient sunlight exposure to empty electron traps). Inadequate emptying of

electron traps, known as partial bleaching (Stokes, 1999), leads to an overestimation of sample age and is discussed in a subsequent section.

Several minerals are known to visibly luminesce when exposed to optical or heat stimulation, though quartz and feldspar grains are most commonly used given their ubiquity in most terrestrial environments (Aitken, 1985, 1998). These two minerals have structural differences that control their abilities to effectively trap and release radiation, altering their sensitivity to luminesce and producing variations in signal brightness and bleaching capabilities (Rhodes, 2011). For example, quartz minerals have been shown to bleach more quickly than feldspar minerals (Godfrey-Smith et al., 1998; Wintle and Murray, 2006), which increases the likelihood of complete bleaching prior to deposition. However, quartz minerals tend to saturate at relatively low doses of radiation (e.g., 200 to 400 Gy), which limits the capabilities of using quartz for luminescence samples older than ~200 ka (Rhodes, 2011). Additionally, it has been shown that quartz minerals extracted from geologically 'younger' sedimentary deposits can suffer from low luminescence sensitivity (e.g., Rhodes and Pownall, 1994; Lian et al., 2002; Preusser et al., 2006, 2009; Fuchs and Owen, 2008; Munyikwa et al., 2011). Pietsch et al. (2008) measured sensitivity at several locations along a stream in New South Wales and found that sediment closer to the headwaters exhibited a lower luminescence sensitivity than sediment further downstream. They concluded that downstream transport provides numerous cycles of irradiation and bleaching, which in turn increases the luminescence sensitivity of quartz (Pietsch et al., 2008). On the contrary, feldspars produce a brighter luminescence signal by an order of magnitude greater than for quartz minerals (Aitken, 1998), allowing for higher precision luminescence measurements (Li et al., 2007, 2014). The disadvantage of using feldspar grains,

however, is the inherent possibility of luminescence signal fading that results in an underestimation of age if unaccounted for (e.g., Rhodes, 2011).

Signal fading, referred to as "anomalous fading" (Wintle, 1973), describes the release, or "leaking," of some of the electron traps over time. Many researchers believe that anomalous fading affects all feldspar samples (e.g., Huntley and Lamothe, 2001), while others have argued that fading is dependent upon the luminescence properties of feldspars and/or user methodologies (e.g., Preusser et al., 2005). Given the advantages of using feldspars for luminescence dating, anomalous fading remains one of the largest hindrances to the forward advancement of dating feldspars (Roberts, 2012).

2.2.2 Optical Luminescence Age Determination

Luminescence age determination relies on the relationship between two components, the equivalent dose and the dose rate. These two values are determined by independent procedures for which a variety of techniques and their associated advantages exist (summarized by Aitken, 1998). The equivalent dose and dose rate values are then combined to determine the time elapsed since sediment burial (i.e., the age of a landform since deposition). The purpose of this section on age determination is to provide a brief overview of luminescence analysis; the specific techniques used for this research and the reasoning behind them are discussed within Chapter 4, which includes the age determination equation and description of procedures.

A sample's equivalent dose represents the total radiation energy accumulated within particle grains since the last exposure to sunlight, known as a bleaching event. The equivalent dose value is determined within the laboratory by irradiating samples with known doses of radiation and comparing the intensity of the resulting luminescence signal to the natural

luminescence signal in order to determine the relationship between radiation energy and luminescence. As a whole, equivalent dose determination consists of a series of heating, irradiating, and measuring of luminescence signals. A sample's dose rate represents the radiation dose per unit time received by the particles grains within the sample while buried. The dose rate is dependent upon several factors that influence the amount of radiation received through cosmic dosing and the surrounding environment, including elevation, sediment depth, density, age, and water content (Aitken, 1985). Cosmic dose contributions are typically calculated using the equations of Prescott and Hutton (1994), and elemental (environmental) dose rate contributions can be measured in situ during collection (i.e., in the field) using a portable spectrometer, independently using high-resolution gamma mass spectrometry, or inductively coupled plasma-mass spectroscopy (ICP-MS) and -atomic emission spectroscopy (ICP-AES).

2.3 Applications and Developments of Luminescence Dating

2.3.1 Applications of Luminescence Dating

While its introduction as a dating technique has been fairly recent, luminescence dating has been used for a variety of sediments, including those of aeolian, volcanic, fluvial, and glacial deposits. Extensive reviews of sediment types and the corresponding uses of luminescence dating can be found in Prescott and Robertson, 1997, Lian and Roberts, 2006, Bateman, 2008, Rittenour et al., 2008, and Rhodes, 2011.

The widespread use of luminescence dating over its relatively recent past speaks to its advantages over other chronometric dating techniques, specifically the commonly used technique of radiocarbon dating. Radiocarbon dating requires sufficient organic material for analysis, which can be hard to find in environments where organic material is often limited or absent, such

as high-latitude aeolian environments where decomposition rates are slow (Bateman and Murton, 2006). Where organics are found, there is often uncertainty regarding whether the organic material is detrital, or if some of the material has been recycled from older carbon. In high-latitude areas where permafrost limits decay, there is a high potential for organic preservation and thus a higher chance of recycling organics (e.g., Nelson et al., 1988; Bateman and Murton, 2006). Another advantage of luminescence dating is that it extends the age range significantly for dating sediment. Optical luminescence is widely used for dating sediment less than a decade in age ranging up to 200,000 years, with recent research indicating potential for greater than 1,000,000 years (Pickering et al., 2013; Arnold et al., 2014), whereas radiocarbon dating has generally been found useful for dating organic material ranging from a few hundred years to ~50 ka (Lian and Roberts, 2006). Luminescence dating can help provide researchers with a more complete past extending back many years, with the potential of providing sediment or landform ages throughout the whole of the Quaternary period.

2.3.1.1 Luminescence Dating of Aeolian Sediment

Luminescence dating has been used for determining numerous chronologies of aeolian sediment and was first used in India, where TL was applied for the dating of aeolian sand deposits (Singhvi et al., 1982). Within North America, Forman and Maat (1990) used TL dating to develop the first luminescence chronology on dunes within of the Central Great Plains. Since these initial studies, researchers have worked globally to document Pleistocene and Holocene sand-dune and loess stratigraphies (see Wintle, 1993; Rhodes 2011). Aeolian-based luminescence studies have been shown to provide a variety of information about past environmental or climatic conditions, including changes in paleowind direction or intensity (e.g.,

Bigelow et al., 1990) and timing of dune stabilization in relation to changes in vegetative cover (e.g., Wolfe et al., 2011). Luminescence dating is particularly well suited for dating aeolian environments for several reasons, including the abundance of quartz and feldspar grains, the preferred minerals used in luminescence dating, within aeolian deposits. Additionally, aeolian grains normally receive adequate exposure to daylight during wind transportation, which is necessary for producing accurate luminescence ages. Lastly, luminescence dating serves as a viable option where radiocarbon dating is not possible due to a lack accumulated organic material and or organic material that does not represents a direct measurement of aeolian activity.

2.3.2 Limitations of Luminescence Dating

As with any chronometric dating technique, limitations to luminescence dating do exist, and, if unaccounted for, can result in under- or overestimated predictive ages. One of the assumptions of luminescence dating is that the sediment grains are fully bleached before their burial upon deposition, meaning that electron traps were emptied during transport. Length of sunlight exposure and the intensity of sunlight are environmental factors that affect the extent to which electron are released from traps (Rhodes, 2011). These factors are determined by the method of sediment transport leading up to deposition and latitude determines intensity of sunlight. Inadequacies of either factor lead to partial bleaching, in which traps are only partially emptied prior to deposition and results in an age overestimation. Partial bleaching has been shown to be particularly problematic for sediment within glacial and periglacial environments (Prescott and Robertson, 1997; Bateman, 2008; Fuchs and Owen, 2008), where fluvial transport often occurs in deep or muddy water or sediment carried within or beneath glacial ice (Prescott

and Robertson, 1997). Conversely, aeolian sediment has a higher probability of each grain receiving sufficient daylight exposure during wind transport (e.g., Aitken, 1985, 1998). In high-latitude areas where sunlight is less direct than lower latitudes, seasonal effects have been considered and studies show differing results regarding their influence. For example, Mejdal and Funder (1994) showed insufficient bleaching within the Arctic Circle in Greenland; however, Berger and Anderson (2000) demonstrated a very low OSL signal on modern (i.e., near-zero age) sediments within two Alaskan lakes, which suggests full resetting is possible even at high latitudes.

Dose rate measurements rely on a value for water content that adequately represents the historical water content since burial, which realistically often varies over time from factors such as a change in water table or permafrost levels. Uncertainties pertaining to water content values can lead to substantial changes in dose rate calculations and subsequently age estimates. For sand-sized grains, it has been shown that the total dose rate varies approximately 1% with a 1% change in water content (Rhodes, 2011). Water contained within sediment pores absorbs radiation, so water content values must be measured during collection or within the laboratory. An important consideration is that the water content measured while sampling should be representative of historical water content as much as possible. Because water can cause a lowering of the dose rate as it hinders radiation from infiltrating a particle, changes in water content can result in age underestimation (Preusser et al., 2008; Lukas et al., 2012). For luminescence samples with assumed past variability in water content, such as former changes in water table levels, further measures may need to be taken, such as modeling past changes in water content (e.g., Mann et al., 2002). This highlights the importance of understanding the

paleoenvironmental setting and history of a sampling area in order to produce accurate dose rate calculations and luminescence age estimates.

Limitations of luminescence dating faced by researchers have fostered rapid advancements in this field. The high variability experienced between the luminescence properties of quartz and feldspar, individual sediment deposits based on depositional processes, and variability between individual grains of the same deposit encourage that researchers report and validate the specific process of luminescence dating being used, which "has led to a degree of quality control rarely seen with other dating methods. This practice of reporting experimental detail, and therefore the sharing of methodology, has also resulted in the rapid advance of the technique" (Lian and Roberts, 2006, p. 2450).

2.3.3 Development of IRSL Techniques

Following the use of TL for dating, the realization that sunlight (i.e., optical stimulation) could bleach sediments gave way to the use of optical means to measure luminescence through OSL (Huntley et al., 1985). Optical dating has been widely used for a variety of applications, including archaeology, seismology, and geomorphology, and is particularly useful for geomorphologists and those developing chronologies of different landforms. Several thorough reviews detail such applications, including those of Duller (2004) and Lian and Roberts (2006).

The use of infrared stimulation, or IRSL dating, was pioneered by Hutt et al. (1988), and has since seen a shift toward expanding the use of feldspar dating through IRSL dating. Quartz grains do not have the ability to trap, store, and release radiation within crystal lattices that feldspar grains possess. Feldspar also extends the dating range for sediments, beyond 100ka years. However, much remains to be understood about the processes surrounding feldspars,

particularly methods to counter anomalous fading. The first observance of anomalous fading came through TL dating of volcanic feldspars (Wintle, 1973), which led to the common hypothesis that anomalous fading occurs due to quantum tunneling mechanics (e.g., Aitken, 1985; Visocekas, 1985). Unstable traps tend to release some of the electron traps--or transfer them from nearby traps--which causes an underestimation of calculated sample age. Some argue that feldspar fading tends to occur ubiquitously (e.g., Huntley and Lamothe, 2001), while others state that feldspar fading is dependent on sediment origin (e.g., Visocekas and Guerin, 2006). As scientists continue to investigate the specific causes of signal fading, they have used a variety of methods to combat the effects of anomalous fading in order to expand the use of feldspar dating.

Initial attempts to diminish the effects of anomalous fading came from studies that aimed to track signal decay, or fading, rates. This is done with a fade test that measures signal decay after irradiation and calculates a fading rate (Huntley and Lamothe, 2001; Auclair et al., 2003). Fade rate corrections can then be made using the calculated fading rate (Huntley and Lamothe, 2001). Lamothe et al. (2003) simplified this method by incorporating the environmental dose and dose rate values into the fading equations. While these methods offer a plausible means for diminishing the effects of anomalous fading, they are often time consuming and rely on the accuracy of equivalent dose and dose rate measurements. The processes are dependent on each other and so any inaccuracies are emphasized in the results. Thus, alternative methods that avoid signal fading are better suited for IRSL dating because they do not require calculating fade corrections.

Due to complications of using fade rate measurements, methods have recently shifted towards developing methods that target a more stable (i.e., non-fading) signal. These methods, first proposed by Thomsen et al. (2008) and utilized by Buylaert et al. (2009), are known as

elevated temperature, two-step post-IR (pIR) protocols that utilize a lower preheat temperature (e.g., 50°C), followed by IRSL measurement at a higher temperature (e.g., 225-320°C) (Table 2.1). A lower preheat temperature is intended to clear out unstable traps before luminescence measurements have been made, thereby ensuring the measurement comes from electron traps less prone to fading (i.e., more stable) rather than luminescence from unstable traps (Thomsen et al., 2008). While the development and testing of pIR techniques continues, these methods have served as a breakthrough in targeting anomalous fading, which has allowed for the expanded use of feldspars in luminescence dating.

Table 2.1. Treatment process of the applied post-IR IRSL SAR protocol (following Buylaert et al., 2009).

Step	Treatment	Observed
1	Give dose, D_i	
2	Preheat, 250 C, 60 s	
3	IR stimulation, 100 s at 50°C	L_i*
4	IR stimulation, 100 s at 225°C	L_i**
5	Give test dose, D_T	
6	Preheat, 250 C, 60 s	
7	IR stimulation, 100 s at 50°C	
8	IR stimulation, 100 s at 225°C	T_i**
9	IR stimulation, 400 s at 290°C	
10	Return to Step 1	

*Referred to as IR at 50°C
**Referred to as post-IR IR at 225°C

2.3.4 Aeolian Luminescence Studies of Alaska

The prevalence of loess throughout Alaska has led to the majority of luminescence research conducted on aeolian material to focus on loess. The well-known loess sequences near Fairbanks, Alaska have received the bulk of luminescence research within Alaska, including the

Halfway House loess (Westgate et al., 1985; Westgate et al., 1990; Oches et al., 1998; Auclair et al., 2007) and the Gold Hills loess (e.g., Preece, 1991; Preece et al., 1999; Berger, 2003). Some of the earliest luminescence studies of loess within central Alaska were conducted by Berger et al. (1994), who used TL to date bracketing loess surrounding the Old Crow tephra to ≥ 140 ka (below the tephra) and 110 ka (above the tephra). Berger et al. (1996) also used TL at a nearby exposure to show similar bracketing ages of the Old Crow tephra ranging from 144 ka (below the tephra) to 128 ka (above the tephra). Paleosols within loess sequences at Gold Hill near Fairbanks were dated using TL and IRSL to bracket the ages of the associated Sheep Creek tephra between 75 ka and 30 ka (Berger, 2003). Several other studies used TL dating to determine the ages of loess within the area (e.g., Wintle and Westgate, 1986; Berger et al., 1994; Berger and Péwé, 2001; Berger, 2003).

In addition to the loess deposits of central Alaska, the Tanana and Nenana river valleys are well-known for their abundance of archaeological material that dates the first populations into eastern Beringia, and possibly the New World (Graf and Bigelow, 2011). Due to the presence of cultural material found within aeolian deposits across the valleys, most archaeological studies within central Alaska to date have utilized radiocarbon dating to provide chronologic framework; however, Reuther (2013) used a combination of IRSL and radiocarbon for geoarchaeological and paleoecological analysis of the Tanana Valley.

Despite the appeal of using luminescence dating for aeolian material, the application of this dating technique has not always been successful for dating aeolian deposits in Alaska and elsewhere. For example, Auclair et al. (2007) conducted three types of fading tests on feldspar grains sampled from tephra and loess and determined that the IRSL ages of loess were reasonable, but the measured fading rate (g-value) used on the tephra resulted in age

underestimation (Auclair et al., 2007). Berger (2003) found that IRSL ages of loess near Fairbanks were underestimated and stratigraphically inconsistent in comparison with TL ages, which he suggested may be due to variations in feldspar grains that affected the use of fade corrections following Huntley and Lamothe (2001). At the Halfway House site in central Alaska, Oches et al. (1998) reported IRSL ages that were discordant from their more reliable TL ages. Age discrepancies have been reported elsewhere; for example, Berger et al. (2000) received similarly inconsistent IRSL ages in relation to TL ages of lake core sediments from northern Alaska that the authors suggested were a result of mineralogical variation among the polymineral samples. Within the northern Great Plains, complications with luminescence dating of quartz grains appeared as low luminescence signals in aeolian studies, which has led to the use of IRSL dating of feldspar grains, rather than OSL dating, throughout the region (Munyikwa et al., 2011; Halfen et al., 2015). Similarly, Reuther (2013) references dim luminescence of quartz grains and avoided quartz OSL analysis by adopting IRSL analysis instead. Given the complications faced by researchers pertaining to available chronologic dating methods and previous preferential interest of research in loess deposits in central Alaska, sand dune chronologies throughout central Alaska are lacking in relation to loess deposits of the region.

Recent investigations of a dune field in the TRL of central Alaska brought to light initial complications using luminescence dating, but subsequently produced promising results using a pIR IRSL protocol. The Wood River dunes comprise a relatively small dune field within the Tanana River Lowlands (TRL) that covers 45 km^2 and consists of a predominately northeast-southwest trending linear dune complex, currently stabilized by tree and shrub growth. Nineteen luminescence samples collected from the dune crests, flanks, and basal portions of the dune were initially processed using IRSL dating that employed the standard fade rate corrections

(Huntley and Lamothe, 2001). Because the resulting ages of the dunes were anomalously young in comparison to regional aeolian proxies, the samples were subsequently dated using a post-IR IRSL protocol recently deemed successful for dating loess in the Fairbanks area (Roberts, 2012) (Table 2.2). P. Hanson and A. Young at the University of Nebraska–Lincoln Geochronology Laboratory conducted initial and subsequent IRSL analyses. The use of the pIR IRSL protocol produced reasonable ages in relation to regional proxies (e.g., Potter et al., 2008, 2011, 2014; Esdale et al., 2012; Reuther, 2013), and dating of the Wood River dunes served as an exploratory investigation of dune activity within the TRL. Given the success of the first use of this protocol to date a stabilized central Alaskan dune field, the pIR IRSL method, central to this research, was adopted to further test the pIR protocol and provide information regarding the timing of aeolian activity and stabilization of the Nenana dune field.

Table 2.2. Wood River dune IRSL age estimates using standard age correction method (Huntley and Lamothe, 2001), which yielded anomalously young ages, versus subsequent post-IR age estimates in agreement with regional proxy data (Johnson et al., 2012).

Sample #	Std. Age (ka)	Post-IR Age (ka)
AK 1-2	4.92 ± 0.33	11.86 ± 0.92
AK 1-3	11.10 ± 1.01	12.64 ± 1.14
AK 2-1	6.95 ± 0.48	10.62 ± 0.88
AK 2-2	6.92 ± 0.45	9.65 ± 0.73
AK 3-1	6.12 ± 0.46	10.24 ± 0.95
AK 3-2	6.59 ± 0.41	10.06 ± 0.81
AK 4-1	10.11 ± 0.65	15.40 ± 1.32
AK 4-2	6.61 ± 0.61	11.87 ± 1.47
AK 5-3	6.06 ± 0.60	10.38 ± 0.97
AK 6-1	8.55 ± 0.62	14.22 ± 1.40
AK 7-4	10.6 ± 0.60	11.62 ± 1.12
AK 7-5	8.39 ± 0.53	11.76 ± 0.93

In summary, multiple researchers have extensively studied loess exposures within central Alaska (Péwé, 1955, 1975; Hamilton 1983, 1988; Begét, 1988, 1990, 1991, 1996, 2001; Begét and Hawkins, 1989; Begét et al., 1990; Westgate et al., 1990; Preece et al., 1991, 1999; Berger et al., 1994, 1996, 2000; Muhs et al., 2001; Lagroix and Banjeree, 2002; Berger, 2003; Muhs et al., 2003), but there remains a paucity of information regarding central Alaskan sand dunes by comparison (e.g., Collins, 1985; Lea 1990, 1996; Lea and Waythomas, 1990; Esdale et al., 2012; Johnson et al., 2012), and even fewer within the Tanana River Lowlands (Johnson et al., 2012). Given the lack of knowledge surrounding the Nenana dunes and the potential of dating success using a pIR protocol, this research documents the timing of aeolian activity and stabilization of the Nenana dune field. This project serves as one of the first studies within central Alaska to use a post-IR IRSL protocol for dating sand dunes and provides further testing of the protocol, which is significant for assessing its potential as a dating technique in sand dune settings. As a corollary to the primary objective of documenting aeolian activity, a discussion is included of the resulting luminescence ages within a paleoenvironmental context of the region.

Chapter 3 Regional Setting and Study Area

The Tanana River Lowlands (TRL) is a broad valley region located within the Tanana-Kuskokwim Lowland Basin (Wahrhaftig, 1965), which defines this east-central division of Alaska (Fig. 3.1). This region is bounded to the north by the Tanana-Uplands and the northern foothills of the Alaska Range to the south. Multiple streams flowing northward, some of which originate in the Alaska Range to the south, dissect the landscape, and their sediment-rich loads have deposited coarse bed load material as expansive alluvial fans that extend into the lowland region (e.g., Péwé, 1975; Collins, 1985; Wahrhaftig, 1985). Remnant stream channels, oxbow lakes, and natural levees signify previous migrations of streams. Several bedrock outcroppings serve as topographic highs across the valley, including the Blair Lakes outcropping in the southeastern portion of the TRL. Much of the bedrock is composed of Precambrian and Paleozoic schist that is highly weathered (Soil Survey Staff, 2007).

During the Pleistocene, glaciers existed to the north, south, and east of the plains and smaller glaciers within the Yukon-Tanana Uplands, but the TRL remained unglaciated (Péwé, 1975) and instead served as an accumulation basin for sediment during the recent glacial and interglacial periods. As such, the majority of the TRL consists of Quaternary deposits, including alluvium from the nearby streams, colluvium from the surrounding upland areas, and aeolian deposits (Péwé et al., 1966; Péwé 1975; Collins, 1985; Foster and Keith, 1994). Windblown silt mantles the topographic highs within the area, including cliff-top terraces, sand dunes, and bedrock outcroppings (Black, 1951; Péwé, 1975; Wahrhaftig, 1985; Muhs et al., 2003). It is well-established that aeolian sediment is prevalent throughout the TRL (Fig. 2.1), shown particularly through extensive research of loess deposits north of the Tanana river near Fairbanks

(Muhs et al., 2003). To date, however, little is known of the sand dune deposits within the lowlands.

Figure 3.1. Physiographic regions of central Alaska (Wahrhaftig, 1965). Tanana River Lowlands (TRL) lies within the Tanana-Kuskokwim Lowland and south of the Yukon-Tanana Upland.

Climate of the TRL is continental subarctic, with winter temperatures averaging -19°C and mean summer temperature of 14°C (National Climatic Data Center, 2015). Monthly temperature and precipitation averages are provided for the village of Nenana in Table 3.1.

Table 3.1. Temperature and precipitation data for Nenana from 1981–2010 (Data from NCDC, 2015).

Month	Precip. (cm)	Minimum Temp. (°C)	Mean Temp. (°C)	Maximum Temp. (°C)
January	1.37	-25.9	-21.2	-16.3
February	1.07	-23.4	-17.6	-11.7
March	0.66	-18.8	-11.8	-4.8
April	0.81	-7.3	-0.7	5.9
May	1.96	1.8	8.7	15.7
June	3.63	7.6	14.7	21.8
July	7.21	9.9	16.1	22.2
August	5.31	7.1	12.8	18.5
September	3.23	1.3	6.6	11.8
October	2.18	-8.8	-4.9	-0.9
November	1.80	-20.4	-16.0	-11.6
December	1.37	-24.2	-19.2	-14.2

Due to the presence of the Alaska Range to the south, air masses tend to lose the majority of their moisture before reaching the TRL, resulting in an annual average annual precipitation of only 25–40 cm for the region (Muhs et al., 2001; Bigelow and Edwards, 2001). This part of central Alaska currently experiences seasonal winds, with primarily southwesterly winds during the summer months and northeasterly winds during the winter months (Figs. 3.2 and 3.3).

The TRL consists of discontinuous permafrost, which varies by depth throughout the area (Wahrhaftig, 1965; Péwé, 1975). Permafrost is largely responsible for frequent ground saturation and the marshy conditions of the low-lying areas within the TRL, as it hinders the downward infiltration of groundwater in the area (Wahrhaftig, 1985).

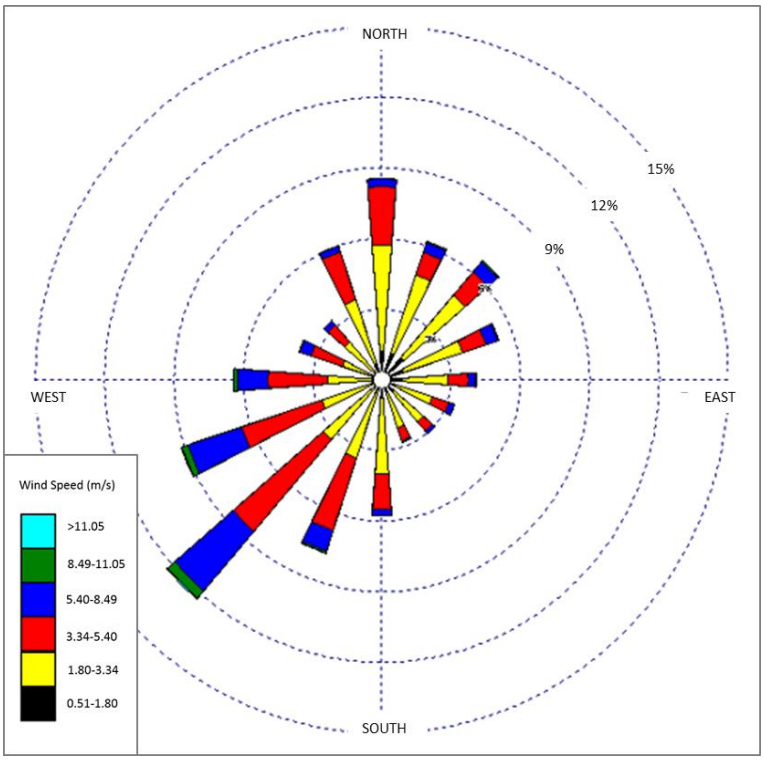

Figure 3.2. Seasonal wind rose showing prevailing wind direction during June 1961–1990 in Fairbanks (Figure modified from: http://www.wcc.nrcs.usda.gov; data from National Climatic Data Center).

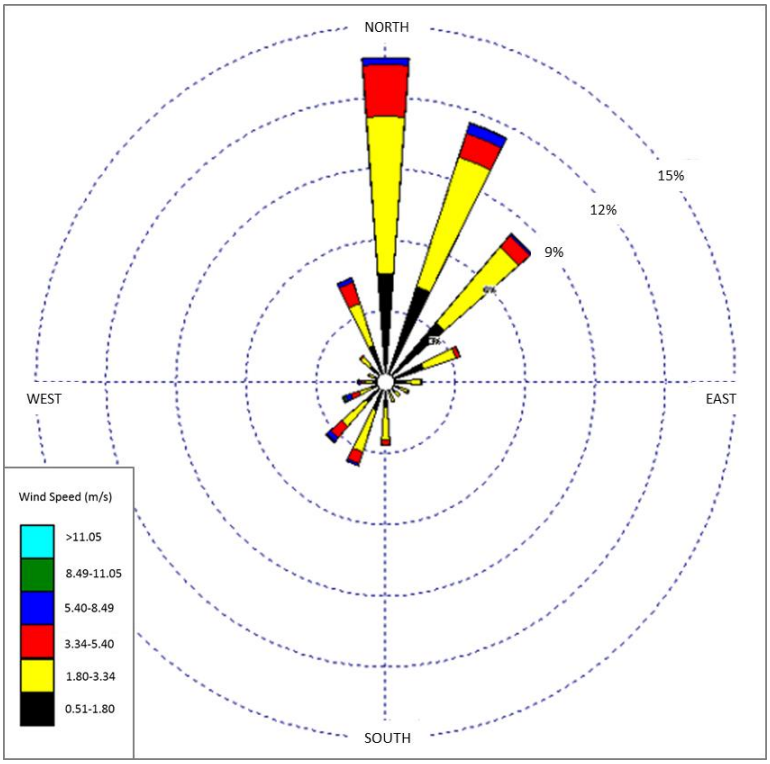

Figure 3.3. Seasonal wind rose showing prevailing wind direction during Dec. 1961–1990 in Fairbanks (Figure modified from: http://www.wcc.nrcs.usda.gov; data from National Climatic Data Center).

An expansive dune field exists to the west of Nenana River, known as the Kantishna sand sea (Collins, 1985), and two substantially smaller dune fields are located within the TRL: the Nenana and Wood River dune fields (Fig. 3.4). The Nenana dune field has been recognized in the literature (Péwé, 1975; Collins, 1985), but lacks detailed study. Collins (1985) describes these dunes south of Nenana as three small groupings of dunes, which occupy the easternmost reach of the aforementioned expansive dune field west of the Tanana River.

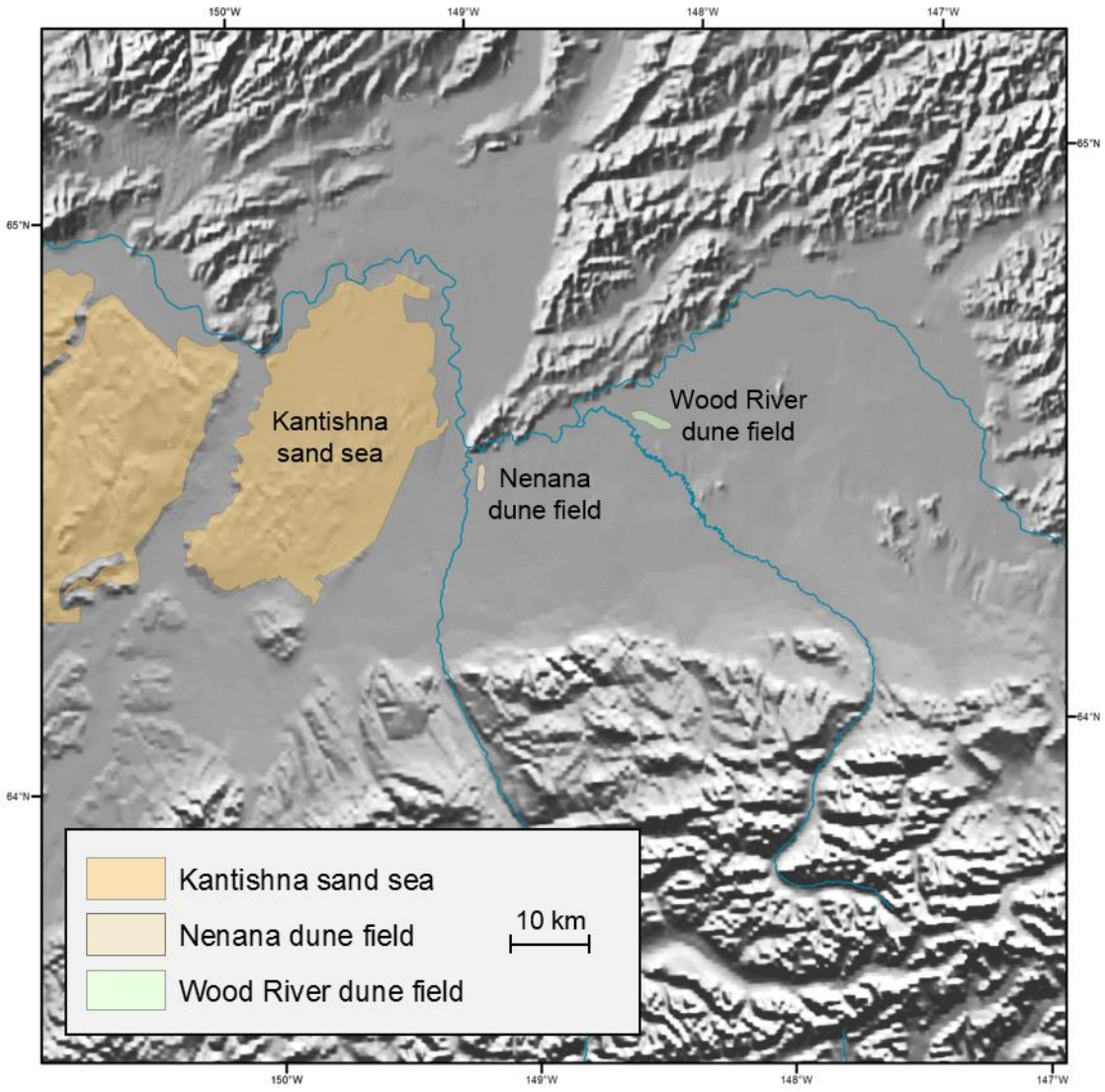

Figure 3.4. Proximal extent of the expansive Kantishna sand sea (from Collins, 1985) in relation to the relative extents of the Nenana and Wood River dune fields within the Tanana River Lowlands.

This smaller concentration of dunes consists of discontinuous, vegetated dunes that are currently irregular in form and in many cases affected by human development (Fig. 3.5), but as noted by Collins (1985), the dunes maintain the muted presence of dune ridges trending in an east-northeast direction. Several of the dune uplands intersect with roads and the major highway running south from the village of Nenana, known as the Parks Highway, which provided access to dune stratigraphy during sampling.

Figure 3.5. Remnants of aeolian deposits that have been scraped away to build a landing strip by the landowner (pers. comm.). Location is about 0.5 km north of the Chevron site (Photograph: C. Messner).

Surrounding the dunes are areas characteristic of the lowland, marshy setting of the TRL (Fig. 3.6). The Wood River dune field covers a larger area, 45 km^2, and also consists of discontinuous vegetated dunes (Péwé et al., 1966; Esdale et al., 2012) (Fig.3.7). The linear dune complex primarily extends northeast-southwest, with the tallest dunes extending as high as 45 m above the surrounding flats (Esdale et al., 2012). Vegetation of the dune uplands is characterized as open, upland dry broadleaf forest (Esdale et al., 2012). Drier, upland areas in undisturbed areas are populated with young birch, spruce, pine, and aspen, while the surrounding low-lying areas are scattered with tamarack, black spruce, and muskeg (Collins, 1985). Well-drained upland dune areas experience relatively mesic and xeric conditions, which can influence dune susceptibility to forest fire.

Figure 3.6. Multiple vegetated, stabilized dunes of the Nenana dune field; view is east from the Parks Highway (Route 3). Note the muskeg, or swampy lowlands within interdunal areas in contrast to the upland (dune) vegetation (Photograph: W. Johnson).

Figure 3.7. Aerial and ground views of several of the Wood River dunes that are currently stabilized by vegetation (Photographs: W. Johnson, W. McLaren, and K. Yeske).

Chapter 4 Methods

4.1 Field Methods

Low-altitude aerial survey of the greater Nenana area was conducted via charter plane and ground survey to evaluate dune field extent and individual dune forms (Fig. 4.1). Eighteen luminescence samples were collected and used to identify periods of aeolian deposition of the Nenana dunes. Sampling strategy targeted multiple site locations throughout the dune field in order to assess the extent of dune activity (Fig. 4.2). This spatial approach limits the level of detail that can be obtained from each dune, so a sampling strategy was derived to capture the maximum- and minimum-limiting ages on several dunes throughout the Nenana and Wood River dune fields.

The principle objective of the sampling method was to gather samples from the crest and base of the dune in order to identify any changes in stratigraphy that could indicate variation of sediment accumulation rates (i.e., rapid vs. slower aggradation). For example, rapid aggradation would be identified by a narrow span in ages between the crest and base of the dune, whereas a wider span of ages would indicate slower aggradation of sediment. Basal samples, or those taken just above depth of permafrost, were extracted in order to provide a maximum-limiting age of dune activity. Near-surface samples were taken from dune crests to gain insight on the most recent activation period and serve as minimum-limiting ages. Where possible, samples were extracted from multiple side slopes (i.e., North, East, South, and West aspects), or dune flanks, as a secondary, exploratory objective, in order to gain insight on the geomorphic context of dune formation.

Figure 4.1. Aerial survey of Nenana area. *Top:* The village of Nenana, AK, and the confluence of the Tanana and Nenana rivers (view northwest). *Bottom:* Aerial view of the Cosna site. Three road cuts reveal dune stratigraphy, and this view indicates a slight east- west trend for dune form (Photographs: W. Johnson and C. Messner).

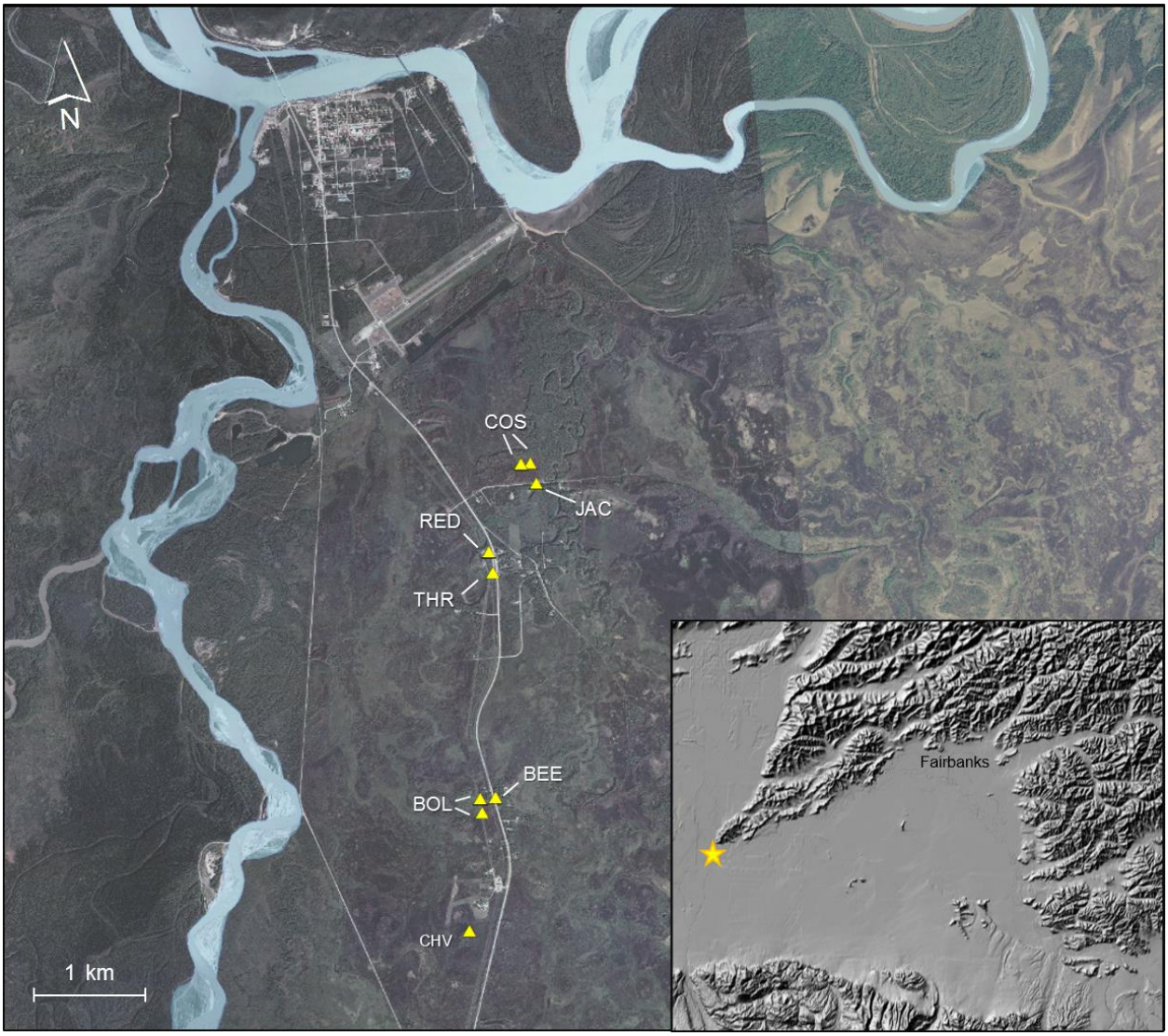

Figure 4.2. Sample sites (yellow triangles) labeled by site location code. Nenana and Tanana rivers bound the dune field to the west and north, respectively. The village of Nenana is located at their confluence, and the yellow star indicates location within the Tanana River Lowlands.

The amorphous nature of the Nenana dunes gives a less clear picture of the age relationship or formation of the dunes than that of a parabolic dune, for example, with obvious orientation indicators. In the case of the ambiguous Nenana dune forms, flank ages that are older than crest ages could indicate some deflation or reactivation of the central portion of the dune occurred, which resulted in more recent deposition. Alternatively, flank ages that are younger

than the dune crest samples could point to other factors that would have triggered later sand deposition, such as an isolated deflation event that could have occurred as a stream meander eroded an existing dune form downwind. In order to minimize the probability of including sediment from the zone of pedoturbation, samples were taken from deeper than 0.9 m below surface; however, in two cases samples were extracted from depths of around 0.6 m to capture the shallowest stratigraphic contact of the site locations' stratigraphy.

Hand excavation from exposed soil profiles was used for dunes bisected by road cuts and dune side slopes. At sites where excavating a soil profile was not feasible due to dense vegetation, hand bucket auguring was used to collect samples. Dune stratigraphy was described for excavated profiles, and changes in color, texture, and moisture were recorded where bucket auguring was employed. To prevent light contamination, the samples were collected in opaque, steel tubes that were gently hammered into the profile or pushed into the top of a sediment-filled auger bucket (Fig. 4.3). Tubes were firmly packed with sediment to eliminate potential mixing within the tube that could potentially result in inaccurate ages, and both ends were tightly sealed with opaque caps fixed with black vinyl electrical tape. Representative samples used to determine water content and dose rate were also collected, either within 30 cm of the sample tube in sediment exposures, or from within the auger bucket.

Figure 4.3. Various sampling techniques used in the field. *Top left:* At road cut sites where establishment of stratigraphic profiles was possible, tubes were hammered in to the sediment and then sealed with black vinyl end caps. *Bottom:* Bucket auguring was employed to collect luminescence samples at sites without natural exposures. *Top right:* The tubes were then inserted into the auger bucket to capture the sediment (Photographs: W. Johnson and C. Messner).

4.2 Laboratory Pretreatment of Luminescence Samples

Pre-treatments for optical samples followed standard procedure in preparation of the IRSL single aliquot regenerative (SAR) analysis for feldspar grains (Murray and Wintle, 2000). For the pretreatment of samples prior to IRSL analysis, sediment was extracted from steel tubes under dim amber light, and 5 cm of material from each end of the tube was discarded to lessen chances of using partially bleached material. Samples were wet sieved to target 63-250 µm grains and then treated with 1N HCl to remove carbonates. Remaining sediment was floated in 2.58 g/cm^3 sodium polytungstate ($Na_6[H_2W_{12}O_{40}]$) to eliminate heavy minerals. Samples were then dry sieved to remove grains finer than 90 µm. All samples were analyzed using the pIR IRSL SAR protocols described in Buylaert et al. (2009; Table 2.1), and analyzed on Risø and Daybreak TL/OSL readers at the Utah State University Luminescence Laboratory.

4.3 Post-IR IRSL Age Determination

Elemental concentrations of bulk sediment taken from a 30 cm radius surrounding the luminescence sample or from within the auger bucket were used for dose rate estimates. Inductively coupled plasma-mass spectrometry (ICP-MS) and -atomic emission spectroscopy (ICP-AES) were used to analyze bulk sediment for concentrations of K, U, Th, and Rb. Sample depth, elevation, and latitude/longitude were utilized for calculating cosmogenic contributions to dose rates using the equations from Prescott and Hutton (1994). Dose rate values were calculated using the equation from Aitken (1998) by dividing the environmental dose (Gy) by the dose rate (Gy/ka), which represents dosing the sample was exposed to following burial.

Chapter 5 Results

5.1 Post-IR IRSL Results

Luminescence analysis of the Nenana dunes produced age estimates ranging from 16 ka to 10 ka (Table 5.1). The two youngest ages, derived from the Cosna and Jacobson sites, were extracted at depths less than one meter below the crest of the dune in order to capture the lower boundary of the silt (loess) cap found at both site locations (COS-1, 10.36 ± 0.97 ka; JAC-1, 10.44 ± 0.98 ka, respectively). Oldest ages came from samples retrieved from the greatest depths below the surface (with one exception, BOL-4, discussed below) from the Jacobson, Cosna, and Red Tower sites (JAC-3, 7.68 mbs, 15.57 ± 1.66; COS-3, 10.1 mbs , 15.74 ± 1.78 ka; RED-2, 6.34 mbs, 16.02 ± 1.72 ka, respectively). Figure 5.1 displays relative depths and resulting ages across sample locations.

Table 5.1: Equivalent dose, dose rate, and post-IR IRSL age estimates for the Nenana dunes.

Field Site Sample Name	Depth (m)	Latitude, Longitude	Num. of aliquots[1]	Dose Rate (Gy/ka)	De[2] (Gy)	IRSL age[3] (ka)
Cosna site						
COS-1	0.93	64.533050, -149.059522	23 (44)	4.22 ± 0.24	43.79 ± 2.23	**10.36 ± 0.97**
COS-2	1.23	64.533050, -149.059522	18 (21)	2.96 ± 0.15	35.83 ± 3.85	**12.11 ± 1.23**
COS-3	10.10	64.533050, -149.059522	17 (23)	2.32 ± 0.16	36.47 ± 4.06	**15.74 ± 1.78**
COS-4	1.29	64.533024, -149.059559	23 (29)	2.84 ± 0.15	37.32 ± 1.70	**13.14 ± 1.19**
COS-5	1.04	64.533024, -149.061374	18 (25)	2.99 ± 0.15	37.95 ± 2.55	**12.70 ± 1.17**
COS-6	1.40	64.533064, -149.059642	26 (29)	2.72 ± 0.19	32.73 ± 2.23	**12.04 ± 1.25**
Jacobsons site						
JAC-1	0.62	64.531293, -149.058741	18 (18)	3.97 ± 0.22	41.47 ± 2.27	**10.44 ± 0.98**
JAC-2	1.23	64.531293, -149.058741	21 (24)	2.94 ± 0.15	33.31 ± 2.59	**11.31 ± 1.06**
JAC-3	7.68	64.531293, -149.058741	19 (20)	2.44 ± 0.18	37.94 ± 2.33	**15.57 ± 1.66**
Red Tower site						
RED-1	1.58	64.525989, -149.067326	22 (25)	2.22 ± 0.12	28.62 ± 1.45	**12.91 ± 1.17**
RED-2	6.34	64.526121, -149.068872	22 (25)	1.99 ± 0.14	31.95 ± 2.99	**16.02 ± 1.72**
Three Towers site						
THR-1	2.42	64.524149, -149.068327	21 (25)	2.73 ± 0.15	31.12 ± 1.93	**11.39 ± 1.06**
Beekeeper site						
BEE-1	0.90	64.505335, -149.071071	24 (25)	2.86 ± 0.15	33.24 ± 2.06	**11.62 ± 1.06**
Boulden site						
BOL-1	1.60	64.505830, -149.074479	21 (22)	2.34 ± 0.18	28.71 ± 1.34	**12.27 ± 1.28**
BOL-2	1.25	64.504163, -149.073943	20 (23)	2.36 ± 0.20	30.02 ± 2.05	**12.71 ± 1.46**
BOL-3	1.40	64.505343, -149.074078	21 (22)	2.42 ± 0.13	31.21 ± 1.41	**12.87 ± 1.16**
BOL-4	6.20	64.505343, -149.074078	24 (25)	2.25 ± 0.18	29.36 ± 1.70	**13.02 ± 1.42**
Chevron site						
CHV-1	0.67	64.494362, -149.078072	20 (20)	2.67 ± 0.21	37.44 ± 1.46	**14.0 ± 1.49**

[1] Number of aliquots used in age calculation and number of aliquots analyzed in parentheses.
[2] Equivalent dose (De) calculated using the Central Age Model (CAM) of Galbraith and Roberts (2012).
[3] Age analysis using the elevated temperature (225°C) post-IR IRSL protocol of Buylaert et al. (2009) on 1-5 mm small-aliquots of potassium feldspar. IRSL ages are not corrected for fading.

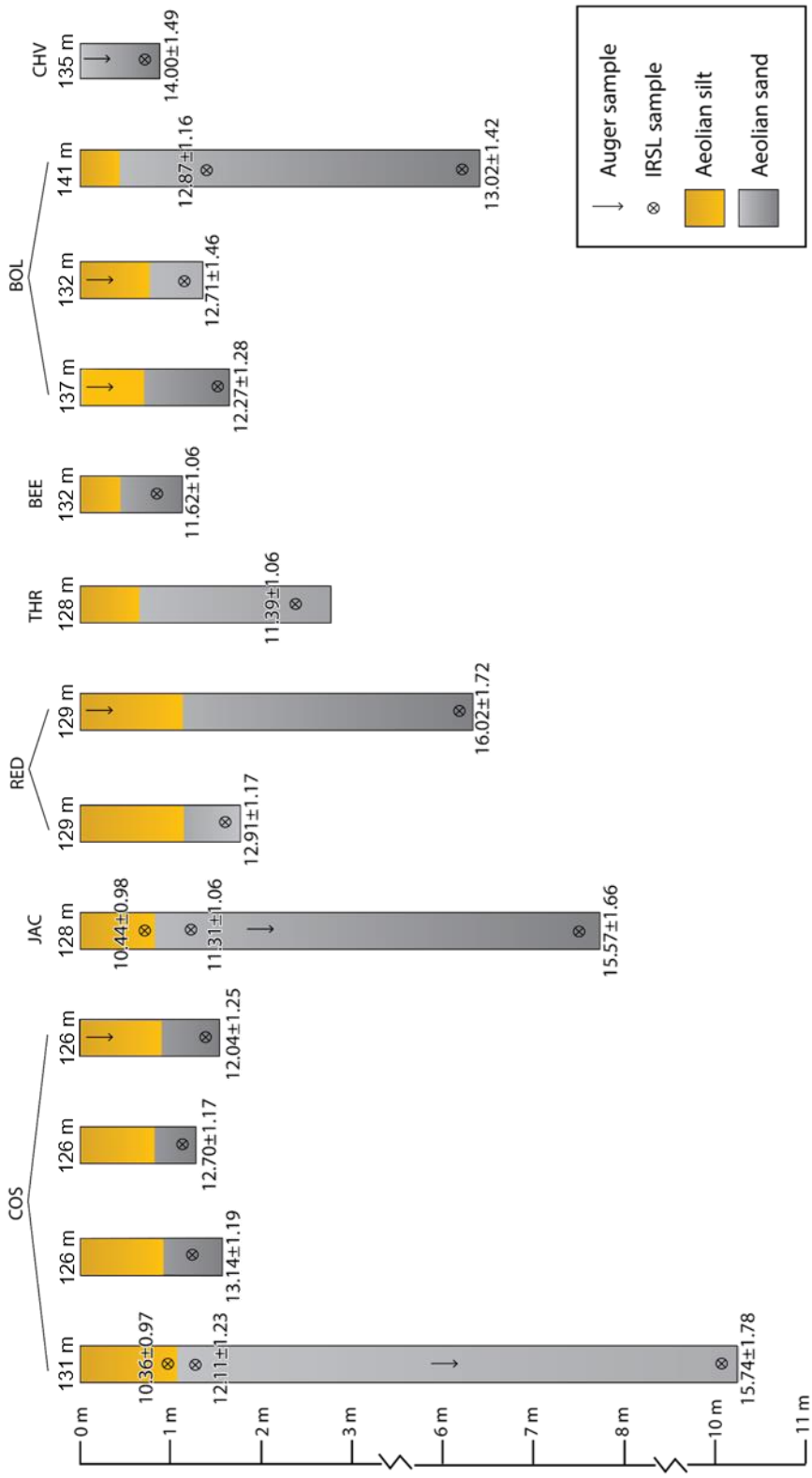

Figure 5.1. Post-IR IRSL age estimates from the Nenana dunes and generalized stratigraphy. Yellow color represents the silty, Holocene-age loess mantle present at most sample sites; gray represents underlying dune sand.

5.2 Site Stratigraphy

The soil survey of the Greater Nenana area records two main soils groups within the vicinity of the Nenana dune field, including Eielson very fine sandy loam (29EL03) and Faa silt loam (29FAI01). Soil orders of these two soil series are Entisols and Inceptisols, respectively, which are characterized by weakly developed soils and are common among high-latitude climates where pedogenic and decompositional processes are often gradual given the short growing season, cold climate, and acidic plant material (Soil Survey Staff, 2007). Parent material associated with the Nenana site locations did not always match up to dunes identified in the field; for example, the Red Tower, Three Towers, and Chevron sites are listed as Eielson very fine sandy loam with alluvium as a parent material, rather than "loess over aeolian sand" as the other sites were (Soil Survey Staff, 2007). However, the field observations listed herein align generally with soil survey descriptions, including minimal surface soil development and parent material consisting of a yellowish brown loess cap (10YR 5/4) overlying very fine to fine grayish brown aeolian sand (2.5 Y 5/2). Additionally, both soil survey and site observations indicate mottling of iron oxides, as well as clean, pebble-free sand indicative of an aeolian origin of sediment. Aeolian bedding averaging ~1 cm in width was visible at several site locations, and paleosols were not visible at any site locations within profiles created for sampling and bucket auguring. Supplemental images of site locations and samples are included in Appendix B.

5.2.1 Cosna site (64.533, -149.060)

The Cosna site is the northernmost sampling location and is ~3.4 km south of the village of Nenana and consists of an isolated dune that has an elongated axis extending east-west in direction (Collins, 1985). It is estimated that the dune footprint covers approximately 9,000 m^2,

and the crest of the dune is located ~131 m above sea level. Gravel roads dissect the dune exposing eastward, southward, and westward facing road cuts.

An eastward road cut exposes ~4.5 m of dune stratigraphy. A yellow loess cap of extends from the crest of the dune down to a depth of ~0.7 m with well-sorted gray aeolian sand below. Clearly defined bedding between 0.5–1.0 cm in width is visible on the eastward facing exposure and dips at approximately 35° (Fig. 5.2). The dip is approximately that of the modern angle of repose of recently disturbed sand and solidifies that the eastward side of the dune represents the slip face of the dune, which indicates primary dune forming paleowinds were westerly. A profile face was cleaned between 0.7–1.4 m below the crest of the dune in order to examine the stratigraphy for sampling and capture the boundary between the loess and sand deposits (Fig. 5.3). Sample COS-1 was extracted at 0.9 m below the surface from within the lower part of the loess cap and just above the sand contact. Sample COS-2 was extracted from 1.2 m below the surface in the upper part of the sandy material in order to capture the most recent visible sand aggradation before the transition to silt aggradation began. A bucket auger was used to extend the profile from the road downwards to a depth of 10.1 m below the crest of the dune. Permafrost prevented further auguring below this depth. No significant changes were observed in particle size or color within the gray aeolian sand unit. Sample COS-3 yielded a luminescence age of 15.74 ± 1.78 ka.

Figure 5.2. Present and original slip face of the Cosna dune. The dip of the preserved dune bedding is the same as that of the angle of repose for the recently disturbed sand (~35°) indicating the lee side of the dune during original formation (Photographs: W. Johnson and C. Messner).

Figure 5.3. East-facing road-cut exposure at the Cosna site. Profile was created in upper part of dune and then a bucket auger was used to sample below depth of road surface (Photographs: W. Johnson and C. Messner).

Southern and western flanks of the dune were also dissected by road cuts that revealed similar stratigraphy (aeolian sand capped by loess) to that found at the larger eastern road cut exposure. A south-facing profile was cleaned exposing sediment 0.6–1.5 m below the dune surface. Possible mixing of sediment appeared evident in the south-facing profile as well as presence of several krotovina. Care was taken to sample from homogenous sediment in order to avoid sample contamination. Sub-horizontal aeolian bedding, between 0.5–1.0 cm in width, as well as mottling and undulating contact boundaries between the loess and sand components were present at both south- and west-facing exposures. Sample COS-4 was extracted from below the loess-sand contact at a depth of 1.3 m below the dune surface and yielded a luminescence age of 13.14 ± 1.19 ka. A west-facing profile was cleaned and extended 0.6–1.1 m below the dune surface. COS-5 was extracted from the gray aeolian sand at a depth of 1.0 m below the dune surface and yielded a luminescence age of 12.70 ± 1.17 ka.

There was no road cut on the northern side of the dune, so a bucket auger was used to extract COS-6 from a depth of 1.4 m below the surface. In the interdunal area, permafrost was present at 1.5 m below the surface, so COS-6 was taken just above the depth of permafrost. Analysis of COS-6 yielded a luminescence age of 12.04 ± 1.25 ka.

5.2.2 Jacobson site (64.531, -149.059)

The Jacobson site is located ~3.7 km south of the village of Nenana. The site is also accessed by Cosna Rd., which dissects the dune. An isolated dune form is present at the sampling area, with another exposure visible 75 m east that appears to have been a part of the original dune form. If this is the case, the Jacobson dune would also exhibit an elongated axis in the east-west direction with an estimated footprint as large as ~4,600 m^2. Dune crest elevation is

~127.5 m above sea level, and the road cut exposure at the Jacobson site exposes ~3.5 m of dune stratigraphy.

A profile, cleaned to expose the top 1.5 m of the dune for luminescence sampling, indicated the dune is covered by ~0.7 m of well-sorted yellow loess containing a weakly-developed surface soil underlain by well-sorted sand. Faint, horizontal aeolian bedding <1 cm in width was visible throughout the sand deposit. Several krotovina were identified within the profile, ranging in size from <5 cm to >10 cm in diameter filled with yellowish brown sediment (Fig. 5.4). Krotovina were distinguishable by their darker, brown color, which contrasted with the surrounding gray sand. Two IRSL samples were extracted from the JAC profile: sample JAC-1 was taken from within the yellow loess layer at 0.6 m depth, just above the transition between loess and sand, and sample JAC-2 was extracted just below the stratigraphic contact within the aeolian gray sand at a depth of 1.2 m below the crest of the dune. Post-IR dating yielded luminescence ages of 10.44 ± 0.98 ka for JAC-1 and 11.31 ± 1.06 ka for JAC-2.

A third IRSL sample (COS-3) was collected via auguring downwards from 2 m below the dune crest. No significant changes in stratigraphy occurred to a depth of 5.4 m, at which point some mottling in the form of red, iron-oxide nodules was noted. Sample COS-3 was extracted from 7.7 m below the dune crest and analysis yielded a luminescence age of 15.57 ± 1.66 ka.

Figure 5.4. Patches of darker colored sediment indicate several krotovina (back-filled burrows) at the Jacobson site (Photograph: C. Messner).

5.2.3 Red Tower site (64.526, -149.067)

The Red Tower site is located ~4 km south of Nenana and is possibly an extension of the Three Towers dune that extends southward from the site. A gravel driveway separates the two dunes, which are estimated to have a combined original footprint as large as ~85,800 m^2. The elevation of the Red Tower dune is approximately 129 m above sea level. Parks Highway

dissects the Red Tower dune and exposes ~4 m of dune stratigraphy on both side of the highway, indicating an elongated axis oriented in an east-west direction.

A profile was created on the west-facing road cut to expose upper dune stratigraphy for sampling ranging from 0.5–1.6 m below the dune crest. A yellow loess cap contained a weakly-developed surface soil within the top 10 cm of the profile, with the loess-sand contact boundary occurring ~1.1 m below the crest surface. Gray aeolian sand extended below the loess cap. Horizontal aeolian bedding ~1 cm width, was visible throughout the gray sand. Sample RED-1 was taken from a depth of 1.6 m below the dune crest and yielded a luminescence age of 12.91 ± 1.17 ka. A second IRSL sample (RED-2) was taken from across the Parks Highway road cut from atop the dune surface. A bucket auger was used to collect sample RED-2 from a depth of 6.34 m below the surface, which was just above the depth of permafrost. There were no significant changes visible in stratigraphy. Analysis of sample RED-2 yielded a luminescence age of 16.02 ± 1.72 ka.

5.2.4 Three Towers site (64.524, -149.068)

The Three Towers site is located ~0.3 km south of the Red Tower site, and the dune form is dissected by the Parks Highway to reveal ~6.5 m of dune stratigraphy on both sides of the highway. Elevation of the dune crest is approximately 128 m above sea level. A profile was cleaned to expose dune stratigraphy from 1.8–2.8 m below the dune crest. Excavation was conducted at a deeper depth to avoid the uppermost sediment that had been disturbed by humans, as evidenced by human disturbance and some visible slumping near the surface (Fig. 5.5). A well-sorted yellow loess cap extended ~0.6 m below the crest surface, which may reflect post-depositional disturbance, underlain by well-sorted aeolian gray sand. Aeolian bedding dipping

approximately 30° toward the south as well as several lenses of coarse sand were evident between 0.2–0.3 m below the dune crest. Sample THR-1 was extracted from 2.4 m below the dune crest and yielded a luminescence age of 11.39 ± 1.6 ka.

Figure 5.5. Human disturbance (ATV tracks) at the Three Towers site. Inset shows visible slumping due to post-depositional disturbance near dune surface (Photographs: W. Johnson and C. Messner).

5.2.5 Beekeeper site (64.505, -149.071)

The Beekeeper site is located ~6.3 km south of Nenana and is separated from the Boulden site by the Parks Highway. Based on the dune's location, it appears it could be an eastward extension of the sand formation sampled at the Boulden site across the road. A gradually sloping surface exposes ~3 m of dune stratigraphy at the Beekeeper site that may

represent the eastern flank of the Boulden dune. Elevation of the highest part of the dune surface is approximately 132 m above sea level. A profile was constructed extending 1.0 m downwards from the crest of the dune. The stratigraphy consisted of well-sorted yellow loess cap transitioning to well-sorted gray sand ~0.3 m below the crest, which is a thinner loess cap than seen at all but the Chevron site. One IRSL sample (BEE-1) was extracted from within the gray sand at 0.9 m below the surface, which yielded a luminescence age of 11.62 ± 1.06 ka.

5.2.6 Boulden site (64.506, -149.074)

The Boulden site is located ~6.3 km south of Nenana and ~0.1 km west of the Beekeeper site and the Parks Highway and consists of an isolated dune with an elongated axis in a north-south direction. Dune crest elevation is approximately 141 m above sea level, and the dune appears to cover ~137,600 m^2. Given the lack of road cut exposures, all samples were extracted using a bucket auger. Sample BOL-1 was taken at the northern flank of the dune from 1.6 m below the surface. Analysis yielded a luminescence age of 12.27 ± 1.28 ka. About 60 m to the south of BOL-1, samples BOL-3 and BOL-4 were taken from the crest of the dune at depths 1.4 m and 6.2 m below the surface, respectively. BOL-3 yielded a luminescence age of 12.87 ± 1.16 ka and BOL-4 yielded a luminescence age of 13.02 ± 1.42 ka. BOL-2 was taken ~124 m south of the crest at the southern flank of the dune from 1.25 m below the surface. Analysis of BOL-2 yielded a luminescence age of 12.71± 1.46 ka.

5.2.7 Chevron site (64.494, -149.078)

The Chevron site is the southernmost site location, located ~7.6 km south of Nenana and ~0.3 km west of the Parks Highway. An isolated dune form at the site appears to have a slightly

elongated axis in the north-south direction. Dune crest elevation is approximately 135 m above sea level, and the footprint of the dune is estimated to be ~49,500 m^2. As with the Boulden site, the lack of road cut exposures required that a bucket auger be used for sampling. The stratigraphy at this site was notably different from all other sample locations.

A yellow loess cap was absent at the Chevron site; instead, pale brown sediment (10YR 6/3) extended from the surface to the maximum auguring depth of 4.2 m. Sediment was nearing saturation and permafrost below this depth. It is possible that human disturbance is responsible for the lack of a loess cap, or perhaps a natural fire that would have decreased vegetation, allowing for deflation of the surface sediment. However, given the average 1 m thickness of the yellow loess cap seen at other sites, it seems unlikely that either of these disturbances could be responsible for removing the entirety of the loess cap. A third possibility, and the most likely explanation, is that a localized difference in vegetation could account for the lack of a loess deposit. Given that a presence of vegetation worked to trap finer, silt-sized particles at the other site locations, it may be that the Boulden site was devoid of ample trapping vegetation, which could explain the lack of a loess cap seen at the site. Further investigation of the Boulden stratigraphy as well as surrounding areas is necessary for definitive statements to be made.

Chapter 6 Discussion

A luminescence-generated chronology indicates dune activity extended from the Late Pleistocene (16 ka) and into the early Holocene (11–10 ka). Basal samples, or those taken as deep as or deeper than the elevation of interdunal areas, suggest dune activity occurred during the Older Dryas (16 ka), with the most recent dune activity, or those samples taken at shallower depths, occurring as late as the beginning of the Holocene Thermal Maximum (HTM; 11–8 ka). The sand dunes were then covered by a Holocene-age loess cap; the only dune without a loess cap was that at the Chevron site (Fig. 5.1).

All IRSL ages are stratigraphically consistent and correspond with aeolian activity throughout the TRL and adjoining valleys, primarily occurring during the Late Pleistocene to early Holocene transition. In particular, the Nenana ages closely align with those of the proximal Wood River dune field, which has similar aeolian stratigraphy, vegetation patterns, and resides within the same climatic zone. The section that follows includes supporting evidence for ages produced within this research through examining paleoclimatic and -environmental conditions at the end of the Pleistocene. In lieu of independent age control within the Nenana dunes, proxy data, such as landform ages, sediment cores, and pollen data, is used to determine whether the ages are representative of past aeolian activity and whether the pIR IRSL protocol is a reliable method for dating sand dunes within central Alaska.

Given the limited number of chronologically-based dune studies in central Alaska, proxies from other parts of Alaska and evidence from northwestern Canada are included within the discussion to provide a regional perspective. This research serves as a starting point for understanding the chronology of aeolian activity of the Nenana dune field, and this chapter

closes with suggested future studies to expand upon and augment further investigations of the Nenana dune field and surrounding area.

6.1 Comparison of Nenana Ages with Regional Proxies

The Nenana luminescence ages that indicate sand deposition within the Nenana dune field occurred as early as 16 ka and transitioned towards dune stabilization and accumulation of loess between 11 ka and 10 ka. This chronology aligns well with evidence of widespread aeolian activity during the Late Pleistocene and into the Holocene period in central Alaska and northwest Canada. A combination of radiocarbon and luminescence ages indicate that sand sheet aggradation occurred during the last glacial maximum, or Duvanny Yar interval (25–14 ka; Hopkins, 1982), in northern Alaska (Hamilton et al., 1984; 1988; Dijkmans and Koster, 1990), and central Alaska (e.g., Hopkins, 1982; Collins, 1985; Lea and Waythomas, 1990; Muhs et al., 2003; Reuther, 2013). In the Tuktoyaktuk Coastlands, the accumulation of sand dunes and sand sheets took place between approximately 30 ka and 8 ka, with stabilizing conditions occurring during the Holocene (Bateman and Murton, 2006). Throughout these areas, the deglaciation of the ice sheets near the end of the Pleistocene was responsible for an influx of sediment into glacially-fed river systems (Fig. 2.3), which include the Tanana and Nenana rivers of central Alaska that likely served as a primary source for the TRL aeolian sediment (Péwé, 1975; Collins, 1985; Muhs and Budahn, 2006).

Southwesterly winds characterize current wind systems in central Alaska during the summer months (Collins, 1985; National Climatic Data Center, 2015) (Fig. 3.2). Although the exact direction of the dune forming paleowinds cannot be determined from this study, dune morphology suggests southwesterly winds were also largely responsible for the deflation and

accumulation of sand and loess that formed the Nenana dunes. Muted signs of bedding within the Nenana dunes favor a north-northeast dune orientation (Collins, 1985), as well as the north–south positioning of the Nenana dunes east of the Nenana River also support this hypothesis. Furthermore, reported ages from the loess north of Fairbanks support the timing of southwesterly winds within the TRL during the Late Pleistocene to early Holocene transition (Muhs et al., 2003), and geochemical evidence of the loess deposits confirmed the Tanana River to the south as their primary sediment source (Muhs and Budahn, 2006). It is possible that strong katabatic winds provided the necessary transport capacity for aeolian deflation within the Nenana valley as the ice sheets retreated (Thorson and Bender, 1985), while in regions farther from the Alaska Range, such as the Kantishna sand sea, northeasterly winds had more influence (Collins, 1985; Lea, 1996). Conversely, differing paleowinds for the Tanana River Lowlands and Kantishna sand sea could have been reflective of different periods of aeolian activity. For example, the Kantishna sand sea may also be a result of the topography of the region, specifically the morphology and orientation of the southwestern tip of the Yukon-Tanana Upland (Fig. 3.4), which may have generated localized winds channeling across the lowlands.

The transition between the Late Pleistocene and early Holocene (16–11 ka) brought increases in air temperature and resulting deeper thaws (e.g., Hopkins, 1982; Edwards et al., 2001), which may have increased sediment supply for aeolian landforms. Aeolian activity continued throughout this period in central Alaska (e.g., Hopkins, 1982; Lea and Waythomas, 1990; Lea, 1996; Dilley, 1998; Reuther, 2013), and in areas of northwest Canada, including central Alberta and Saskatchewan between 16 ka and 11 ka (Wolfe et al., 2004). While aeolian activity is reported in the Tuktoyaktuk Coastlands for this period, Bateman and Murton (2006) detailed a shift towards accumulation dominated by sand sheets during this time, rather than sand

dunes. Surface armoring of sediment may have decreased supply, and warmer temperatures were accompanied by a rapid increase in moisture and vegetation ~14 ka that may also have limited aeolian activity (Edwards et al., 2001; Bateman and Murton, 2006). Within the Tanana River Lowlands (TRL), however, dune formation did not appear to be limited; the Nenana dune maximum-limiting ages indicate that dune formation occurred as long ago as 16 ka and likely continued until 11–10 ka (Table 5.1). Preserved bedding visible at several sample sites as well as a lack of observed paleosols implies that the rate of sand aggradation kept ahead of pedogenic processes, occurring rapidly enough to prevent surface stabilization and soil development; however, finer sampling resolution is necessary to provide information on whether dune aggradation rates remained consistent and for verification that periods of erosion did not remove sediment from within the dune, including paleosols that represent periods of dune stability.

The Holocene Thermal Maximum brought increasing summer insolation and moister conditions (Hopkins, 1982) that seemingly led to the time-transgressive expansion of the boreal forest throughout interior Alaska and western Canada around 10–9 ka that stabilized aeolian sediment within the region (e.g., Wolfe et al., 2011). The expansion of boreal forest coincides with the minimum-limiting ages of the Nenana dune field of 11–10 ka and is believed to be the primary cause for the slowing of dune sand aggradation and gradual stabilization.

Around the time of dune stabilization, a transition from sandy to silty sediment occurred in the Nenana dune field between 11 ka and 10 ka (Table 5.1). Some aeolian records from central Alaska indicate an earlier such change occurring 14–13 ka that is likely tied also to the spread of the boreal forest throughout central Alaska (e.g., Reuther, 2013). Muhs et al. (2003) proposed that Holocene loess accumulation was due in large part to the ability of vegetation to trap silt-sized particles. Due to their finer texture, the finer material would likely not have damaged the

underlying vegetation (Collins, 1985). The presence of vegetation probably affected the accumulation of the loess cap in a similar fashion that occurred as the Nenana dunes began to stabilize with vegetation. This can be seen today near Delta Junction in central Alaska, where detailed mapping of loess distribution (Lindholm et al., 1959; Péwé and Holmes, 1964) revealed that most loess is found within the boreal forest, whereas many upland surfaces above the tree line consist of little to no loess covering (Muhs et al., 2003). Similarly, a decrease in wind intensity may have led to less carrying capacity during this time, and moister conditions may have helped establish vegetation to trap smaller windblown particles (Reuther, 2013).

Given the abundance of stabilizing forest vegetation found throughout the Nenana dune field, Holocene reactivation does not seem likely once loess accumulation began around 10 ka. While loess accumulation is documented throughout the early Holocene (e.g., Muhs et al., 2003; Reuther, 2013), surrounding aeolian deposits within the Tanana Valley appeared to have become more stabilized by the mid-Holocene (6 ka) in comparison to the Late Pleistocene to early Holocene transition (Dilley, 1998; Reuther, 2013). In the adjacent Wood River dune field, in-situ archaeological artifacts yielded ages from within the upper loess deposits establishing stable conditions throughout the Holocene (Esdale et al., 2012), which further supports the notion that the Nenana dunes did not experience widespread reactivation during the Holocene. However, it is possible that the lack of silt seen at the Chevron site could be an indication of localized reactivation, possibly influenced by wildfire, as seen elsewhere in central Alaska (e.g., Reuther, 2013).

6.1.1 Wood River Age Comparison

Luminescence ages of the Wood River dunes provide a significant proxy comparison to those of the Nenana dunes. Both dune fields are within the TRL and are likely sourced primarily by adjacent alluvial systems. In addition, dunes at both locations are relatively similar in form and are currently stabilized with arboreal (tree and shrub) vegetation. Dune stratigraphy of the Wood River dunes is generally uniform consisting of 1–3.5 m of aeolian silts underlain by > 7 m of thinly bedded aeolian sands. Given these similarities, it is reasonable that luminescence ages documenting sand and loess deposition for the two dune fields overlap and show good agreement with each other. For example, the Wood River ages document aeolian deposition occurring between 15.40 ka and 9.65 ka. By comparison, the Nenana ages document aeolian deposition occurring between 16.02 ka and 10.36 ka. Accelerator mass spectrometry (AMS) radiocarbon ages taken from intact archaeological components throughout the Wood River silt deposits yielded mid- to early-Holocene ages of 6310–6480 cal yrs BP, 4340–4520 cal yrs BP, 1830–1990 cal yrs BP, and 260–310 cal yrs BP (reported to 2 Sigma cal yrs BP) (Esdale et al., 2012). These Holocene ages indicate that it is likely the Wood River dunes remained relatively stable throughout the Holocene during the accumulation of a loess cap, which is believed to also be the case for the Nenana dunes.

6.2 Future Studies

IRSL ages provide a chronological framework for aeolian activity of the Nenana dune field during the Late Pleistocene and early Holocene. Results indicate that luminescence analysis using a post-IR IRSL protocol is a useful technique for dating sand dunes of central Alaska and

serve as a starting point for future research aiming to expand upon the understanding of aeolian paleolandscapes within central Alaska.

Goals of this research were to provide age estimates on multiple dunes throughout the Nenana dune field by sampling crest, flank, and basal portions of the dunes. In-depth stratigraphic and chronologic analysis of the Nenana dunes would provide age control at a finer resolution for the timing of aeolian activity of these dunes. Continuous stratigraphic analysis, such as incremental sampling that extends from the crest down to the underlying sediment of each dune, is helpful for identifying whether sand accumulation was continuous, or if there were periods of disruption, such as erosion events, that were not apparent from observations of this project. Limited property access as well as limited time and resources precluded such investigations for this research, but future efforts conducting more complete stratigraphic and chronologic testing would provide finer sampling resolution for the dune chronology. Additionally, independent age control, such as that provided from radiocarbon samples taken at the same depths as luminescence samples, is an important component for chronologic studies. This can be difficult in aeolian settings, where sufficient organic material is often absent, but remains important nonetheless. Ideally, further investigations of the Nenana dunes would include a sampling strategy that allows for a source of age control to corroborate existing ages of Nenana dune formation and stabilization. This is currently being done at an archaeological investigation within the TRL on an alluvial terrace near Blair Lakes, an older archaeological site that has been resampled for luminescence dating in order to provide a method of independent age control for existing AMS ^{14}C radiocarbon ages. Preliminary results show relatively good agreement between a pIR IRSL luminescence sample age and an AMS ^{14}C age taken at nearly the same depth (J. Esdale, pers. comm.). Further attention to archaeological sites within the region (e.g., Upward

Sun River Site) will allow for supplementary IRSL testing using a pIR protocol where dating was previously limited.

The Nenana River channel and floodplain likely served as the primary sediment source for the Nenana dunes, given its proximity to the dunes and the existing literature on paleowinds within the TRL during dune activation periods. Future analysis consisting of samples taken from multiple locations along both rivers, has the potential to illustrate information about the sediment sources for the Nenana dunes within the TRL. In conjunction with geochemical research that would investigate sediment sourcing, research addressing paleowinds spanning the late glacial and interglacial periods would supplement the conflicting results of previous research regarding paleowinds within this time period.

A valuable extension of this study would be an extensive examination of the intersecting geomorphic systems in the area. For example, the periphery of the Nenana dune field consists of a dense network of meander scars, oxbow lakes, and meandering streams that have undoubtedly influenced these dune systems with respect to sediment supply, stabilization, sediment source, and erosion. Further testing could include radiocarbon dating of the alluvial sediments in order to provide further minimum-limiting ages of dune stabilization. Luminescence dating may prove problematic given the most recent fluvial origin of sediment (Rittenour, 2008), but could also provide an option for investigating the fluvial systems. An improved understanding of the adjoining geomorphic systems would give a clearer picture of the interaction of these systems, which is much more telling than examining the dune fields alone. Halfen et al. (2015) emphasized that relations between fluvial and aeolian geomorphic processes remain poorly understood: the authors proposed a sediment-state theory for the Central Plains dunes in which they describe rivers serving as sediment supply with respect to dune activity. Given the

complexity of geomorphic systems, it is appropriate to assume that similar linkages played a role with the Alaskan dunes.

Chapter 7 Conclusions

Since the initial mapping of surficial deposits of central Alaska by Péwé (1955), it has been well-recognized that aeolian deposits are ubiquitous throughout the area. Substantial loess deposits throughout Fairbanks have been thoroughly researched regarding the timing of aeolian accumulation as well as the sourcing of sediment (e.g., Muhs et al., 2003; Muhs and Budahn, 2006). The Tanana and Nenana valleys have also been the focus of extensive archaeological studies that have revealed the oldest known peopling sites of North America (e.g., Holmes and Dilley, 1996; Potter et al., 2008, 2011, 2014; Graf and Bigelow, 2011; Reuther 2013). Future studies of aeolian deposits will be strengthened with the incorporation of archaeological data, as prehistoric human behavior inherently reflects regional environmental conditions. Integrating cultural data with geologic and geographic studies produces a more dynamic interpretation of the region.

What is lacking from the published body of literature within central Alaska is detailed information concerning some of the smaller, isolated dune fields of central Alaska, including the Nenana dune field. The paucity of dune field data within the region is partially due to a lack of viable dating methods of aeolian stratigraphy. The majority of previous aeolian research sites examine cultural materials or organics within paleosols and tephra beds that provided the necessary organic material used for radiocarbon analysis. Without these conditions, however, organic material is often lacking in aeolian settings and prevents radiocarbon dating.

Luminescence dating is an ideal method for dating aeolian deposits in that it provides a direct age for the deposit being sampled and doesn't require a buildup of organic material. Instead, luminescence dating utilizes quartz and feldspar grains, which are common throughout

aeolian deposits. Until recently, luminescence dating of central Alaska has produced only limited success, as quartz grains within this high-latitude region tend to exhibit a dim sensitivity to luminescence (e.g., Munyikwa et al., 2011; Reuther, 2013). While feldspars emit a higher intensity signal and can be used to date older sediment using IRSL, they have been often been avoided as feldspar grains have been shown to suffer from anomalous fading (Wintle, 1973), which underestimates luminescence ages.

The first attempt of using an elevated temperature post-IR IRSL protocol (following Buylaert et al., 2009) in central Alaska was successful for dating Fairbanks loess (Roberts, 2012). A separate study of a vegetated dune field also located within the Tanana River Lowlands (TRL) showed similarly promising results in relation to surrounding aeolian proxy data (Johnson et al., 2012). These studies and their use of a post-IR IRSL protocol served as impetus for this research, while preliminary results of a post-IR luminescence age show general agreement with a corroborating AMS ^{14}C age (J. Esdale, pers. comm.), which is promising for continued use of this technique.

This research sought to answer the question of when aeolian activity occurred in the form of dune formation and stabilization for the Nenana dunes of the TRL. Eighteen IRSL samples were collected from dune crests and basal depths above permafrost in order to identify changes in stratigraphy and determine whether sand accumulation was rapid or gradual. Dune flanks were sampled, where possible, as an exploratory focus since the Nenana dune form was largely amorphous, lacking distinct morphology in most cases.

An elevated temperature post-IR IRSL protocol following Buylaert et al. (2009) revealed sand accumulation occurring as early as 16 ka and as late as 11 ka with stratigraphic and reasonable agreement between sites. Two IRSL samples taken from the yellow loess yielded

ages around 10 ka, indicating a shift from sand to loess accumulation between 11 ka and 10 ka. All ages passed dose recovery tests and align with ages taken from a proximal dune field within the TRL with similar stratigraphy, vegetation, and climatic influences. Additionally, the Nenana IRSL ages generally align with regional paleoenvironmental proxies, including numerous radiocarbon ages from aeolian settings of the Tanana and Nenana valleys. Given that the IRSL ages seem reasonable stratigraphically and regionally, the elevated temperature post-IR IRSL protocol is considered a valid method for dating sand deposits within central Alaska.

In addition to investigating the timing of aeolian activity and testing the potential of a post-IR IRSL protocol, this research sought to place the chronologic information within a paleoenvironmental context. While the limited chronologic data provided in this study are unable to definitively answer questions regarding the paleowinds, sourcing, and climatic and environmental changes that dictated the formation of the Nenana dunes, this study serves as a starting point for further aeolian research and can add to the existing literature of environmental changes that occurring during the Late Pleistocene and early Holocene periods.

Late Glacial and early Holocene ages of the Nenana dunes support the potential for early archaeological components found within similar settings throughout the Nenana and Tanana valleys. The aeolian settings of many of the primary archaeological sites, including the Upward Sun River Site, Shaw Creek Flats, and Swan Point, consist of loess deposits underlain by aeolian sand, which is analogous to the Nenana dune stratigraphy. The majority of cultural artifacts within the bottom portion of the loess yield ages in agreement with the Nenana ages above the loess-sand contact that document the most recent sand accumulation occurring around 11 ka, followed by a shift to silt accumulation 11 ka and 10 ka. In sum, the timing of aeolian activity and dune stabilization is in agreement with the growing body of archaeological research

conducted throughout central Alaska and adds to the chronological framework that is imperative for developing understanding of the earliest peopling of North America.

References

Abbott, M.B., Finney, B.P., Edwards, M.E., Kelts, K.R., 2000. Lake-level reconstructions and paleohydrology of Birch Lake, central Alaska, based on seismic reflection profiles and core transects. Quaternary Research 53, 154–166.

Ager, T.A., 1983. Holocene vegetational history of Alaska. In: Wright Jr., H.E. (Ed.), Late Quaternary Environments of the United States, The Holocene, Vol. 2. University of Minnesota Press, Minneapolis, pp. 128–141.

Ager, T.A., Brubaker, L., 1985. Quaternary palynology and vegetation history of Alaska. In: Bryant Jr., V.M., Holloway, R.G. (Eds.), Pollen Records of Late-Quaternary North American Sediments. American Association of Stratigraphic Palynologists Foundation, Dallas, Texas, pp. 353–383.

Aitken, M.J., 1985. Thermoluminescence Dating. Academic Press, London.

Aitken, M.J., 1998. An Introduction to Optical Dating. Oxford University Press, Oxford.

Anderson, P.M., Brubaker, L.B., 1994. Vegetation history of northcentral Alaska: a mapped summary of Late-Quaternary pollen data. Quaternary Science Reviews 13, 71–92.

Anderson, P.M., Edwards, M.E., Brubaker, L.B., 2004. Results and paleoclimate implications of 35 years of paleoecological research in Alaska. In: Gillespie, A.R., Porter, S.C., Atwater, B.F., (Eds.), The Quaternary Period in the United States. Developments in Quaternary Science 1. Elsevier, Amsterdam, pp. 427-440.

Arnold, L.J., Demuro, M., Parés, J.M., Pérez-González, A., Arsuaga, J.L., Bermúdez de Castro, J.M., Carbonell, E., 2014. Evaluating the suitability of extended-range luminescence dating techniques over early and Middle Pleistocene timescales: Published datasets and case studies from Atapuerca, Spain, Quaternary International, *in press*, doi:10.1016/j.quaint.2014.08.010.

Auclair, M., Lamothe, M., Huot, S., 2003. Measurement of anomalous fading for feldspar IRSL using SAR. Radiation Measurements 37, 487–492.

Auclair, M., Lamothe, M., Lagroix, F., Banerjee, S.K., 2007. Luminescence investigation of loess and tephra from Halfway House section, Central Alaska. Quaternary Geochronology 2, 34–38.

Barber, V.A., Finney, B.P., 2000. Late Quaternary paleoclimatic reconstructions for interior Alaska based on paleolake-level data and hydrologic models. Journal of Paleolimnology 24, 29–41.

Bartlein, P.J., 1997. Paleoclimatic variations in Beringia: Large-scale controls and regional responses in general circulation model simulations. In: Edwards, M.E., Sher, A.V.,

Guthrie, R.D. (Eds.), Terrestrial Paleoenvironmental Studies in Beringia. The Alaska Quaternary Center, University of Alaska, Fairbanks, Alaska, pp. 43–47.

Bateman, M.D., Murton, J.B., 2006. The chronostratigraphy of Late Pleistocene glacial and periglacial aeolian activity in the Tuktoyaktuk Coastlands, NWT, Canada. Quaternary Science Reviews 25, 2552–2568.

Begét, J.E., 1988. Tephras and sedimentology of frozen loess. In: Senneset, K. (Ed.), Fifth International Permafrost Conference Proceedings, Vol. 1. Tapir, Trondheim, pp. 672–677.

Begét, J.E., 1990. Middle Wisconsin climate fluctuations recorded in central Alaskan loess. Géographie Physique et Quaternaire 44, 3–13.

Begét, J.E., 1991. Paleoclimatic significance of high latitude loess deposits. In: Weller, G. (Ed.), International Conference on the Role of the Polar Regions in Global Change, Vol. II. Geophysical Institute, University of Alaska, Fairbanks, Alaska, pp. 594–598.

Begét, J.E., 1996. Tephrochronology and paleoclimatology of the last interglacial-glacial cycle recorded in Alaskan loess deposits. Quaternary International 34–36, 121–126.

Begét, J.E., 2001. Continuous Late Quaternary proxy climate records from loess in Beringia. Quaternary Science Reviews 20, 499–507.

Begét, J.E., Hawkins, D.B., 1989. Influence of orbital parameters on Pleistocene loess deposition in central Alaska. Nature 337, 151–153.

Begét, J.E., Stone, D.B., Hawkins, D.B., 1990. Paleoclimatic forcing of magnetic susceptibility variations in Alaskan loess during the Quaternary. Geology 18, 40–43.

Berger, G.W., 1978. Thermoluminescence dating of the Pleistocene Old Crow tephra and adjacent loess, near Fairbanks, Alaska. Canadian Journal of Earth Sciences 24, 2975–1984.

Berger, G.W., 2003. Luminescence chronology of late Pleistocene loess-paleosol and tephra sequences near Fairbanks, Alaska. Quaternary Research 60, 70–83.

Berger, G.W., Anderson, P.M., 2000. Extending the geochronometry of arctic lake cores beyond the radiocarbon limit by using thermoluminescence. Journal of Geophysical Research 105, 15439–15455.

Berger, G.W., Boardman, P.C., Brubaker, L.B., Anderson, P.M., 2000. Mineralogical controls on luminescence ages for a core from Ahaliorak Lake, northern Alaska. Geological Society of America, Abstracts with Programs 32, A324.

Berger, G.W., Péwé, T.L., 2001. Last interglacial age of the Eva Forest Bed, central Alaska, from thermoluminescence dating of bracketing loess. Quaternary Science Reviews 20, 485–498.

Berger, G.W., Péwé, T.L., Westgate, J.A., Preece, S.J., 1996. Age of Sheep Creek tephra (Pleistocene) in central Alaska from thermoluminescence dating of bracketing loess. Quaternary Research 45, 263–270.

Berger, G.W., Pillans, B.J., Palmer, A.S., 1994. Test of thermoluminescence dating of loess from New Zealand and Alaska. Quaternary Science Reviews 13, 309–333.

Bigelow, N.H., 1997. Late Quaternary vegetation and lake level changes in central Alaska. Ph.D. dissertation, Department of Anthropology, University of Alaska, Fairbanks, Fairbanks.

Bigelow, N.H, Begét, J.E., Powers, W.R., 1990. Latest Pleistocene increase in wind intensity recorded in eolian sediments from central Alaska. Quaternary Research 34, 160–168.

Bigelow, N.H., Edwards, M.E., 2001. A 14,000 yr paleoenvironmental record from Windmill Lake, central Alaska: Lateglacial and Holocene vegetation in the Alaska range. Quaternary Science Reviews 20, 203–215.

Bigelow, N.H., Powers, W.R., 2001. Climate, vegetation, and archaeology 14,000-9000 cal yr B.P. in central Alaska. Arctic Anthropology 38, 171–195.

Black, R.F., 1951. Eolian deposits of Alaska. Arctic 4, 89–111.

Buylaert, J.P., Murray, A.S., Thomsen, K.J., Jain, M., 2009. Testing the potential of an elevated temperature IRSL signal from K-feldspar. Radiation Measurements 44, 560–565.

Carter, L.D., Robinson, S.W., 1978. Eolian sand and interbedded organic horizons at Kealok Creek on the Arctic Coastal Plain of Alaska: possible regional implications. U.S. Department of the Interior Geological Survey, Open File Report 78–320.

Collins, F.R., 1985. A map showing a vegetated dune field in central Alaska. U.S. Geological Survey, Miscellaneous Field Studies Map MF-1708.

David, P.P., 1977. Sand dune occurrences of Canada: a theme and resource inventory of eolian landforms in Canada. Indian and Northern Affairs, National Parks Branch, Contract No. 74-230, pp. 183.

Demuro, M., Arnold, L.J., Froese, D.G., Roberts, R.G., 2013. OSL dating of loess deposits bracketing Sheep Creek tephra beds, northwest Canada: Dim and problematic single-grain OSL characteristics and their effect on multi-grain age estimates. Quaternary Geochronology 15, 67–87.

Dijkmans, J.W.A., Koster, E.A., 1990. Morphological development of dunes in a subarctic environment, central Kobuk valley, north-western Alaska. Geografiska Annaler 72A, 93–109.

Dilley, T.E., 1998. Late Quaternary loess stratigraphy, soils, and environments of the Shaw Creek Flats paleoindian sites, Tanana Valley, Alaska. Ph.D. dissertation, Department of Geosciences, University of Tucson, Tucson.

Duller, G.A.T., 2004. Luminescence dating of quaternary sediments: recent advances. Journal of Quaternary Science 19, 183–192.

Dyke, A.S., 2004. An outline of North American deglaciation with emphasis on central and northern Canada. In: Ehlers, J.J., Gibbard, P.L. (Eds.), Quaternary Glaciations e Extent and Chronology, Part II. Elsevier, London, pp. 373–424.

Dyke, A.S., 2005. Late Quaternary vegetation history of northern North America based on pollen, macrofossil, and faunal remains. Géographie physique et Quaternaire 59, 211–262.

Dyke, A.S., Moore, A., Robertson, L., 2003. Revised North America deglaciation maps. Geological Survey of Canada, Open File 1574.

Edwards, M.E., Mock, C.J., Finney, B.P., Barber, V.A., Bartlein, P.J., 2001. Potential analogues for paleoclimatic variations in eastern interior Alaska during the past 14,000 yr: atmospheric-circulation control of regional temperature and moisture responses. Quaternary Science Reviews 20, 189–202.

Esdale, J.A., Gaines, E.P., Yeske, K.S., McLaren, W.E., Shimel, M., Kunesh, J.F., 2012. Cultural Resources Survey and Evaluation, Fort Wainwright and Training Lands, 2010 and 2011. Central for the Environmental Management of Military Lands, Colorado State University, Section 110 Report, pp. 449.

Fernald, A.T., 1964. Surficial geology of the central Kobuk River valley, northwestern Alaska. United States Geological Survey Bulletin 1181-K, K1–K31.

Finkenbinder, M.S., Abbott, M.B., Edwards, M.E., Langdon, C.T., Steinman, B.A., Finney, B.P., 2014. A 31,000 year record of paleoenvironmental and lake-level change from Harding Lake, Alaska, USA. Quaternary Science Reviews 87, 98–113.

Forman, S.L., Maat, P., 1990. Stratigraphic evidence for the late Quaternary dune activity near Hudson on the Piedmont of Colorado. Geology 18, 745–748.

Foster, H.L., Keith, T.E.C., 1994. Geology of the Yukon-Tanana area of east-central Alaska. In: Plafker, G., Berg, H.C., (Eds.), The Geology of Alaska: U.S. Geological Society of America, 205–240.

Fuchs, M., Owen, L.A., 2008. Luminescence dating of glacial and associated sediments: review, recommendations and future directions. Boreas 37, 636–659.

Galbraith, R.F., Roberts, R.G., 2012. Statistical aspects of equivalent dose and error calculation and display in OSL dating: an overview and some recommendations. Quaternary Geochronology 11, 1–27.

Godfrey-Smith, D.I., Huntley, D.J., Chen, W.H., 1988. Optical dating studies of quartz and feldspar sediment extracts. Quaternary Science Reviews 7, 373–380.

Graf, K.E., Bigelow, N.H., 2011. Human response to climate during the Younger Dryas chronozone in central Alaska. Quaternary International 242, 434–451.

Halfen, A.F., Lancaster, N., Wolfe, S.A., 2015. Interpretations and common challenges of aeolian records from North American dune fields. Quaternary International, *in press*, http://dx.doi.org/10.1016/j.quaint.2015.03.003.

Hamilton, T.D., Ager, T.A., Robinson, S.W., 1983. Late Holocene ice wedges near Fairbanks, Alaska U.S.A.: Environmental setting and history of growth. Arctic and Alpine Research 15, 157–168.

Hamilton, T.D., Ashley, G.M., Reed, K.M., van Etten, D. P, 1984: Stratigraphy and sedimentology of Epiguruk Bluff. A preliminary Account. In: Reed, R.M., Bartsch-Winkler, S. (Eds.). The U. S. Geological Survey in Alaska: Accomplishments during 1982. U. S. Geological Survey Circulation 939, 12–15.

Hamilton, T.D., Craig, J.L., Sellmann, P.V., 1988. The Fox permafrost tunnel: a late Quaternary geological record in central Alaska. Geological Society of America Bulletin 100, 948–969.

Hinzman, L.D., Kane, D.L., 1992. Potential response of an Arctic watershed during a period of global warming. Journal of Geophysical Research 97, 2811–2820.

Holmes, C.E., 1996. Broken Mammoth. In: West, F.H. (Ed.), American Beginnings: The Prehistory and Paleoecology of Beringia, University of Chicago Press, Chicago, 312–318.

Holmes, C.E., 2001. Tanana River Valley Archaeology Circa 14,000 to 9,000 B.P. Arctic Anthropology 38, 154–170.

Holmes, C.E., Vanderhoek, R., Dilley, T.E., 1996. Swan Point. In: West, F.H., (Ed.), American Beginnings: The Prehistory and Paleoecology of Beringia. University of Chicago Press, 319–323.

Hopkins, D.M., 1982. Aspects of the paleogeography of Beringia during the late Pleistocene. In: Hopkins, D.M., Matthews Jr., J.V., Schweger, C.E., Young, S.B. (Eds.), Paleoecology of Beringia. Academic Press, New York, 3–28.

Huntley, D.J., Godfrey-Smith, D.I., Thewalt. M.L.W., 1985. Optical dating of sediments. Nature 313, 105–107.

Huntley, D.J., Lamothe, M., 2001. Ubiquity of anomalous fading in K-feldspars and the measurement and correction for it in optical dating. Canadian Journal of Earth Science 38, 1093–1106.

Hütt, G., Jaek, I., Tchonka, J., 1988. Optical dating: K-feldspars optical response stimulation spectra. Quaternary Science Reviews 7, 381–385.

Jensen, B.J., 2013. Tephrostratigraphy and paleoenvironments of the late Quaternary in eastern Beringia. PhD thesis, University of Alberta, Edmonton.

Johnson, W.C., Hanson, P.R., Halfen, A.F., Gaines, E.P., 2012. Success in dating late-Pleistocene dunes in central Alaska using a Post-IR IRSL protocol: UK Luminescence and ESR Meeting, Aberystwyth, September.

Kaufman, D.S., 29 others, 2004. Holocene thermal maximum in the western Arctic (0–180°W). Quaternary Science Reviews 23, 529–560.

Kocurek, G., Lancaster, N., 1999. Aeolian system sediment state: theory and Mojave Desert Kelso dune field example. Sedimentology 46, 505–515.

Kokorowski, H.D., Anderson, P.M., Mock, C.J., Lozhkin, A.V., 2008. A Re-evaluation and Spatial Analysis for a Younger Dryas Climatic Reversal in Beringia. Quaternary Science Reviews 27, 1710–1722.

Lagroix, F., Banerjee, S.K., 2002. Paleowind directions from the magnetic fabric of loess profiles in central Alaska. Earth and Planetary Science Letters 195, 99–112.

Lagroix, F., Banerjee, S.K., 2004. The regional and temporal significance of primary aeolian magnetic fabrics preserved in Alaskan loess. Earth and Planetary Science Letters 225, 369–385.

Lamothe, M., Auclair, M., Hamzaoui, C., Huot, S., 2003. Towards a prediction of long-term anomalous fading of feldspar IRSL. Radiation Measurements 37, 493–498.

Lancaster, N., 1995. Geomorphology of Desert Dunes. Routledge, London.

Lancaster, N., 2009. Aeolian Features and Processes. In: Young, R., Norby, L. (Eds.), Geological Monitoring. Geological Society of America, Boulder, pp. 1-25.

Lea, P.D., 1990. Pleistocene periglacial eolian deposits in southwestern Alaska: sedimentary facies and depositional processes. Journal of Sedimentary Petrology 60, 582–591.

Lea, P.D., 1996. Vertebrate tracks in Pleistocene eolian sand-sheet deposits of Alaska. Quaternary Research 45, 226–240.

Lea, P.D., Waythomas, Christopher F., 1990. Late-Pleistocene eolian sand sheets in Alaska. Quaternary Research 34, 269 – 281.

Li, B., Jacobs, Z., Roberts, R.G., Li, S.H., 2014. Review and assessment of the potential of post-IR IRSL dating methods to circumvent the problem of anomalous fading in feldspar luminescence. Geochronometria 41, 178–201.

Li, S.H., Chen Y.Y., Li, B., Sun, J.M., Yang, L.R., 2007. OSL dating of sediments from desert in northern China. Quaternary Geochronology 2, 23–28.

Lian, O.B., Huntley, D.J., Wolfe, S.A., 2002. Optical dating of eolian sand from the Canadian prairies. Geographie Physique et Quaternaire 56, 191–202.

Lian, O.B., Roberts, R.G., 2006. Dating the Quaternary: progress in luminescence dating of sediments. Quaternary Science Reviews 25, 2449–2468.

Lindholm, G.F., Thomas, L.A., Davidson, D.T., Handy, R.L., Roy, C.J., 1959. Silts near Big Delta and Fairbanks. In: Davidson, D.T., Roy, C.J. (Eds.), The geology and engineering characteristics of some Alaskan soils. Iowa State University Bulletin 186, 33–70.

Lukas, S., Preusser, F., Anselmetti, F.S., Tinner, W., 2012. Testing the potential of luminescence dating of high-alpine lake sediments. Quaternary Geochronology 8, 23–32.

Manley, W.F., 2002. Postglacial Flooding of the Bering Land Bridge: A Geospatial Animation. Volume 1. INSTAAR, University of Colorado, Boulder. Electronic data available at http://instaar.colorado.edu/QGISL/bering_land_bridge/. Last accessed May 15, 2015.

Mann, D.H., Heiser, P.A., Finney, B.P., 2002. Holocene history of the Great Kobuk sand dunes, northwestern Alaska. Quaternary Science Reviews 21, 709–731.

Mejdal, V., Funder, S., 1994. Luminescence dating of Late Quaternary sediments from East Greenland. Boreas 23, 525–535.

Muhs, D.R., Ager, T.A., Begét, J., 2001. Vegetation and paleoclimate of the last interglacial period, central Alaska. Quaternary Science Reviews 20, 41–61.

Muhs, D. R., Ager, T.A., Bettis, E.A., McGeehin, J.P., Been, J.M., Begét, J.E., Pavich, M.J., Stafford, Jr., T.W., Stevens, D.A.S.P., 2003. Stratigraphy and palaeoclimatic significance of Late Quaternary loess–palaeosol sequences of the Last Interglacial–Glacial cycle in central Alaska. Quaternary Science Reviews 22, 1947–1986.

Muhs, D.R., Budahn, J.R., 2006. Geochemical evidence for the origin of late Quaternary loess in central Alaska. Canadian Journal of Earth Science 43, 323–337.

Muhs, D.R., Wolfe, S.A., 1999. Sand dunes of the northern Great Plains of Canada and the United States. In: Lemmen, D.S., Vance, R.E. (Eds.), Holocene Climate and Environmental Change in the Palliser Triangle: a Geoscientific Context for Evaluating the Effects of Climate Change on the Southern Canadian Prairies. Geological Survey of Canada, Bulletin 534, 183–197.

Murray, A.S., Roberts, R.G., 1998. Measurement of the equivalent dose in quartz using a regenerative-dose single-aliquot protocol. Radiation Measurements 29, 503–515.

Murray, A.S., Wintle, A.G., 2000. Luminescence dating of quartz using an improved single-aliquot regenerative-dose protocol. Radiation Measurements 32:57–73.

Munyikwa, K., Feathers, J.K., Rittenour, T.M., Shrimpton, H.K., 2011. Constraining the Late Wisconsinan retreat of the Laurentide ice sheet from western Canada using luminescence ages from postglacial aeolian dunes. Quaternary Geochronology 6, 407–422.

Murton, J.B., Frechen, M., Maddy, D., 2007. Luminescence dating of mid- to Late Wisconsinan aeolian sand as a constraint on the last advance of the Laurentide Ice Sheet across the Tuktoyaktuk Coastlands, western Arctic Canada. Canadian Journal of Earth Science 44, 857–869.

National Climatic Data Center, 2015. Annual Climate Normals (Temperature and Precipitation) for Nenana, AK. Last accessed: July 26, 2015.

National Climatic Data Center, 2015. Monthly wind roses for Fairbanks, AK. Available online via: http://www.wcc.nrcs.usda.gov/climate/windrose.html. Last accessed: July 17, 2015.

Nelson, R.E., Carter, D.L., Robinson, S.W., 1988. Anomalous radiocarbon ages from a Holocene detrital organic lens in Alaska and their implications for radiocarbon dating and palaeoenvironmental reconstructions in the Arctic. Quaternary Research 29, 66–71.

Oches, E.A., Banerjee, S.K., Solheid, P.A., Frechen, M., 1998. High-resolution proxies of climate variability in the Alaskan loess record. In: Busacca, A.J. (Ed.), Dust Aerosols, Loess Soils and Global Change. Washington State University College of Agriculture and Home Economics, Miscellaneous Publication No. MISC0190, Pullman, 167–170.

Péwé, T.L., 1955. Origin of the upland silt near Fairbanks, Alaska. Geological Society of America Bulletin 66, 699–724.

Péwé, T.L., 1965. Middle Tanana River Valley. In: Péwé, T.L., Ferrains, O.J., Nichols, D.R., Karlstrom, T.N.V., (Eds.) Guide to the Quaternary Geology: Central and South-Central Alaska, Division of Geological and Geophysical Surveys, Department of Natural Resources, College, Alaska, 36–54.

Péwé, T.L., 1975. Quaternary geology of Alaska. U.S. Geological Survey Professional Paper 835, 145 pp.

Péwé, T.L., Holmes, G.W., 1964. Geology of the Mt. Hayes D-4 Quadrangle, Alaska. U.S. Geological Survey. Miscellaneous Geological Investigations Map I-394. U.S. Government Printing Office, Washington D.C.

Péwé, T.L., Wahrhaftig, C., and Weber, F., 1966. Geologic map of the Fairbanks quadrangle, Alaska. U.S. Geological Survey, Miscellaneous Geological Investigations Map I-455, scale 1:250,000.

Pickering, R., Jacobs, Z., Herries, A.I.R., Karakanas, P., Bar-Mathews, M., Woodhead, J.D., Kappen, P., Fisher, E., Marean, C.W., 2013. Paleoanthropologically significant South African sea caves dated to 1.1–1.0 million years using a combination of U–Pb, TT-OSL and palaeomagnetism. Quaternary Science Reviews 65, 39–52.

Pietsch, T.J., Olley, J.M., Nanson, G.C., 2008. Fluvial transport as a natural luminescence sensitiser of quartz. Quaternary Geochronology 3, 365–376.

Potter, B.A., Irish, J.D., Reuther, J.D., Gelvin-Reymiller, C., Holliday, V.T., 2011. A terminal Pleistocene child cremation and residential structure from eastern Beringia. Science 331, 1058–1062.

Potter, B.A., Irish, J.D., Reuther, J.D., McKinney, H.J., 2014. New insights into Eastern Beringian mortuary behavior: A terminal Pleistocene double infant burial at Upward Sun River. Proceedings of the National Academy of Sciences 111, 17060–17065.

Potter, B.A., Reuther, J.D., Bowers, P.M., Gelvin-Reymiller, C., 2008. Little Delta Dune Site: A Late Pleistocene multi-component Site in central Alaska. Current Research in the Pleistocene 25, 132–135.

Preece, S.J., 1991. Tephrostratigraphy of the late Cenozoic Gold Hill Loess, Fairbanks area, Alaska. M.S. thesis, University of Toronto, Toronto.

Preece, S.J., Westgate, J.A., Stemper, B.A., Péwé, T.L., 1999. Tephrochonology of late Cenozoic loess at Fairbanks, central Alaska. Geological Society of America Bulletin 111, 71–90.

Prescott, J.R., Hutton, J.T., 1994. Cosmic ray contributions to dose rates for luminescence and ESR dating: large depths and long-term time variations. Radiation Measurements 23, 497–500.

Prescott, J.R., Robertson, G.B., 1997. Sediment dating by luminescence: a review. Radiation Measurements 27, 893–922.

Preusser, F., Andersen, B.G., Denton, G.H., Schlüchter, C., 2005. Luminescence chronology of Late Pleistocene glacial deposits in north Westland, New Zealand. Quaternary Science Reviews 24, 2207–2227.

Preusser, F., Chithambo, M.L., Götte, T., Martini, M., Ramseyer, K., and others, 2009. Quartz as a natural luminescence dosimeter. Earth-Science Reviews 97, 184–214.

Preusser, F., Degering, D., Fuchs, M., Hilgers, A., Kadereit, A., Klasen, N., Krbetschek, M., Richter, D., Spencer, J.Q.G., 2008. Luminescence dating: basics, methods and applications. Eiszeitalter und Gegenwart 57, 95–149.

Preusser, F., Ramseyer, K., Schlüchter, C., 2006. Characterisation of low OSL intensity quartz from the New Zealand Alps. Rad. Measurements 41, 871–877.

Reuther, J.D., 2013. Late glacial and early Holocene geoarchaeology and terrestrial paleoecology in the lowlands of the middle Tanana Valley, subarctic Alaska. PhD thesis (University of Arizona, Tucson).

Rhodes, E.J., 2011. Optically Stimulated Luminescence Dating of Sediments over the Past 200,000 Years. Annu. Reviews Earth Planet. Science 39, 461–488.

Rhodes, E.J., Pownall, L., 1994. Zeroing of the OSL signal in quartz from young glaciofluvial sediments. Radiation Measurements 23, 329–333.

Rittenour, T.M., 2008. Luminescence dating of fluvial deposits: applications to geomorphic, palaeoseismic and archaeological research. Boreas 37, 613–635.

Singhvi, A.K., Sharma, Y.P., Agrawal, D.P., 1982. Thermoluminescence dating of sand dunes in Rajasthan, India. Nature 295, 313–315.

Soil Survey Staff, Natural Resources Conservation Service, United States Department of Agriculture. 2007. Soil Survey of Greater Nenana Area, Alaska.

Soil Survey Staff, Natural Resources Conservation Service, United States Department of Agriculture. Web Soil Survey. Available online at http://websoilsurvey.nrcs.usda.gov/. Last accessed: July 1, 2015.

Steffen, D., Preusser, F., Schlunegger, F., 2009. OSL quartz age underestimation due to unstable signal components. Quaternary Geochronology 4, 353–362.

Stokes, S., 1999. Luminescence dating applications in geomorphological research. Geomorphology 29, 153–171.

Thiel, C., Buylaert, J.P., Murray, A., Terhorst, B., Hofer, I., Tsukamoto, S., Frechen, M., 2011. Luminescence dating of the Stratzing loess profile (Austria) – Testing the potential of an elevated temperature post-IR IRSL protocol. Quaternary International 234, 23–31.

Thomsen, K.J., Murray, A.S., Jain, M., Bøtter-Jensen, L., 2008. Laboratory fading rates of various luminescence signals from feldspar-rich sediment extracts. Radiation Measurements 43, 1474–1486.

Thorson, R.M., Bender, G., 1985. Eolian deflation by ancient katabatic winds: A late Quaternary example from the north Alaska Range. Geological Society of America Bulletin 96, 702–709.

Vlag, P.A., Oches, E.A., Banerjee, S.K., Solheid, P.A., 1999. The paleoenvironmental-magnetic record of the Gold Hill Steps loess section in central Alaska. Physics and Chemistry of the Earth A 24, 779–783.

Visocekas, R., 1985. Tunneling radiative recombination in labradorite: its association with anomalous fading of thermoluminescence. Nuclear Tracks and Radiation Measurements 10, 521–529.

Visocekas, R., Guerin, G., 2006. TL dating of feldspars using their far-red emission to deal with anomalous fading. Radiation Measurements 41, 942–947.

Wahrhaftig, C., 1965. Physiographic Divisions of Alaska. United States Government Printing Office, Washington D.C.

Wahrhaftig, C., 1985. Quaternary and Engineering Geology in the central part of the Alaska Range. Geological Survey Professional Paper 293, 116 pp.

Westgate, J.A., Stemper, B.A., Péwé, T.L., 1990. A 3 m.y. record of Pliocene–Pleistocene loess in interior Alaska. Geology 18, 858–861.

Westgate, J.A., Walter, R.C., Pearce, G.W., Gorton, M.P., 1985. Distribution, stratigraphy, petrochemistry, and palaeomagnetism of the late Pleistocene Old Crow tephra in Alaska and the Yukon. Canadian Journal of Earth Sciences 22, 893–906.

Wintle, A.G., 1973. Anomalous fading of thermoluminescence in mineral samples. Nature 245, 143–44.

Wintle, A.G., 1993. Luminescence dating of aeolian sands: an overview. Geological Society, London, Special Publications 72, 49-58.

Wintle, A.G., Murray, A.S., 2006. A review of quartz optically stimulated luminescence characteristics and their relevance in single-aliquot regeneration dating protocols. Radiation Measurements 41, 369–391.

Wintle, A.G., Westgate, J.A., 1986. Thermoluminescence age of Old Crow tephra in Alaska. Geology 14, 594–597.

Wolfe, S., Bond, J., Lamothe, M., 2011. Dune stabilization in central and southern Yukon in relation to early Holocene environmental change, northwestern North America. Quaternary Science Reviews 30, 324–334.

Wolfe, S.A., Gillis, A., Robertson, L., 2009. Late Quaternary Eolian Deposits of Northern North America: Age and Extent. Geological Survey of Canada. Open File 6006.

Wolfe, S.A., Huntley, D.J., Ollerhead, J., 2004. Relict late Wisconsinan dune fields of the northern Great Plains, Canada. Géographie Physique et Quaternaire 58, 323– 336.

Wolfe, S.A., Paulen, R.C., Smith, I.R., Lamothe, M., 2007. Age and paleoenvironmental significance of late Wisconsinan dune fields in the Mount Watt and Fontas River map areas, northern Alberta and British Columbia. Geological Survey of Canada: Current Research 2007 B4, pp. 10.

APPENDICES

Appendix A. Supplemental Data

Appendix B. Sample Site Images

Claire Anna Messner

Submitted as supplemental material for the thesis:

Post-IR IRSL dating of the Nenana dune field in the Tanana Lowlands, central Alaska

Appendix A. Supplemental Data

Table A.1. Dose rate, water content, and sample information for the Nenana dune samples.

Sample Name	USU num.	K %	Rb ppm	Th ppm	U ppm	Depth (m)	Wt. % H2O	Elev. (m)	Latitude/Longitude
THR-1	USU-1536	1.04	39	5	1.1	2.42	3.70%	128	64.524149, -149.068327
RED-1	USU-1537	0.89	30.6	2.8	0.9	1.58	1.56%	129	64.525989, -149.067326
RED-2	USU-1538	0.85	25.4	3.4	1	6.34	16.44%	129	64.526121, -149.068872
JAC-1	USU-1539	1.53	70.3	8.5	1.7	0.62	1.28%	128	64.531293, -149.058741
JAC-2	USU-1540	1.08	42.8	4.7	1.3	1.23	7.21%	128	64.531293, -149.058741
JAC-3	USU-1541	1.2	48.1	4.9	1.1	5.66	5.52%	128	64.531293, -149.058741
COS-1	USU-1542	1.77	76.8	9.5	1.8	0.93	9.47%	131	64.533050, -149.059522
COS-2	USU-1543	1.17	46.5	4.6	1.1	1.23	1.35%	131	64.533050, -149.059522
COS-3	USU-1544	1.03	38.4	4.1	1.1	5.7	19.33%	131	64.533050, -149.059522
COS-4	USU-1545	1.17	47.2	4.7	1.1	1.29	1.28%	126	64.533024, -149.059559
COS-5	USU-1546	1.14	42.8	4.8	1.1	1.04	2.70%	126	64.533024, -149.061374
COS-6	USU-1547	1.23	47.4	5.1	1.1	1.40	5.46%	126	64.533064, -149.059642
BEE-1	USU-1548	1.17	38.5	3.8	1.1	0.90	3.22%	132	64.505335, -149.071071
CHV-1	USU-1549	1.15	45.5	5.5	1.4	0.67	19.31%	135	64.494362,-149.078072
BOL-1	USU-1550	1	38.1	4.4	1.2	1.60	18.72%	137	64.505830, -149.074479
BOL-2	USU-1551	1.05	39.1	4.8	1.2	1.25	22.48%	132	64.504163, -149.073943
BOL-3	USU-1552	0.99	34.7	3.7	1.1	1.4	10.04%	141	64.505343, -149.074078
BOL-4	USU-1553	1.24	43.1	4.2	1.1	6.2	2.03%	141	64.505343, -149.074078

Notes:
1. Radioelemental concentrations determined by ALS Chemex using ICP-MS and ICP-AES techniques, dose rate is derived from concentrations by conversion factors from Guerin et al. 2011.
2. In-situ gravimetric water content, assumed 6±3% for moisture content to represent burial history for values <6%.
3. 17.9% used for H 2 O, the average of USU-1538 and USU-1544.
4. 22.5% used for H 2 O; average %K (1.01%) from USU-1550:1552 used for dose rate calculation.

Table A.2. 48-element geochemical results for Nenana dunes via ICP-MS/ICP-AES at ALS Minerals, Reno, NV.

SAMPLE	Recvd Wt. kg	Ag ppm	Al %	As ppm	Ba ppm	Be ppm	Bi ppm	Ca %	Cd ppm	Ce ppm	Co ppm	Cr ppm	Cs ppm
USU-1536	0.03	0.15	6.21	8.5	580	0.91	0.08	3.43	0.2	40.2	14.4	207	1.16
USU-1537	0.07	0.05	6.08	5.5	520	0.77	0.06	3.46	0.15	26.8	14.4	211	0.75
USU-1538	0.02	0.06	6.29	8	500	0.83	0.07	4.03	0.14	34	16.5	341	0.84
USU-1539	0.02	0.21	6.68	15.7	780	1.46	0.16	1.93	0.15	67.4	14.9	96	2.17
USU-1540	0.07	0.05	5.16	6	610	0.82	0.1	2.49	0.16	37.1	11.4	89	1.01
USU-1541	0.05	0.06	5.94	7.4	620	1.03	0.11	2.92	0.19	40.4	12.8	92	1.24
USU-1542	0.02	0.1	7.19	17.6	870	1.56	0.17	1.87	0.18	73	15.1	97	2.42
USU-1543	0.04	0.05	5.28	6.2	640	0.86	0.09	2.42	0.17	35.4	11.2	96	1.07
USU-1544	0.05	0.05	5.6	6.2	580	0.81	0.08	2.92	0.13	34.6	12.8	109	0.97
USU-1545	0.04	0.05	5.51	7.1	630	0.9	0.09	2.59	0.21	37.5	11.9	100	1.16
USU-1546	0.05	0.12	5.42	6.5	660	0.97	0.08	2.2	0.16	36.3	11.6	84	1.09
USU-1547	0.04	0.08	5.66	7.7	670	1.04	0.09	2.09	0.16	39.2	11.8	79	1.3
USU-1548	0.06	0.12	5.95	7.2	680	0.85	0.07	2.38	0.16	31.5	13	137	1
USU-1549	0.03	0.11	7.13	11.3	730	1.33	0.12	3.11	0.17	49.5	16.7	121	1.66
USU-1550	0.03	0.15	6.87	9.8	610	1.08	0.09	3.99	0.21	40.9	18.8	185	1.22
USU-1551	0.03	0.08	6.28	9.1	640	0.98	0.1	2.93	0.19	41.6	16.4	197	1.23
USU-1552	0.03	0.14	6.07	7.4	590	0.89	0.07	3.4	0.18	32.4	15.4	195	0.97
USU-1553	0.03	0.06	5.26	6.8	710	0.89	0.09	2.37	0.16	32.4	10.3	70	1.17

Table A.2. *(continued)*

SAMPLE	Cu ppm	Fe %	Ga ppm	Ge ppm	Hf ppm	In ppm	K %	La ppm	Li ppm	Mg %	Mn ppm	Mo ppm	Na %
USU-1536	32	3.79	12.4	0.05	1.2	0.04	1.04	19.9	15	1.62	706	0.58	1.67
USU-1537	25.7	3.43	12.25	0.14	1.2	0.039	0.89	13.7	11.7	1.65	673	0.34	1.85
USU-1538	33.7	4.14	12.6	0.06	1.2	0.045	0.85	16.4	13.1	1.83	753	0.52	1.82
USU-1539	36.5	3.9	15.1	0.09	1.3	0.053	1.53	34.3	21.2	1.29	649	0.87	1.45
USU-1540	21.5	2.82	11.2	0.16	1.4	0.033	1.08	19.1	13.7	1.2	554	0.47	1.52
USU-1541	26.4	3.26	12.85	0.15	1.5	0.04	1.2	20.3	15.7	1.33	631	0.62	1.71
USU-1542	39.4	4.09	15.9	0.11	1.3	0.051	1.77	36.9	22.6	1.34	681	0.77	1.42
USU-1543	21.2	2.93	11.2	0.16	1.3	0.034	1.17	17.9	14	1.2	567	0.52	1.5
USU-1544	24.4	3.17	12.05	0.13	1.4	0.037	1.03	17.5	13.6	1.36	641	0.51	1.67
USU-1545	23.3	3.09	11.85	0.14	1.4	0.034	1.17	19.4	14.7	1.26	591	0.59	1.55
USU-1546	23.4	2.97	10.95	0.07	1.3	0.032	1.14	18.4	15.2	1.21	583	0.58	1.47
USU-1547	28.2	3.12	11.85	0.08	1.2	0.038	1.23	20	16.5	1.18	579	0.7	1.52
USU-1548	29.1	3.28	11.15	0.06	1.1	0.034	1.17	16.4	15.6	1.48	626	0.56	1.67
USU-1549	42.2	4.29	14.95	0.1	1.3	0.054	1.15	24.9	21.3	1.68	798	0.55	1.88
USU-1550	43.7	4.41	14.5	0.08	1.5	0.052	1	20.3	18.2	1.92	805	0.74	1.87
USU-1551	38.2	3.97	13.1	0.08	1.3	0.041	1.05	21.1	17.4	1.68	756	0.56	1.73
USU-1552	35	3.71	12.05	0.06	1.4	0.043	0.99	16	15.1	1.69	687	0.56	1.72
USU-1553	24.8	2.74	10.3	0.11	1.4	0.031	1.24	16.4	16.4	1.13	490	0.63	1.47

SAMPLE	Nb ppm	Ni ppm	P ppm	Pb ppm	Rb ppm	Re ppm	S %	Sb ppm	Sc ppm	Se ppm	Sn ppm	Sr ppm	Ta ppm
USU-1536	6.6	54.9	660	10.1	39	<0.002	0.01	1.22	15.5	1	1.1	305	0.47
USU-1537	4.3	53.5	490	5.8	30.6	0.005	0.01	0.92	15.8	<1	0.9	318	0.33
USU-1538	5.9	66.2	640	6.3	25.4	<0.002	0.01	1.14	17.7	<1	1	347	0.43
USU-1539	9.4	44.2	670	13.5	70.3	<0.002	0.01	1.39	15.1	1	1.6	236	0.67
USU-1540	5.5	33.3	510	7.1	42.8	0.004	0.01	1	11.1	<1	1.1	250	0.43
USU-1541	6.2	35	660	7.8	48.1	0.005	<0.01	1.02	12.9	1	1.3	289	0.48
USU-1542	10.2	43.6	840	12.9	76.8	<0.002	0.01	1.54	15.4	1	1.7	233	0.72
USU-1543	5.5	33.1	530	7.6	46.5	0.005	0.01	1.03	11	<1	1.1	244	0.45
USU-1544	5.3	37.8	550	6.9	38.4	0.004	0.01	0.97	14.6	<1	1.1	284	0.43
USU-1545	6.2	34.2	580	8.1	47.2	0.005	0.01	1.02	11.8	1	1.2	257	0.51
USU-1546	6.4	36.8	510	8.7	42.8	<0.002	0.01	1.13	11.8	1	0.9	241	0.44
USU-1547	6.7	35.6	580	8.7	47.4	<0.002	0.01	1.12	12.4	1	1.1	245	0.47
USU-1548	5.8	55	550	8.2	38.5	<0.002	0.01	1.22	13.4	1	0.9	270	0.4
USU-1549	8.2	49.7	950	9.2	45.5	<0.002	0.01	1.12	19.3	1	1.4	335	0.55
USU-1550	6.8	71	810	9.1	38.1	<0.002	<0.01	1.23	20.1	1	1.1	346	0.48
USU-1551	7	62.5	730	8.1	39.1	<0.002	<0.01	1.22	17.9	1	1.1	299	0.5
USU-1552	5.8	63.9	600	8.2	34.7	0.002	0.01	1.23	16.1	1	1	306	0.4
USU-1553	5.9	36.9	500	7.8	43.1	<0.002	0.01	1.14	10.9	1	0.9	252	0.41

Table A.2. *(continued)*

SAMPLE	Te ppm	Th ppm	Ti %	Tl ppm	U ppm	V ppm	W ppm	Y ppm	Zn ppm	Zr ppm
USU-1536	<0.05	5	0.426	0.25	1.1	131	0.7	15.1	60	43.5
USU-1537	<0.05	2.8	0.383	0.16	0.9	126	0.8	13.9	53	38.7
USU-1538	<0.05	3.4	0.443	0.19	1	150	0.8	16.9	57	42.2
USU-1539	<0.05	8.5	0.414	0.39	1.7	116	1.3	18.1	67	49.8
USU-1540	<0.05	4.7	0.348	0.22	1.3	99	0.7	12.9	51	45.2
USU-1541	<0.05	4.9	0.388	0.25	1.1	111	0.8	14.3	61	51.3
USU-1542	0.05	9.5	0.439	0.45	1.8	120	1.3	18	78	48.6
USU-1543	<0.05	4.6	0.346	0.25	1.1	100	0.7	12.9	51	43.4
USU-1544	<0.05	4.1	0.37	0.2	1.1	110	0.7	14	54	46.4
USU-1545	<0.05	4.7	0.377	0.25	1.1	104	0.9	13.4	56	45.7
USU-1546	<0.05	4.8	0.343	0.27	1.1	102	0.7	12.8	49	49.4
USU-1547	<0.05	5.1	0.367	0.28	1.1	102	0.8	12.9	55	45.9
USU-1548	<0.05	3.8	0.355	0.25	1.1	114	0.7	12.8	55	40.9
USU-1549	0.05	5.5	0.488	0.3	1.4	151	0.9	20.2	72	46.4
USU-1550	<0.05	4.4	0.469	0.25	1.2	154	0.9	18.9	68	57.2
USU-1551	<0.05	4.8	0.438	0.27	1.2	140	0.9	18.3	64	44.8
USU-1552	<0.05	3.7	0.393	0.2	1.1	128	0.7	15.1	57	51.9
USU-1553	<0.05	4.2	0.299	0.27	1.1	91	0.7	11.8	48	47.1

Equivalent dose (D_e) Distributions: Probability density functions and radial plots

Figure A.1. Three Towers Site

USU-1536, THR-1

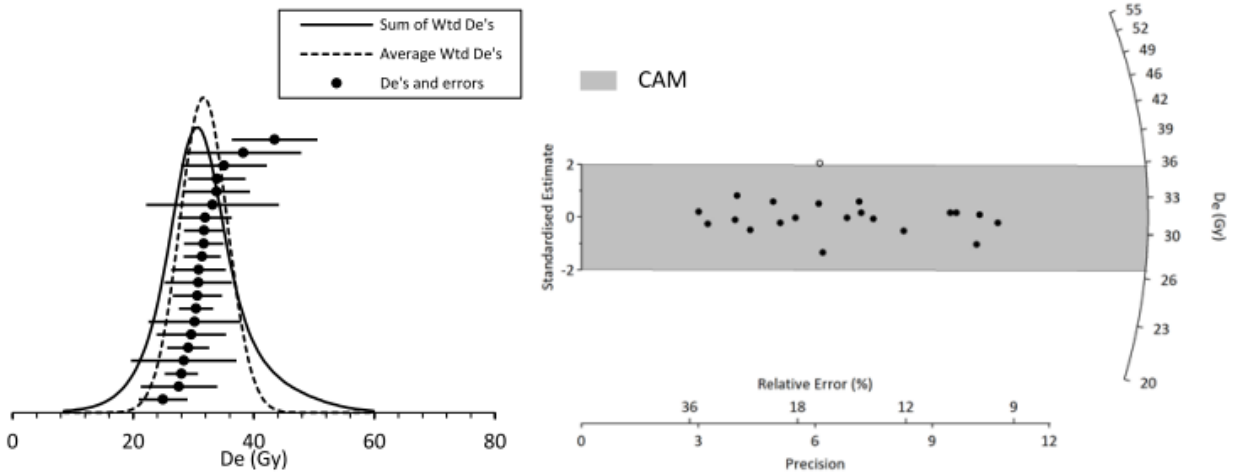

Figure A.2. Red Tower Site

USU-1537, RED-1

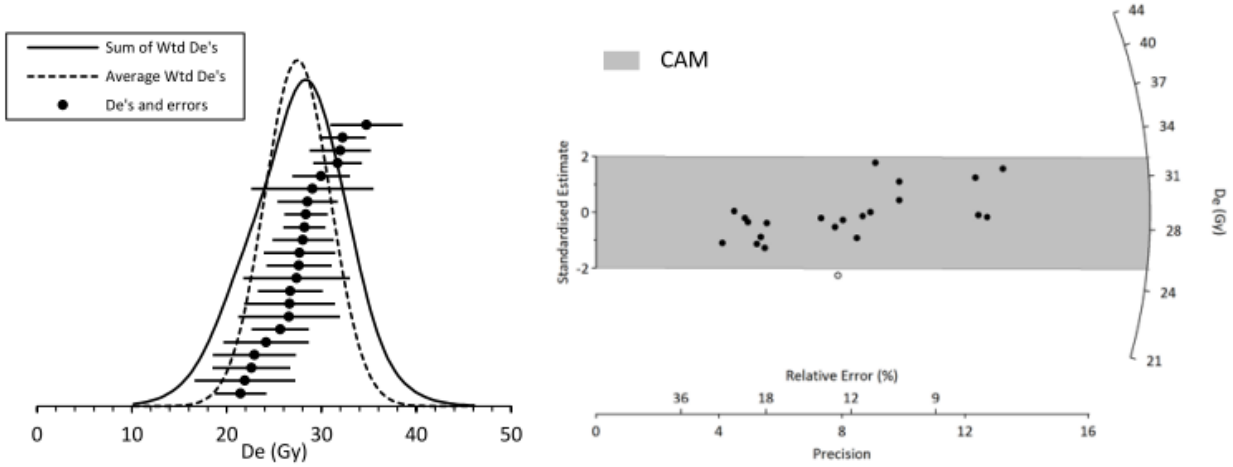

USU-1538, RED-2

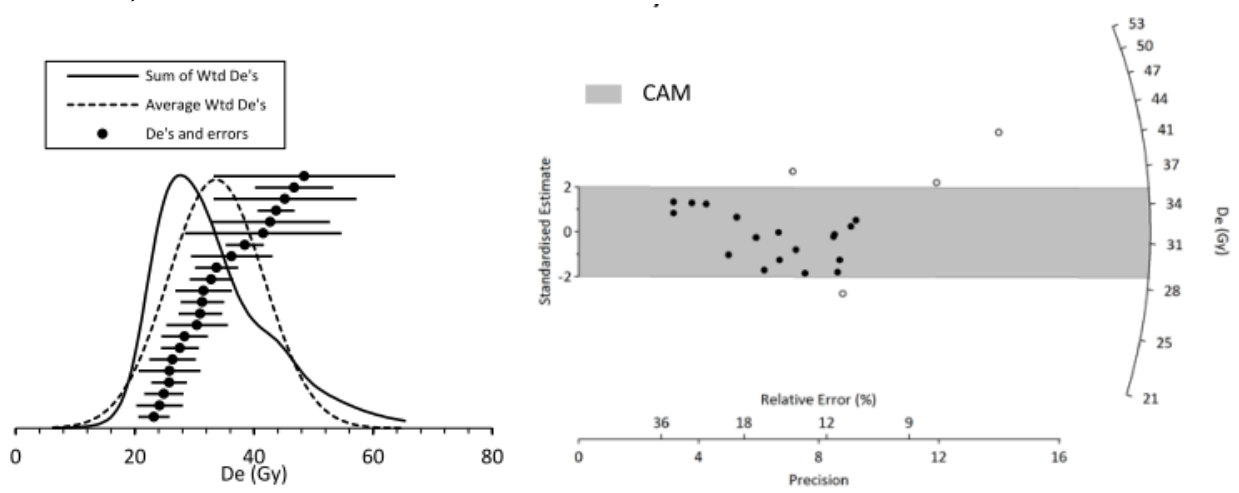

Figure A.3. Jacobson Site

USU-1539, JAC-1

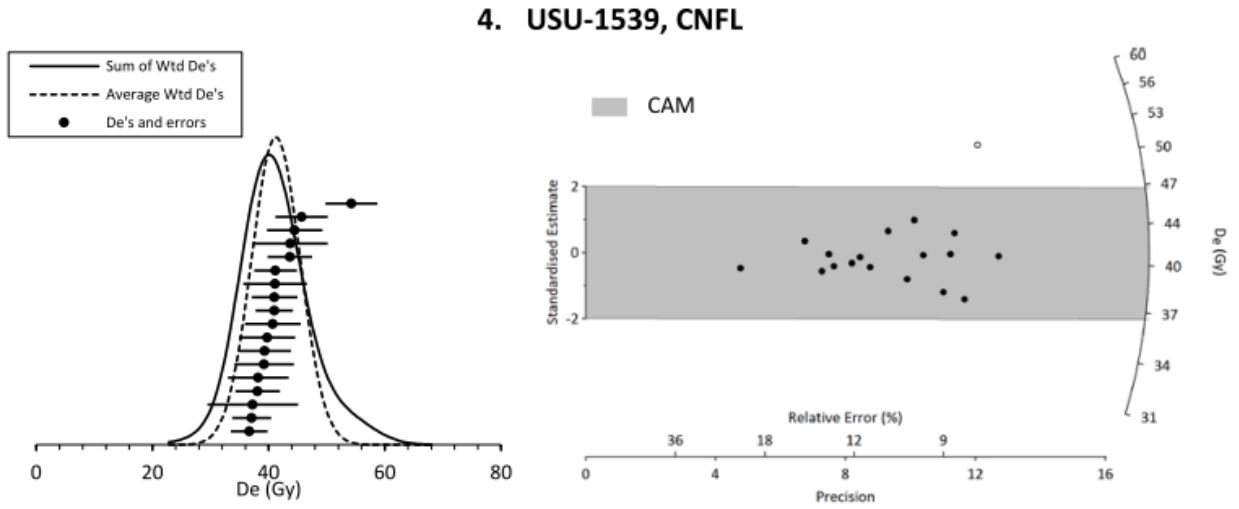

USU-1540, JAC-2

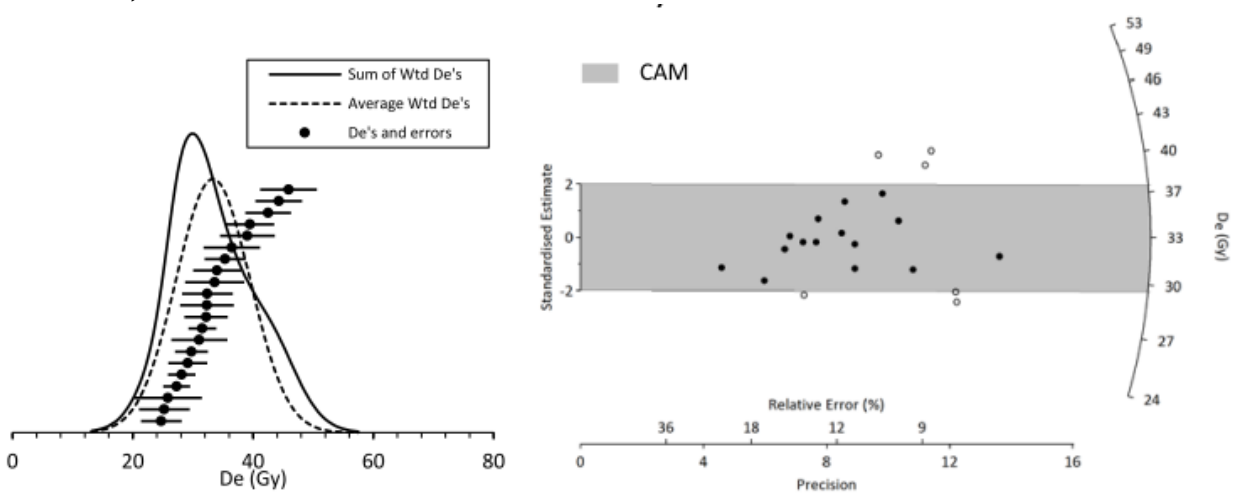

USU 1541, JAC-3

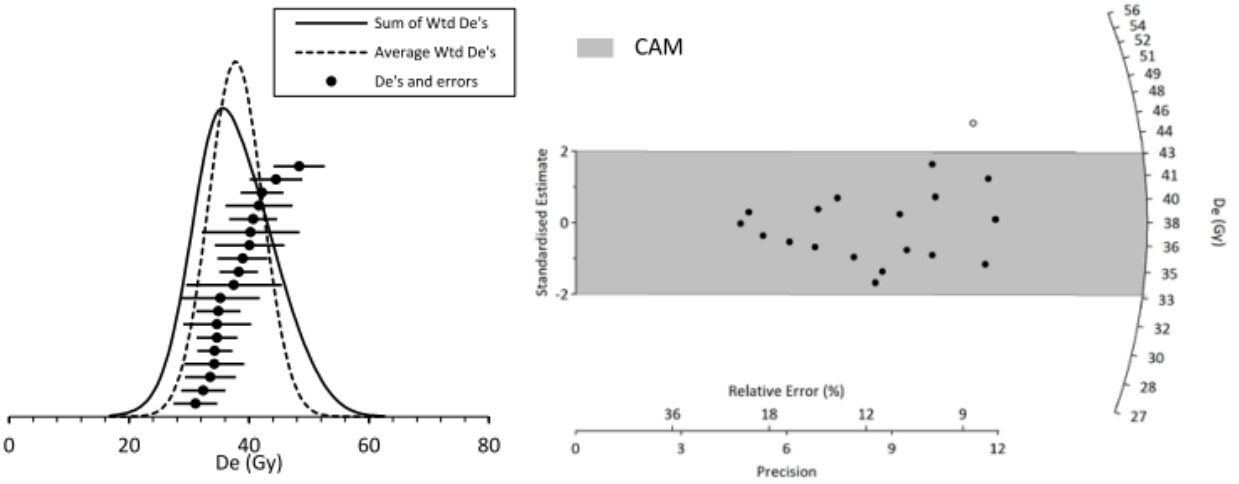

Figure A.4. Cosna Site

USU 1542, COS-1

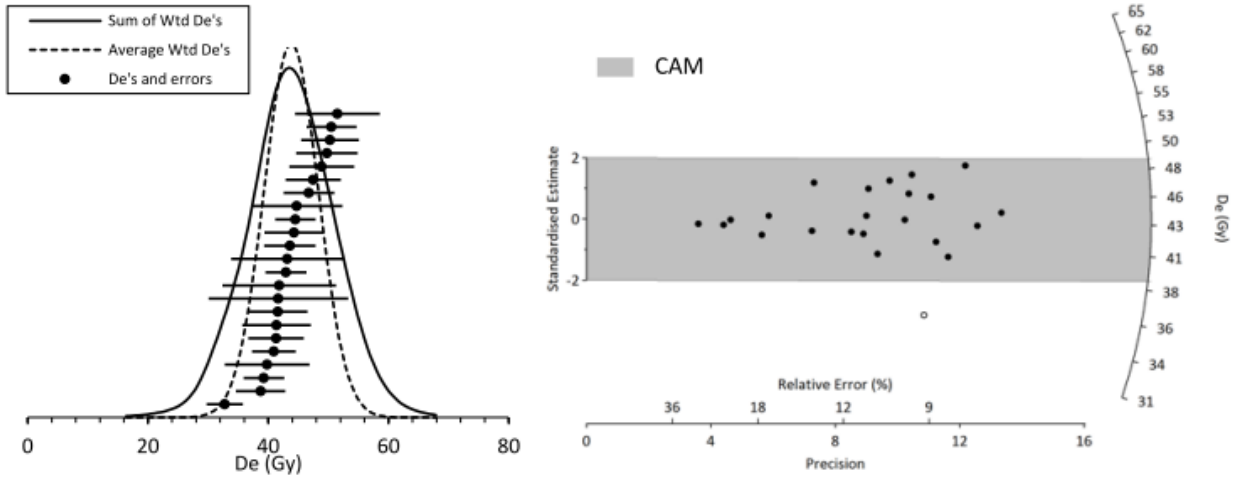

USU-1543, COS-2

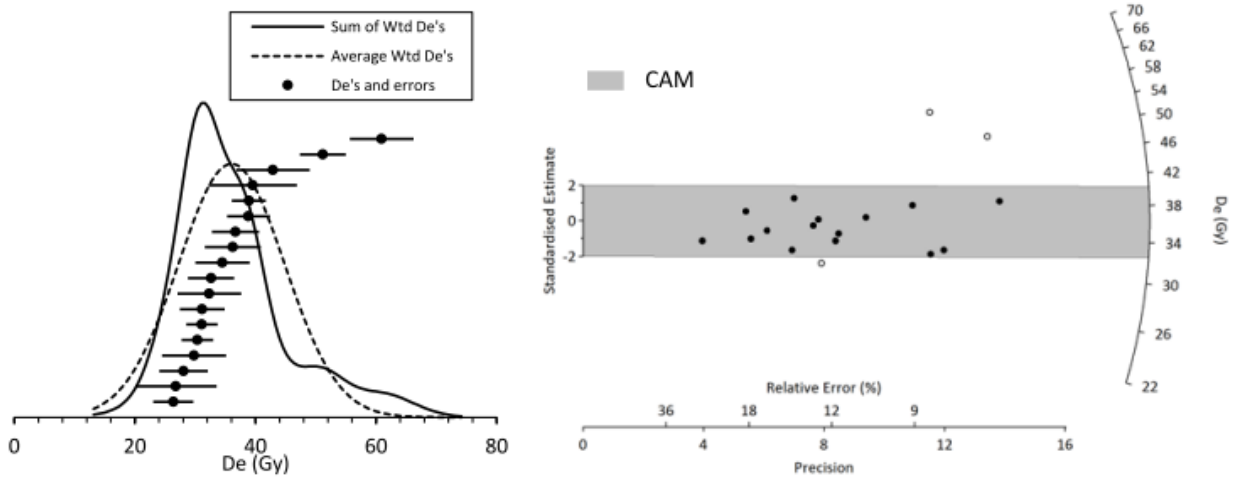

USU-1544, COS-3

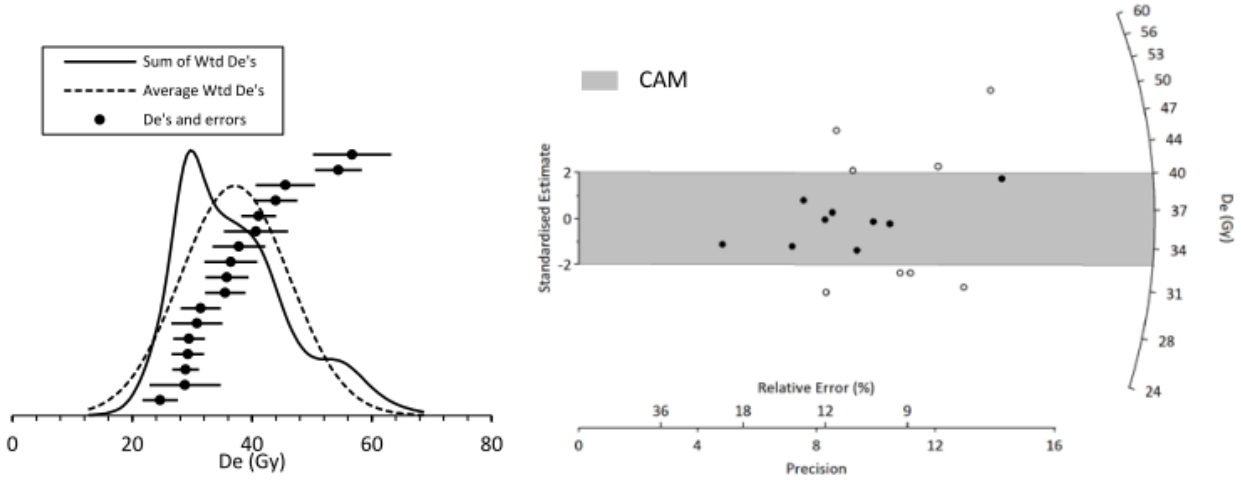

USU-1545, COS-4

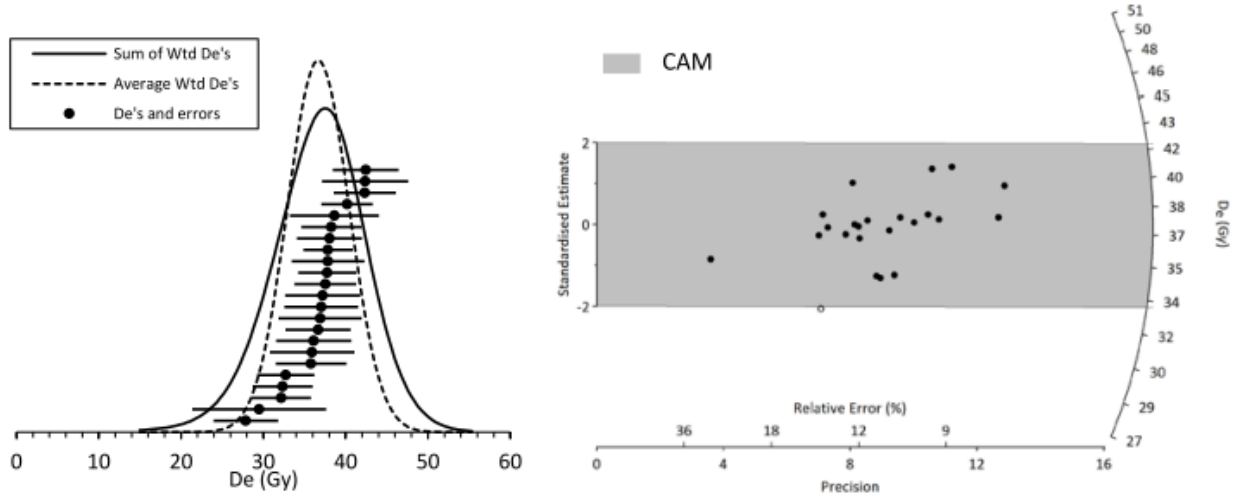

USU-1546, COS-5

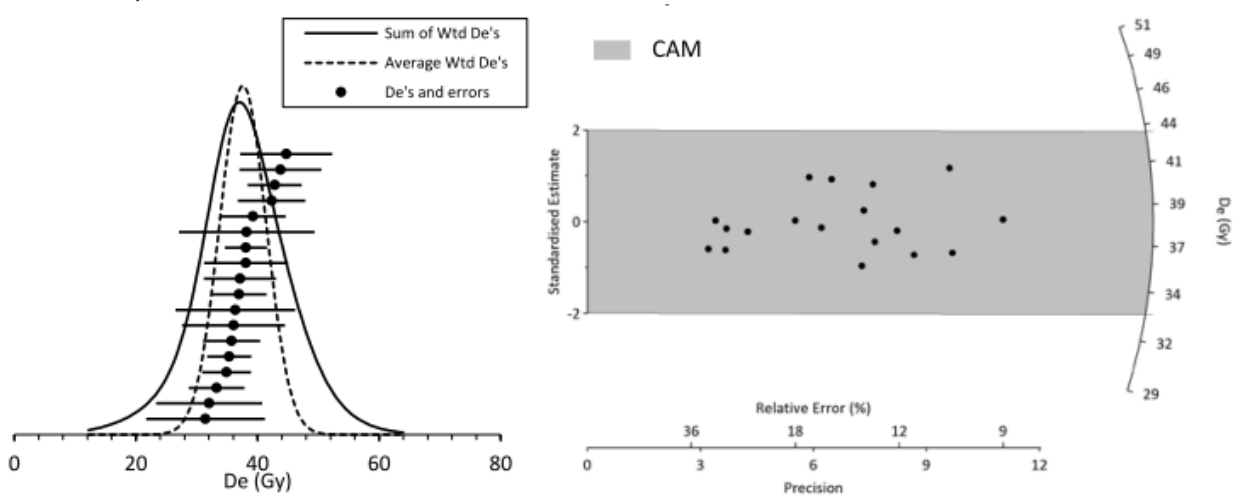

USU-1547, COS-6

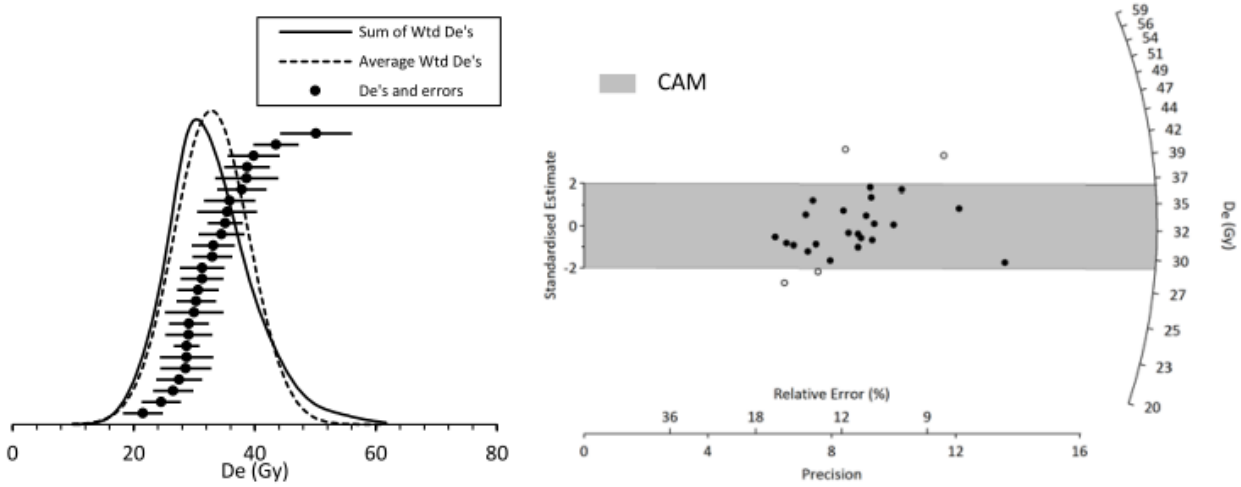

Figure A.5. Beekeeper Site

USU-1548, BEE-1

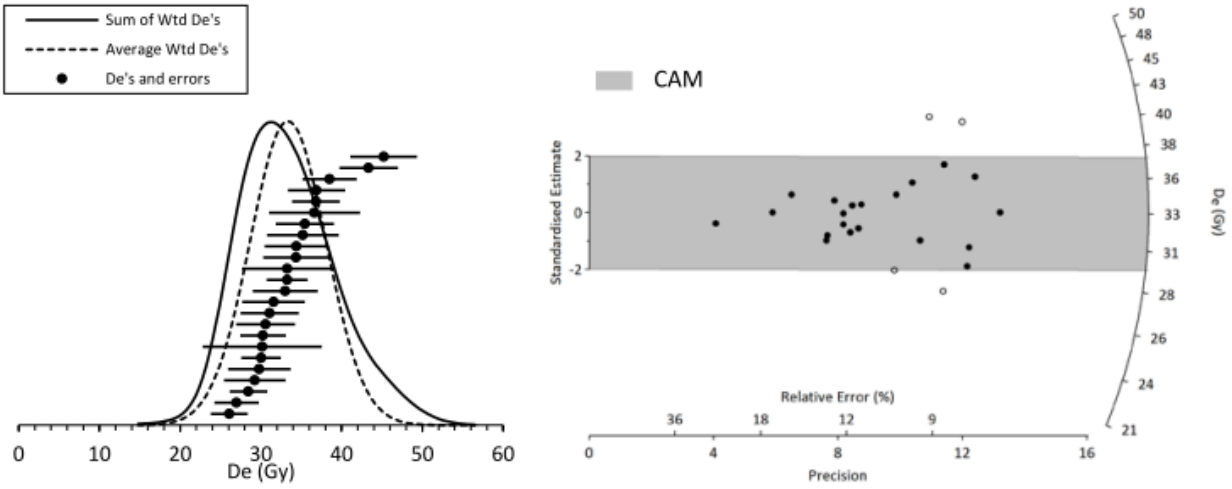

Figure A.6. Chevron Site

USU-1549, CHV-1

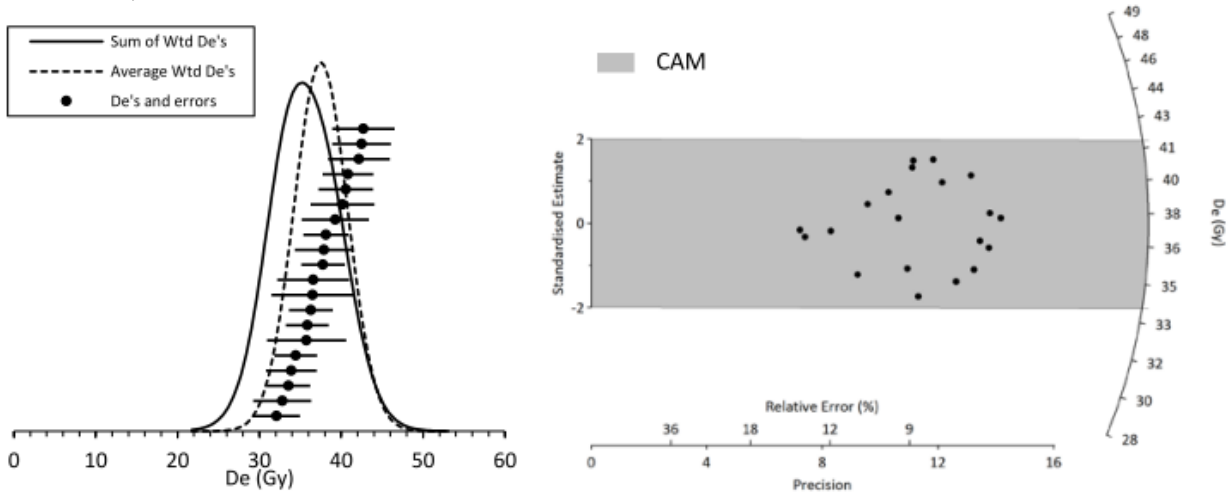

Figure A.7. Boulden Site

USU-1550, BOL-1

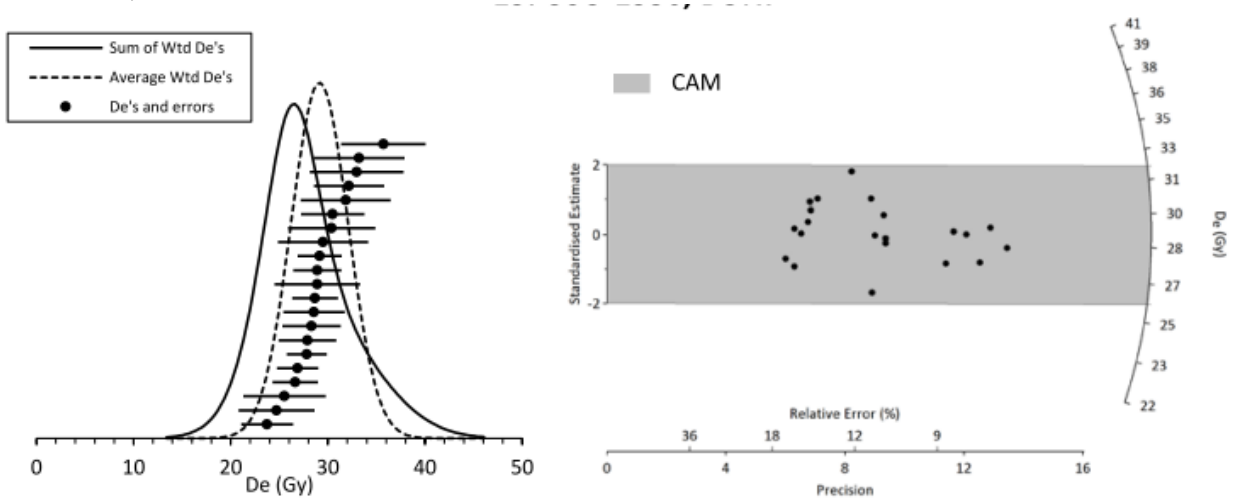

USU-1551, BOL-2

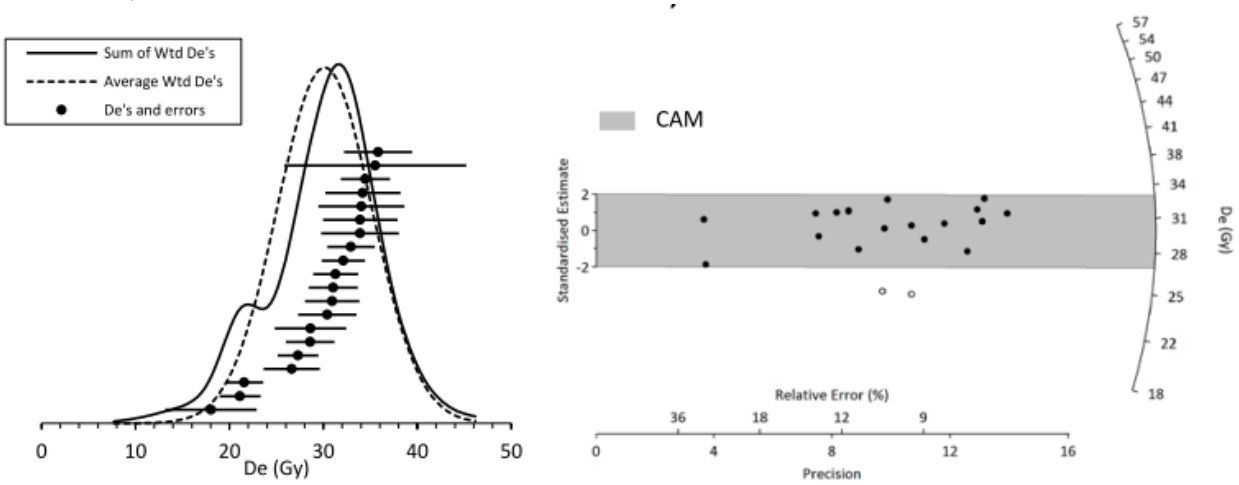

USU-1552, BOL-3

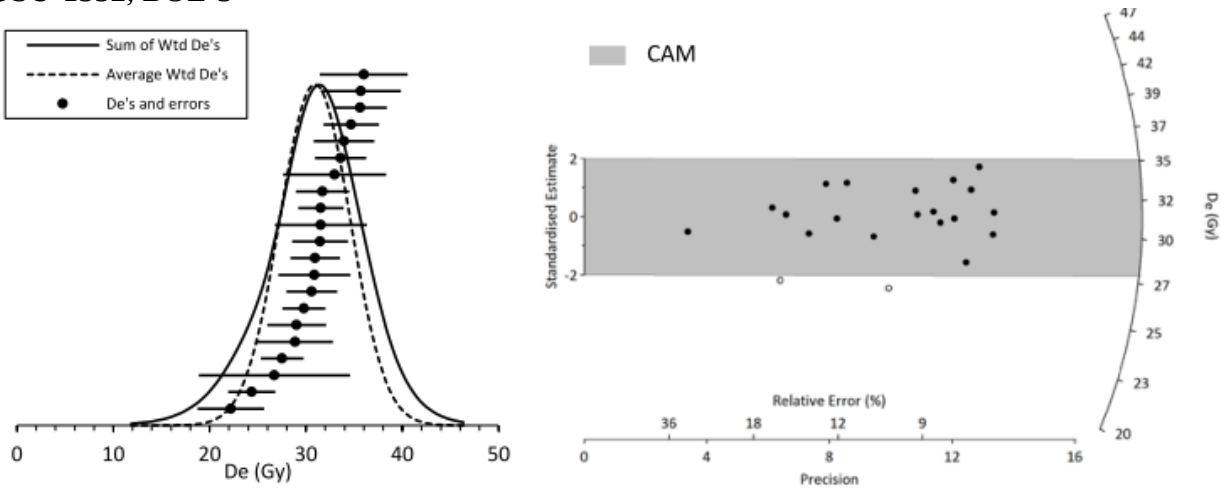

USU-1553, BOL-4

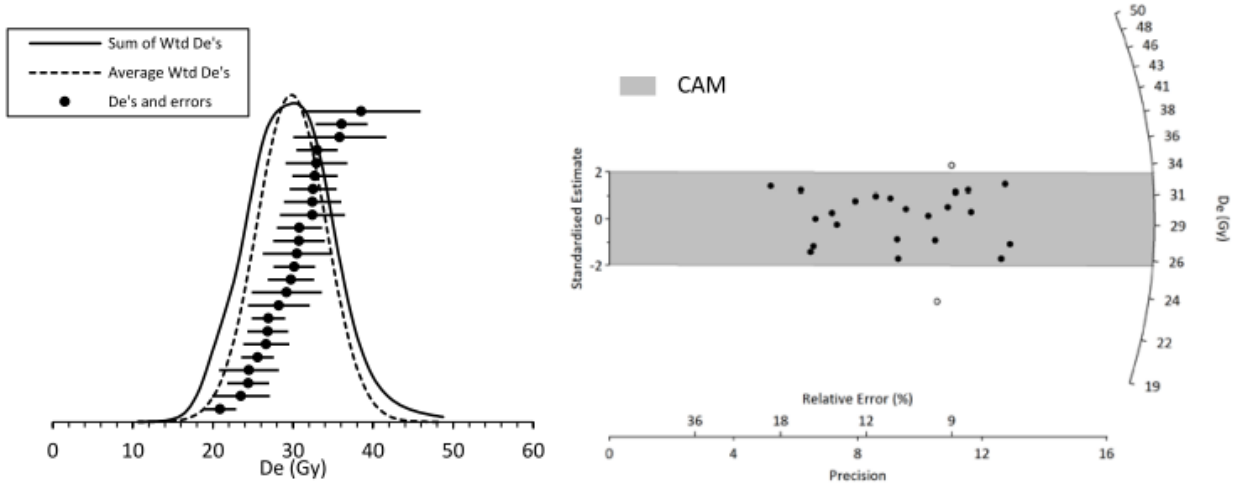

Figure A.8.1. Example of ‘very bright’ @ 1-mm mask:

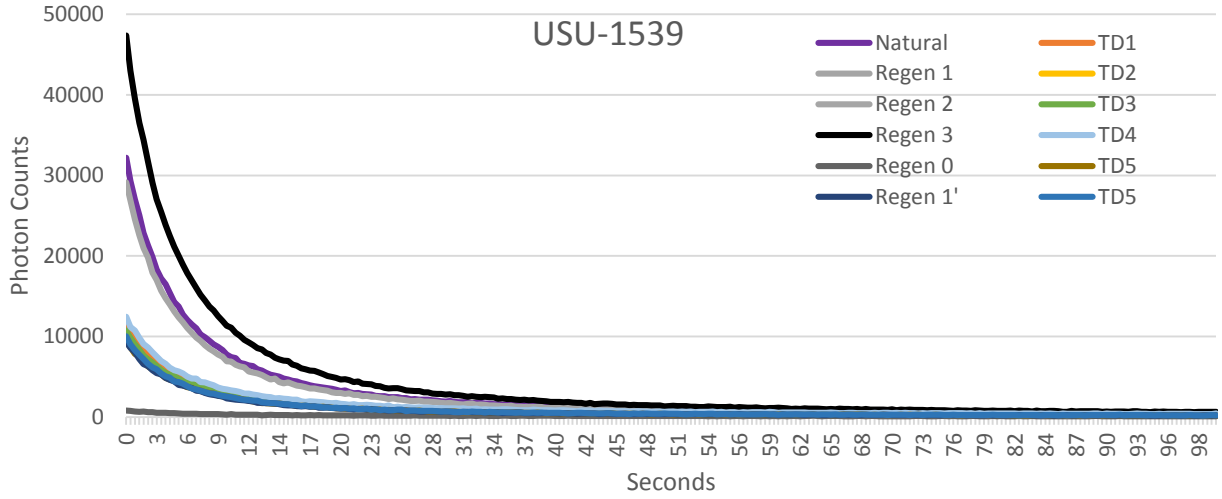

Figure A.8.2. Example of ‘dim’ @ 1-mm mask, required 5-mm mask to produce ‘bright’ signal:

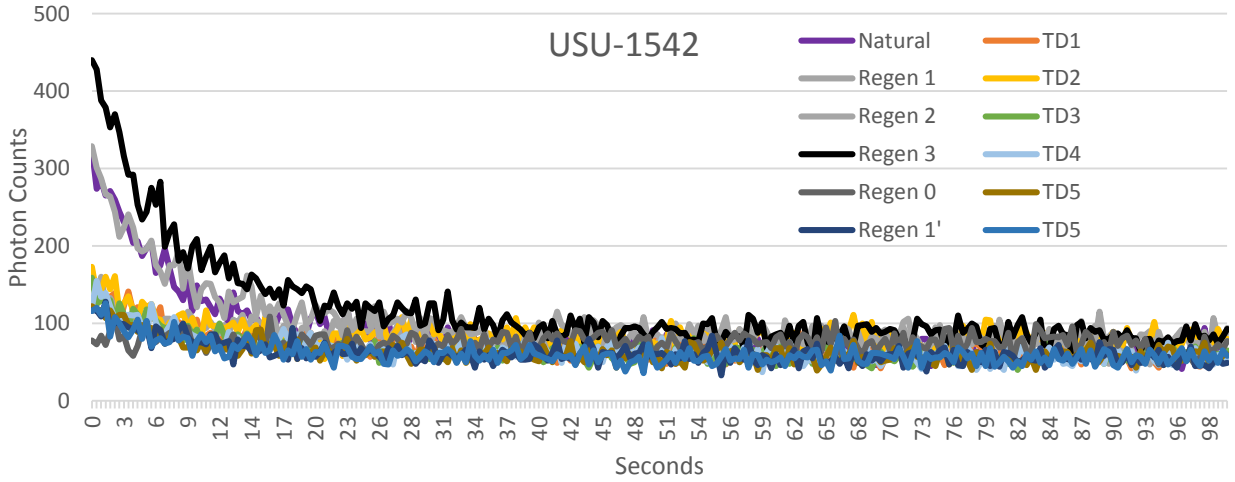

Table A.3. Summary of particle size data. Analyzed using a Malvern Mastersizer 2000.

USU Sample Number	Particle refractive index	Particle absorption index	Dispersant refractive index	Start result channel size	Last result channel size	Obscuration	Residual	Concentration	Span	D [4, 3] - Volume weighted mean	Uniformity	Specific surface area	D [3, 2] - Surface weighted mean	d (0.1)	d (0.5)	d (0.9)
1536a	1.56	0.1	1.33	0.1	1000	7.48	0.264	0.0387	1.812	97.149	0.654	0.168	35.664	32.98	75.769	170.29
1536a	1.56	0.1	1.33	0.1	1000	7.5	0.257	0.0391	1.841	98.521	0.663	0.167	35.964	33.119	76.294	173.55
1536a	1.56	0.1	1.33	0.1	1000	7.5	0.259	0.0389	1.799	95.772	0.632	0.168	35.799	33.034	75.993	169.76
1536a - Avg	1.56	0.1	1.33	0.1	1000	7.49	0.26	0.0389	1.817	97.147	0.65	0.168	35.809	33.044	76.018	171.18
1536b	1.56	0.1	1.33	0.1	1000	6.41	0.284	0.0345	1.808	98.533	0.649	0.161	37.374	33.737	76.879	172.7
1536b	1.56	0.1	1.33	0.1	1000	6.37	0.292	0.0342	1.772	95.754	0.616	0.161	37.236	33.741	76.642	169.51
1536b	1.56	0.1	1.33	0.1	1000	6.4	0.29	0.0344	1.783	97.352	0.637	0.161	37.273	33.752	76.654	170.43
1536b - Avg	1.56	0.1	1.33	0.1	1000	6.39	0.288	0.0344	1.787	97.212	0.634	0.161	37.294	33.743	76.724	170.87
1536c	1.56	0.1	1.33	0.1	1000	6.48	0.364	0.0339	1.786	95.164	0.628	0.166	36.246	32.879	75.729	168.17
1536c	1.56	0.1	1.33	0.1	1000	6.46	0.358	0.034	1.811	97.044	0.647	0.165	36.452	32.995	76.098	170.81
1536c	1.56	0.1	1.33	0.1	1000	6.5	0.36	0.0342	1.8	96.487	0.641	0.165	36.449	33	75.998	169.78
1536c - Avg	1.56	0.1	1.33	0.1	1000	6.48	0.361	0.034	1.799	96.231	0.638	0.165	36.382	32.958	75.941	169.57
1537a	1.56	0.1	1.33	0.1	1000	6.13	0.591	0.1181	1.287	177.31	0.396	0.0453	132.444	85.562	162.62	294.82
1537a	1.56	0.1	1.33	0.1	1000	6.09	0.586	0.115	1.291	175.655	0.399	0.0462	129.995	84.531	161.02	292.47
1537a	1.56	0.1	1.33	0.1	1000	6.28	0.582	0.1215	1.29	178.228	0.397	0.0451	133.009	85.696	163.51	296.66
1537a - Avg	1.56	0.1	1.33	0.1	1000	6.17	0.586	0.1182	1.289	177.064	0.397	0.0455	131.803	85.265	162.38	294.65
1537b	1.56	0.1	1.33	0.1	1000	6.04	0.555	0.1112	1.315	171.721	0.408	0.0473	126.884	81.731	156.68	287.7
1537b	1.56	0.1	1.33	0.1	1000	6.04	0.569	0.1109	1.302	170.565	0.404	0.0474	126.543	81.768	155.87	284.63
1537b	1.56	0.1	1.33	0.1	1000	6.04	0.569	0.111	1.302	170.284	0.404	0.0474	126.548	81.7	155.53	284.17
1537b - Avg	1.56	0.1	1.33	0.1	1000	6.04	0.564	0.111	1.306	170.856	0.406	0.0474	126.658	81.733	156.03	285.49
1537c	1.56	0.1	1.33	0.1	1000	6.04	0.496	0.1036	1.313	159.661	0.406	0.0507	118.354	75.939	145.77	267.26
1537c	1.56	0.1	1.33	0.1	1000	6.11	0.486	0.1048	1.317	159.467	0.407	0.0508	118.17	75.8	145.41	267.26
1537c	1.56	0.1	1.33	0.1	1000	6.02	0.487	0.1025	1.301	157.898	0.402	0.0511	117.382	75.54	144.49	263.53
1537c - Avg	1.56	0.1	1.33	0.1	1000	6.06	0.49	0.1037	1.31	159.008	0.405	0.0509	117.967	75.758	145.22	265.98
1538a	1.56	0.1	1.33	0.1	1000	6.02	0.265	0.03	1.758	99.23	0.549	0.172	34.812	32.032	86.53	184.19
1538a	1.56	0.1	1.33	0.1	1000	5.99	0.254	0.0297	1.749	98.885	0.546	0.173	34.722	31.994	86.467	183.26
1538a	1.56	0.1	1.33	0.1	1000	5.98	0.257	0.0299	1.758	99.652	0.55	0.172	34.948	32.252	86.785	184.83
1538a - Avg	1.56	0.1	1.33	0.1	1000	6	0.258	0.0299	1.755	99.256	0.548	0.172	34.827	32.092	86.594	184.09
1538b	1.56	0.1	1.33	0.1	1000	6.4	0.225	0.0316	1.787	100.047	0.559	0.174	34.474	31.759	86.651	186.59
1538b	1.56	0.1	1.33	0.1	1000	6.4	0.215	0.0318	1.794	100.887	0.56	0.173	34.711	31.809	87.37	188.59
1538b	1.56	0.1	1.33	0.1	1000	6.41	0.216	0.0317	1.764	99.279	0.549	0.174	34.473	31.696	86.765	184.74
1538b - Avg	1.56	0.1	1.33	0.1	1000	6.4	0.219	0.0317	1.781	100.071	0.556	0.174	34.552	31.755	86.927	186.61
1538c	1.56	0.1	1.33	0.1	1000	6.76	0.256	0.0328	1.746	97.246	0.541	0.178	33.774	31.048	85.673	180.67
1538c	1.56	0.1	1.33	0.1	1000	6.77	0.262	0.0329	1.739	97.227	0.539	0.177	33.873	31.166	85.784	180.38
1538c	1.56	0.1	1.33	0.1	1000	6.78	0.259	0.0332	1.771	98.941	0.551	0.176	34.138	31.311	86.458	184.42
1538c - Avg	1.56	0.1	1.33	0.1	1000	6.77	0.259	0.033	1.752	97.805	0.544	0.177	33.927	31.176	85.969	181.79
1539a	1.56	0.1	1.33	0.1	1000	11.59	0.205	0.0282	3.536	65.758	1.1	0.363	16.538	10.371	40.471	153.46
1539a	1.56	0.1	1.33	0.1	1000	11.55	0.21	0.0279	3.401	63.587	1.06	0.366	16.41	10.282	40.125	146.76
1539a	1.56	0.1	1.33	0.1	1000	11.54	0.207	0.0281	3.473	64.64	1.07	0.363	16.516	10.366	40.397	150.65
1539a - Avg	1.56	0.1	1.33	0.1	1000	11.56	0.207	0.0281	3.469	64.662	1.07	0.364	16.488	10.339	40.33	150.23
1539b	1.56	0.1	1.33	0.1	1000	8.73	0.19	0.0208	3.498	64.54	1.09	0.366	16.405	10.268	39.804	149.51
1539b	1.56	0.1	1.33	0.1	1000	8.75	0.192	0.0207	3.409	62.948	1.06	0.367	16.333	10.224	39.591	145.2
1539b	1.56	0.1	1.33	0.1	1000	8.77	0.195	0.0207	3.342	61.865	1.04	0.369	16.279	10.182	39.411	141.9
1539b - Avg	1.56	0.1	1.33	0.1	1000	8.75	0.192	0.0207	3.415	63.118	1.06	0.367	16.339	10.224	39.601	145.46
1539c	1.56	0.1	1.33	0.1	1000	6.8	0.194	0.0161	3.536	65.048	1.1	0.363	16.545	10.393	39.934	151.59
1539c	1.56	0.1	1.33	0.1	1000	6.76	0.192	0.0158	3.173	60.409	1	0.369	16.28	10.229	39.271	134.82
1539c	1.56	0.1	1.33	0.1	1000	6.74	0.195	0.0158	3.263	61.303	1.02	0.367	16.345	10.284	39.449	139
1539c - Avg	1.56	0.1	1.33	0.1	1000	6.77	0.193	0.0159	3.317	62.253	1.04	0.366	16.389	10.302	39.548	141.47
1540a	1.56	0.1	1.33	0.1	1000	6.36	0.449	0.095	1.443	177.771	0.449	0.0574	104.59	78.489	159.47	308.61
1540a	1.56	0.1	1.33	0.1	1000	6.4	0.452	0.0959	1.434	177.584	0.446	0.0572	104.962	78.764	159.52	307.54
1540a	1.56	0.1	1.33	0.1	1000	6.37	0.439	0.0949	1.442	177.362	0.449	0.0574	104.45	78.488	159.03	307.83
1540a - Avg	1.56	0.1	1.33	0.1	1000	6.38	0.447	0.0953	1.44	177.572	0.448	0.0573	104.667	78.58	159.34	307.99
1540b	1.56	0.1	1.33	0.1	1000	6.47	0.288	0.0997	1.457	184.678	0.45	0.0556	107.876	80.45	165.87	322.07
1540b	1.56	0.1	1.33	0.1	1000	6.6	0.314	0.108	1.515	192.156	0.473	0.0526	113.968	81.955	169.42	338.64
1540b	1.56	0.1	1.33	0.1	1000	6.6	0.296	0.1068	1.461	187.653	0.452	0.0532	112.731	81.564	168.39	327.54
1540b - Avg	1.56	0.1	1.33	0.1	1000	6.56	0.299	0.1048	1.477	188.162	0.458	0.0538	111.462	81.327	167.88	329.22
1540c	1.56	0.1	1.33	0.1	1000	7.09	0.327	0.1077	1.466	180.816	0.454	0.0566	106.09	78.639	161.87	315.96
1540c	1.56	0.1	1.33	0.1	1000	7.07	0.342	0.1074	1.452	179.521	0.45	0.0566	106.024	78.924	160.85	312.42
1540c	1.56	0.1	1.33	0.1	1000	7.03	0.331	0.1083	1.505	185.728	0.468	0.0558	107.492	79.318	164.19	326.47
1540c - Avg	1.56	0.1	1.33	0.1	1000	7.06	0.334	0.1078	1.474	182.022	0.458	0.0563	106.531	78.96	162.29	318.14
1541a	1.56	0.1	1.33	0.1	1000	6.41	0.254	0.0369	1.693	101.889	0.534	0.149	40.205	36.622	88.23	186.02
1541a	1.56	0.1	1.33	0.1	1000	6.43	0.247	0.0386	1.739	106.834	0.576	0.141	42.47	36.98	89.29	192.24
1541a	1.56	0.1	1.33	0.1	1000	6.43	0.255	0.0385	1.722	105.484	0.562	0.142	42.369	36.979	89.179	190.55
1541a - Avg	1.56	0.1	1.33	0.1	1000	6.43	0.252	0.038	1.718	104.733	0.558	0.144	41.653	36.859	88.895	189.56
1541b	1.56	0.1	1.33	0.1	1000	6.24	0.239	0.0372	1.695	103.87	0.532	0.142	42.37	37.237	90.108	189.95
1541b	1.56	0.1	1.33	0.1	1000	6.22	0.227	0.0375	1.735	108.142	0.574	0.141	42.66	37.345	90.667	194.67
1541b	1.56	0.1	1.33	0.1	1000	6.23	0.234	0.0373	1.712	104.719	0.54	0.141	42.529	37.308	90.303	191.9
1541b - Avg	1.56	0.1	1.33	0.1	1000	6.23	0.234	0.0373	1.714	105.574	0.549	0.141	42.519	37.297	90.358	192.13
1542a	1.56	0.1	1.33	0.1	1000	6.61	0.212	0.0146	2.225	47.012	0.754	0.392	15.319	9.713	36.105	90.051
1542a	1.56	0.1	1.33	0.1	1000	6.61	0.203	0.0146	2.225	47.742	0.771	0.391	15.338	9.728	36.172	90.201
1542a	1.56	0.1	1.33	0.1	1000	6.61	0.212	0.0145	2.213	46.727	0.748	0.392	15.287	9.698	36.029	89.418
1542a - Avg	1.56	0.1	1.33	0.1	1000	6.61	0.209	0.0146	2.221	47.16	0.758	0.392	15.315	9.713	36.102	89.883

Table A.3. *(continued)*

USU Sample Number	Particle refractive index	Particle absorption index	Dispersant refractive index	Start result channel size	Last result channel size	Obscuration	Residual	Concentration	Span	D [4, 3] - Volume weighted mean	Uniformity	Specific surface area	D [3, 2] - Surface weighted mean	d (0.1)	d (0.5)	d (0.9)
1542b	1.56	0.1	1.33	0.1	1000	7.24	0.197	0.0158	2.194	46.754	0.759	0.396	15.17	9.62	35.776	88.103
1542b	1.56	0.1	1.33	0.1	1000	7.25	0.195	0.016	2.226	48.105	0.788	0.393	15.267	9.682	36.007	89.851
1542b	1.56	0.1	1.33	0.1	1000	7.26	0.193	0.016	2.215	47.835	0.782	0.393	15.261	9.685	35.973	89.364
1542b - Avg	1.56	0.1	1.33	0.1	1000	7.25	0.195	0.0159	2.212	47.565	0.776	0.394	15.232	9.662	35.918	89.102
1542b	1.56	0.1	1.33	0.1	1000	6.89	0.322	0.0678	1.754	183.308	0.522	0.0851	70.522	43.436	168.46	338.88
1542b	1.56	0.1	1.33	0.1	1000	6.85	0.332	0.0673	1.745	182.111	0.519	0.0853	70.322	43.155	167.82	335.99
1542b	1.56	0.1	1.33	0.1	1000	6.87	0.334	0.0679	1.742	182.756	0.518	0.0848	70.771	43.555	168.39	336.95
1542b - Avg	1.56	0.1	1.33	0.1	1000	6.87	0.33	0.0677	1.747	182.725	0.52	0.0851	70.538	43.381	168.22	337.28
1543b	1.56	0.1	1.33	0.1	1000	7.2	0.43	0.0714	1.768	185.076	0.529	0.0847	70.88	43.622	169.61	343.57
1543b	1.56	0.1	1.33	0.1	1000	7.19	0.441	0.0715	1.771	185.537	0.53	0.0844	71.057	43.68	169.95	344.73
1543b	1.56	0.1	1.33	0.1	1000	7.21	0.453	0.0726	1.759	185.961	0.526	0.0835	71.849	44.243	170.69	344.52
1543b - Avg	1.56	0.1	1.33	0.1	1000	7.2	0.441	0.0718	1.766	185.524	0.528	0.0842	71.26	43.847	170.08	344.27
1544a	1.56	0.1	1.33	0.1	1000	6.8	0.356	0.0756	1.963	173.935	0.607	0.0757	79.221	55.98	144.19	338.96
1544a	1.56	0.1	1.33	0.1	1000	6.79	0.37	0.0749	1.92	170.171	0.591	0.0764	78.527	55.724	142.68	329.72
1544a	1.56	0.1	1.33	0.1	1000	6.79	0.365	0.0754	1.962	173.308	0.607	0.0759	79.036	55.93	143.59	337.7
1544a - Avg	1.56	0.1	1.33	0.1	1000	6.79	0.363	0.0753	1.948	172.471	0.602	0.076	78.927	55.877	143.48	335.39
1544b	1.56	0.1	1.33	0.1	1000	7.11	0.247	0.0762	1.973	165.339	0.612	0.0787	76.219	53.85	136.14	322.49
1544b	1.56	0.1	1.33	0.1	1000	7.04	0.25	0.0746	1.98	163.414	0.611	0.0795	75.435	53.456	134.74	320.31
1544b	1.56	0.1	1.33	0.1	1000	7.04	0.248	0.074	1.929	160.062	0.597	0.0802	74.782	53.36	133.12	310.13
1544b - Avg	1.56	0.1	1.33	0.1	1000	7.06	0.248	0.075	1.961	162.938	0.607	0.0795	75.474	53.553	134.65	317.59
1545a	1.56	0.1	1.33	0.1	1000	7.74	0.291	0.0505	1.845	135.523	0.552	0.128	46.758	29.432	122.95	256.32
1545a	1.56	0.1	1.33	0.1	1000	7.74	0.29	0.0526	1.827	135.714	0.547	0.123	48.883	29.909	123.54	255.68
1545a	1.56	0.1	1.33	0.1	1000	7.76	0.288	0.053	1.824	135.624	0.546	0.122	49.133	30.073	123.5	255.29
1545a - Avg	1.56	0.1	1.33	0.1	1000	7.75	0.29	0.052	1.832	135.62	0.548	0.124	48.234	29.803	123.33	255.76
1545b	1.56	0.1	1.33	0.1	1000	7.15	0.333	0.0488	1.859	138.473	0.557	0.122	49.278	30.407	124.98	262.69
1545b	1.56	0.1	1.33	0.1	1000	7.07	0.337	0.0462	1.873	137.207	0.561	0.128	47.005	29.698	123.55	261.07
1545b	1.56	0.1	1.33	0.1	1000	7.09	0.325	0.0482	1.853	137.051	0.555	0.122	49.133	30.249	123.85	259.7
1545b - Avg	1.56	0.1	1.33	0.1	1000	7.1	0.332	0.0477	1.861	137.577	0.558	0.124	48.449	30.115	124.13	261.16
1546a	1.56	0.1	1.33	0.1	1000	6.53	0.348	0.1178	1.586	224.056	0.49	0.0478	125.444	82.409	201.81	402.5
1546a	1.56	0.1	1.33	0.1	1000	6.54	0.347	0.1186	1.583	224.548	0.49	0.0476	125.941	82.749	202.34	403.12
1546a	1.56	0.1	1.33	0.1	1000	6.56	0.347	0.1185	1.576	223.587	0.487	0.0478	125.582	82.683	201.77	400.7
1546a - Avg	1.56	0.1	1.33	0.1	1000	6.54	0.347	0.1183	1.582	224.064	0.489	0.0477	125.655	82.613	201.97	402.11
1546b	1.56	0.1	1.33	0.1	1000	6.57	0.327	0.1173	1.612	222.973	0.498	0.0484	124.042	79.278	200.76	402.88
1546b	1.56	0.1	1.33	0.1	1000	6.53	0.35	0.1166	1.62	223.947	0.5	0.0483	124.099	79.152	201.38	405.42
1546b	1.56	0.1	1.33	0.1	1000	6.49	0.316	0.1155	1.648	225.251	0.509	0.0485	123.782	78.666	201.42	410.53
1546b - Avg	1.56	0.1	1.33	0.1	1000	6.53	0.331	0.1165	1.626	224.057	0.502	0.0484	123.974	79.032	201.19	406.24
1547a	1.56	0.1	1.33	0.1	1000	7.48	0.234	0.044	2.053	155.173	0.624	0.143	41.991	26.596	137.5	308.93
1547a	1.56	0.1	1.33	0.1	1000	7.5	0.221	0.0443	2.051	155.696	0.623	0.142	42.216	26.708	138	309.75
1547a	1.56	0.1	1.33	0.1	1000	7.5	0.233	0.0443	2.054	156.032	0.624	0.142	42.173	26.681	138.29	310.68
1547a - Avg	1.56	0.1	1.33	0.1	1000	7.49	0.229	0.0442	2.053	155.634	0.624	0.142	42.126	26.661	137.93	309.79
1547b	1.56	0.1	1.33	0.1	1000	7.88	0.243	0.0473	2.068	163.389	0.629	0.14	42.834	27.033	144.66	326.21
1547b	1.56	0.1	1.33	0.1	1000	7.92	0.229	0.048	2.071	164.096	0.63	0.139	43.161	27.25	145.07	327.69
1547b	1.56	0.1	1.33	0.1	1000	7.9	0.229	0.0479	2.073	164.667	0.631	0.139	43.173	27.261	145.55	328.95
1547b - Avg	1.56	0.1	1.33	0.1	1000	7.9	0.234	0.0477	2.071	164.05	0.63	0.139	43.055	27.181	145.09	327.62
1548a	1.56	0.1	1.33	0.1	1000	6.61	0.43	0.0854	1.556	162.148	0.484	0.0662	90.603	63.818	144.46	288.54
1548a	1.56	0.1	1.33	0.1	1000	6.53	0.425	0.0811	1.561	161.359	0.485	0.0685	87.539	63.235	143.65	287.47
1548a	1.56	0.1	1.33	0.1	1000	6.64	0.426	0.0861	1.559	162.652	0.485	0.066	90.852	64.004	144.79	289.75
1548a - Avg	1.56	0.1	1.33	0.1	1000	6.59	0.427	0.0842	1.559	162.053	0.484	0.0669	89.639	63.683	144.3	288.59
1548b	1.56	0.1	1.33	0.1	1000	6.98	0.35	0.0936	1.521	167.437	0.475	0.0639	93.856	68.049	149.7	295.81
1548b	1.56	0.1	1.33	0.1	1000	7.04	0.356	0.0958	1.54	170.349	0.482	0.0631	95.129	68.742	151.5	302.08
1548b	1.56	0.1	1.33	0.1	1000	7.09	0.362	0.0964	1.542	170.235	0.485	0.0631	95.015	68.737	150.77	301.3
1548b - Avg	1.56	0.1	1.33	0.1	1000	7.04	0.356	0.0953	1.535	169.341	0.481	0.0634	94.663	68.505	150.65	299.72
1549a	1.56	0.1	1.33	0.1	1000	7.15	0.233	0.0106	2.082	31.12	0.635	0.585	10.256	5.772	26.697	61.36
1549a	1.56	0.1	1.33	0.1	1000	7.16	0.233	0.0107	2.086	31.225	0.636	0.584	10.277	5.792	26.75	61.595
1549a	1.56	0.1	1.33	0.1	1000	7.15	0.253	0.0106	2.081	31.182	0.635	0.584	10.277	5.796	26.745	61.448
1549a - Avg	1.56	0.1	1.33	0.1	1000	7.15	0.24	0.0106	2.083	31.175	0.635	0.584	10.27	5.786	26.731	61.467
1549b	1.56	0.1	1.33	0.1	1000	8.05	0.227	0.0124	2.047	31.378	0.625	0.567	10.577	6.073	27.074	61.505
1549b	1.56	0.1	1.33	0.1	1000	8.03	0.228	0.0124	2.044	31.299	0.623	0.568	10.567	6.069	27.047	61.353
1549b	1.56	0.1	1.33	0.1	1000	8.02	0.227	0.0124	2.055	31.47	0.628	0.566	10.593	6.092	27.092	61.756
1549b - Avg	1.56	0.1	1.33	0.1	1000	8.03	0.227	0.0124	2.049	31.382	0.625	0.567	10.579	6.078	27.071	61.535
1550a	1.56	0.1	1.33	0.1	1000	5.9	0.203	0.0117	2.354	47.573	0.817	0.44	13.65	9.976	34.63	91.5
1550a	1.56	0.1	1.33	0.1	1000	5.89	0.205	0.0117	2.34	46.385	0.786	0.441	13.612	9.94	34.557	90.806
1550a	1.56	0.1	1.33	0.1	1000	5.89	0.205	0.0117	2.376	48.092	0.829	0.438	13.688	10.025	34.705	92.49
1550a - Avg	1.56	0.1	1.33	0.1	1000	5.89	0.204	0.0117	2.357	47.35	0.811	0.44	13.65	9.98	34.63	91.588
1550b	1.56	0.1	1.33	0.1	1000	6.45	0.202	0.0129	2.371	47.016	0.793	0.437	13.723	9.835	34.897	92.568
1550b	1.56	0.1	1.33	0.1	1000	6.47	0.204	0.013	2.384	47.337	0.798	0.435	13.789	9.914	35.007	93.386
1550b	1.56	0.1	1.33	0.1	1000	6.43	0.208	0.0129	2.385	47.115	0.797	0.437	13.729	9.852	34.865	92.992
1550b - Avg	1.56	0.1	1.33	0.1	1000	6.45	0.204	0.0129	2.38	47.156	0.796	0.436	13.747	9.867	34.923	92.982
1551a	1.56	0.1	1.33	0.1	1000	5.64	0.218	0.0143	3.873	91.751	1.2	0.343	17.47	12.108	54.871	224.62
1551a	1.56	0.1	1.33	0.1	1000	5.63	0.216	0.0142	3.928	91.3	1.21	0.345	17.402	12.076	54.294	225.33
1551a	1.56	0.1	1.33	0.1	1000	5.61	0.214	0.014	3.841	88.128	1.17	0.349	17.2	11.933	53.461	217.28
1551a - Avg	1.56	0.1	1.33	0.1	1000	5.63	0.216	0.0141	3.88	90.393	1.19	0.346	17.357	12.038	54.201	222.32

Table A.3. *(continued)*

USU Sample Number	Particle refractive index	Particle absorption index	Dispersant refractive index	Start result channel size	Last result channel size	Obscuration	Residual	Concentration	Span	D [4, 3] - Volume weighted mean	Uniformity	Specific surface area	D [3, 2] - Surface weighted mean	d (0.1)	d (0.5)	d (0.9)
1551b	1.56	0.1	1.33	0.1	1000	6.38	0.248	0.0163	3.954	93.964	1.22	0.341	17.598	12.078	55.598	231.92
1551b	1.56	0.1	1.33	0.1	1000	6.37	0.235	0.0161	3.863	91.71	1.2	0.343	17.479	12.003	55.002	224.45
1551b	1.56	0.1	1.33	0.1	1000	6.38	0.248	0.0163	3.809	91.423	1.17	0.341	17.619	12.093	55.805	224.65
1551b - Avg	1.56	0.1	1.33	0.1	1000	6.38	0.244	0.0162	3.875	92.365	1.2	0.342	17.565	12.058	55.465	226.96
1552a	1.56	0.1	1.33	0.1	1000	13.41	0.301	0.0536	2.34	116.256	0.743	0.226	26.5	17.75	98.067	247.25
1552a	1.56	0.1	1.33	0.1	1000	13.38	0.299	0.0541	2.346	117.268	0.743	0.224	26.772	17.883	98.849	249.75
1552a	1.56	0.1	1.33	0.1	1000	13.37	0.299	0.0542	2.348	117.526	0.743	0.223	26.879	17.922	99.022	250.38
1552a - Avg	1.56	0.1	1.33	0.1	1000	13.39	0.299	0.054	2.344	117.016	0.743	0.225	26.716	17.852	98.645	249.12
1552b	1.56	0.1	1.33	0.1	1000	6.4	0.293	0.025	2.365	115.211	0.75	0.223	26.89	17.889	96.426	245.89
1552b	1.56	0.1	1.33	0.1	1000	6.4	0.293	0.0255	2.418	120.396	0.77	0.218	27.523	18.179	99.079	257.78
1552b	1.56	0.1	1.33	0.1	1000	6.37	0.302	0.0255	2.427	120.918	0.774	0.217	27.587	18.215	99.203	258.95
1552b - Avg	1.56	0.1	1.33	0.1	1000	6.39	0.296	0.0253	2.403	118.841	0.765	0.22	27.33	18.092	98.22	254.08
1553a	1.56	0.1	1.33	0.1	1000	6.82	0.214	0.0888	1.799	182.096	0.554	0.0657	91.286	59.222	158.17	343.74
1553a	1.56	0.1	1.33	0.1	1000	6.81	0.198	0.0852	1.793	180.213	0.553	0.068	88.265	58.805	156.53	339.43
1553a	1.56	0.1	1.33	0.1	1000	6.82	0.226	0.0882	1.779	179.613	0.549	0.0662	90.61	59.165	156.26	337.16
1553a - Avg	1.56	0.1	1.33	0.1	1000	6.82	0.213	0.0874	1.79	180.641	0.552	0.0666	90.035	59.063	156.98	340.12
1553b	1.56	0.1	1.33	0.1	1000	7.13	0.332	0.0927	1.786	180.295	0.551	0.066	90.948	59.002	156.79	338.99
1553b	1.56	0.1	1.33	0.1	1000	7.11	0.334	0.0928	1.803	182.243	0.555	0.0657	91.351	58.948	158.16	344.13
1553b	1.56	0.1	1.33	0.1	1000	7.18	0.33	0.0951	1.835	186.575	0.567	0.0647	92.719	59.772	160.26	353.92
1553b - Avg	1.56	0.1	1.33	0.1	1000	7.14	0.332	0.0935	1.808	183.038	0.558	0.0655	91.666	59.235	158.38	345.62
1552b	1.56	0.1	1.33	0.1	1000	6.4	0.293	0.025	2.365	115.211	0.75	0.223	26.89	17.889	96.426	245.89
1552b	1.56	0.1	1.33	0.1	1000	6.4	0.293	0.0255	2.418	120.396	0.77	0.218	27.523	18.179	99.079	257.78
1552b	1.56	0.1	1.33	0.1	1000	6.37	0.302	0.0255	2.427	120.918	0.774	0.217	27.587	18.215	99.203	258.95
1552b - Avg	1.56	0.1	1.33	0.1	1000	6.39	0.296	0.0253	2.403	118.841	0.765	0.22	27.33	18.092	98.22	254.08
1553a	1.56	0.1	1.33	0.1	1000	6.82	0.214	0.0888	1.799	182.096	0.554	0.0657	91.286	59.222	158.17	343.74
1553a	1.56	0.1	1.33	0.1	1000	6.81	0.198	0.0852	1.793	180.213	0.553	0.068	88.265	58.805	156.53	339.43
1553a	1.56	0.1	1.33	0.1	1000	6.82	0.226	0.0882	1.779	179.613	0.549	0.0662	90.61	59.165	156.26	337.16
1553a - Avg	1.56	0.1	1.33	0.1	1000	6.82	0.213	0.0874	1.79	180.641	0.552	0.0666	90.035	59.063	156.98	340.12
1553b	1.56	0.1	1.33	0.1	1000	7.13	0.332	0.0927	1.786	180.295	0.551	0.066	90.948	59.002	156.79	338.99
1553b	1.56	0.1	1.33	0.1	1000	7.11	0.334	0.0928	1.803	182.243	0.555	0.0657	91.351	58.948	158.16	344.13
1553b	1.56	0.1	1.33	0.1	1000	7.18	0.33	0.0951	1.835	186.575	0.567	0.0647	92.719	59.772	160.26	353.92
1553b - Avg	1.56	0.1	1.33	0.1	1000	7.14	0.332	0.0935	1.808	183.038	0.558	0.0655	91.666	59.235	158.38	345.62

Appendix B. Sample Site Images

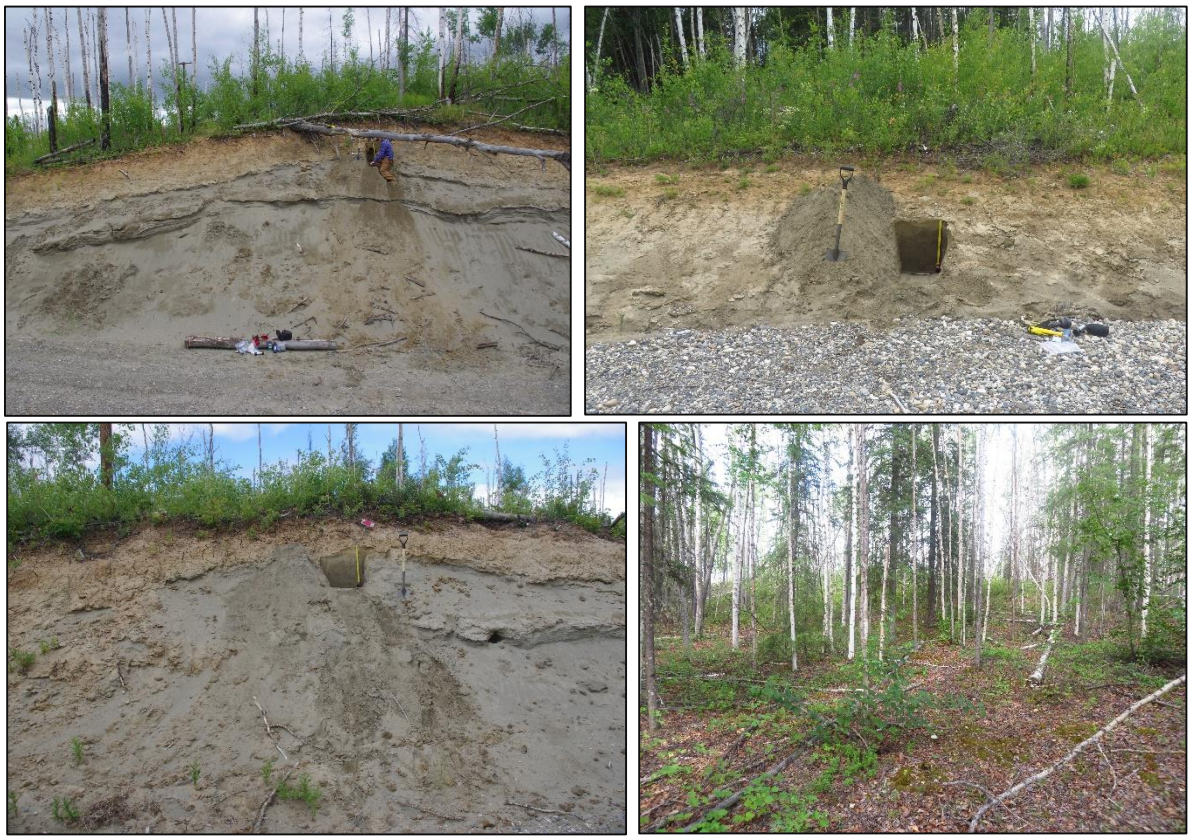

Figure B.1. Four sample locations of the Cosna dune site, from which six samples were taken. *Clockwise from top left:* East-facing road cut exposure with prominent aeolian bedding; west-facing exposure on the west flank of the dune; wooded northern flank/interdunal area; south-facing road cut exposure that also showed prominent aeolian preserved bedding (Photographs: W. Johnson and C. Messner).

Figure B.2. Red Tower site. *Top:* Exposure of dune stratigraphy faces eastward. Bottom: Second Red Tower exposure, located across the Parks Highway. Dune exposure faces westward (Photographs: W. Johnson and C. Messner).

Figure B.3. Jacobson site. Dune exposure faces northward. Loess cap is readily visible (Photograph: W. Johnson and C. Messner).

Figure B.4. Three Towers site. The Parks Highway provided another road cut exposure. Dune exposure faces westward, and Red Tower site is located to the right of the photo (northward) (Photograph: W. Johnson and C. Messner).

Figure B.5. Beekeeper site. Dune stratigraphy rises gradually past the Parks Highway. Exposure faces westward (Photograph: W. Johnson and C. Messner).

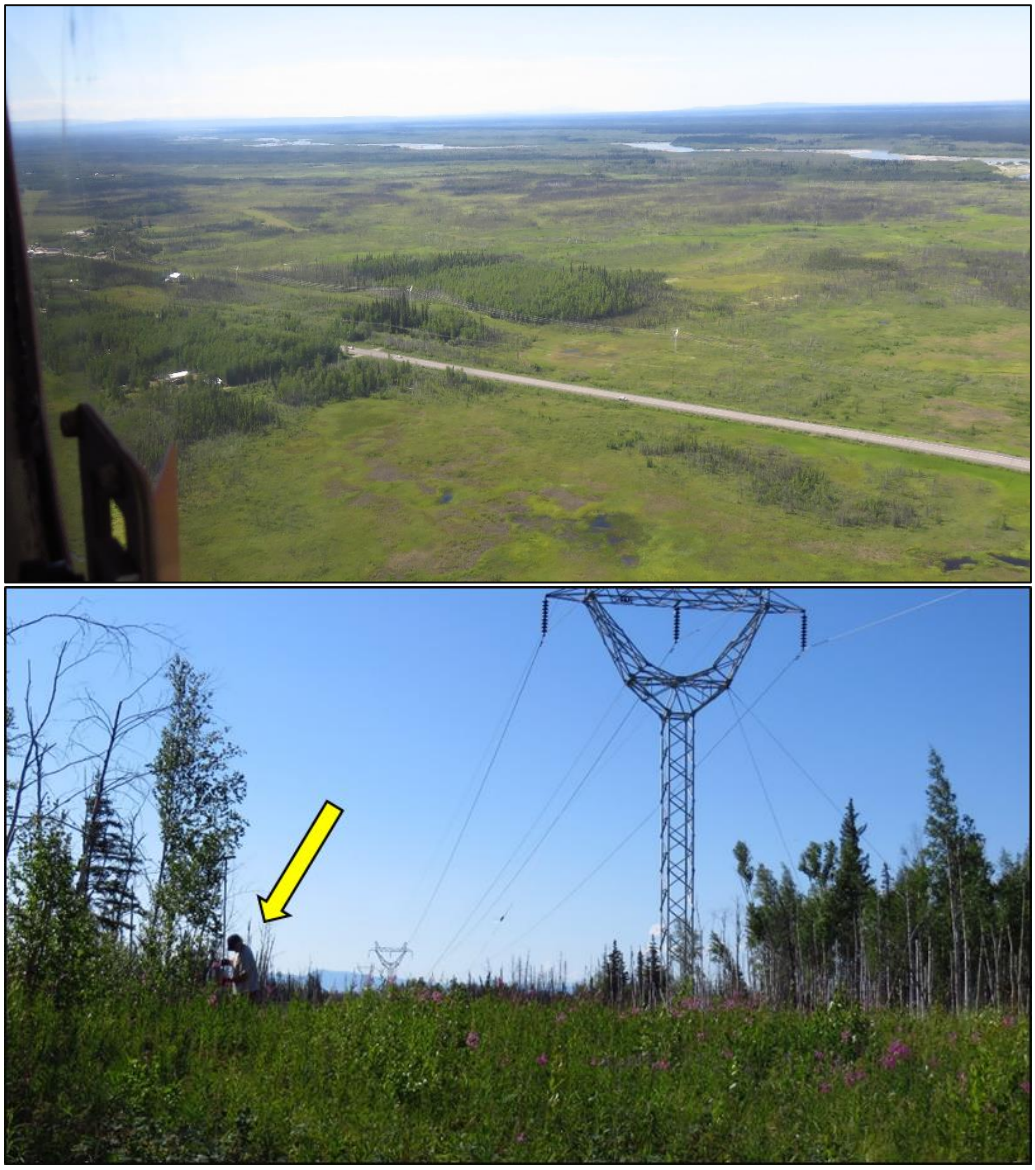

Figure B.6. *Top:* Aerial view of the Boulden site (view southwest). Dense covering of trees stabilizes the Boulden dune that extends north-south. *Bottom:* W. Johnson using a bucket auger to sample deep beneath the crest of the dune (arrow) (Photographs: W. Johnson and C. Messner).

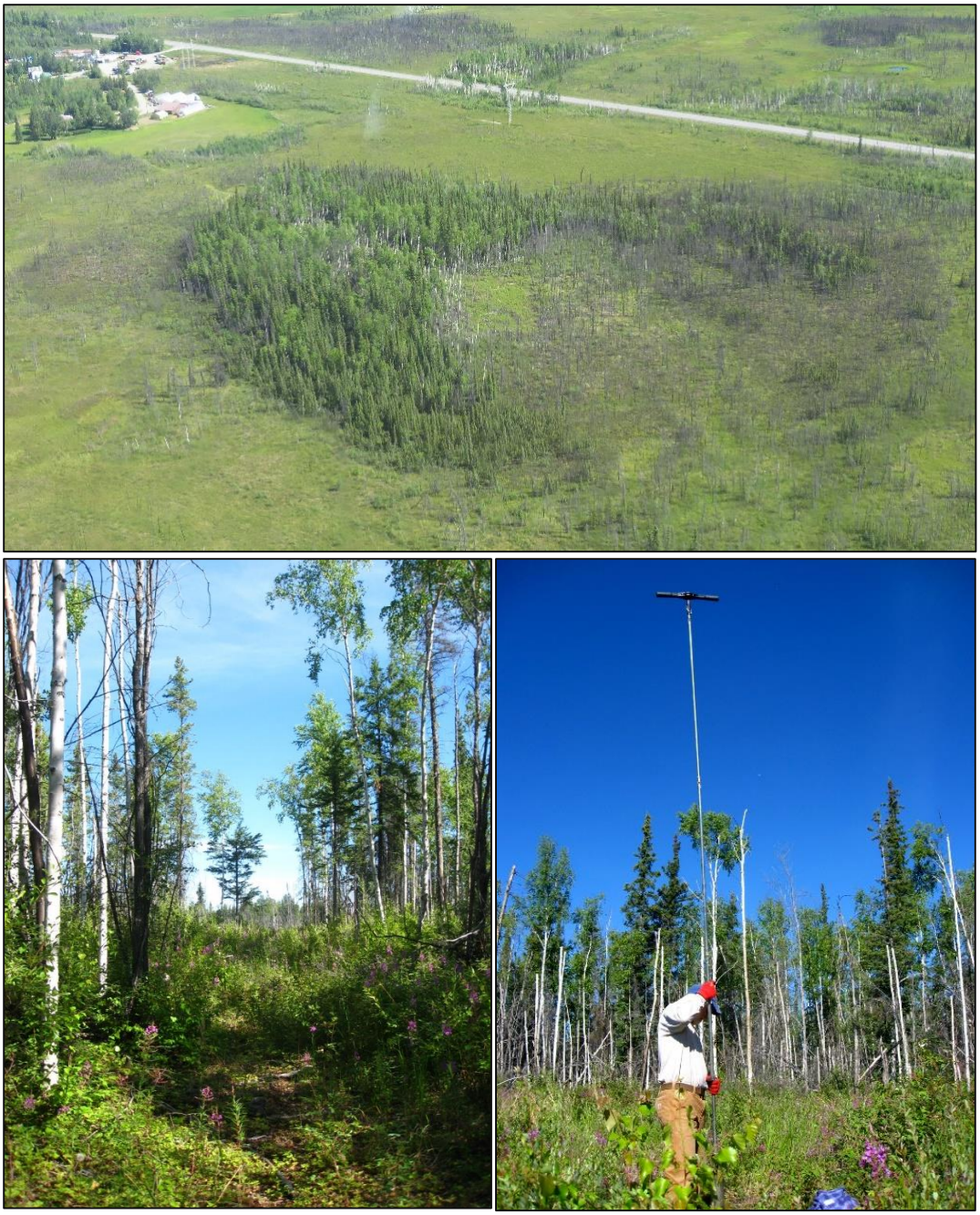

Figure B.7. *Top*: Aerial view of the southern side of the Chevron dune. Landowner mentioned a wildfire had come through the area and stripped the landform of substantial vegetation. *Bottom:* Photos taken from two locations near the crest of the dune. This dune was the only location to have no record of a yellow silty cap overlying dune sand; instead, sediment consisted of gray, silt-sized sediment at all depths (Photographs: W. Johnson and C. Messner).